DISSERTATIONS IN
FORESTRY AND
NATURAL SCIENCES

Teemu Luostari

Non-polynomial Approximation Methods in Acoustics and Elasticity

Publications of the University of Eastern Finland
Dissertations in Forestry and Natural Sciences

UNIVERSITY OF
EASTERN FINLAND

TEEMU LUOSTARI

Non-polynomial approximation methods in acoustics and elasticity

Publications of the University of Eastern Finland
Dissertations in Forestry and Natural Sciences
No 125

Academic Dissertation
To be presented by permission of the Faculty of Science and Forestry for public examination in the Auditorium ML3 in Medistudia Building at the University of Eastern Finland, Kuopio, on October, 25, 2013,
at 12 o'clock noon.

Department of Applied Physics

Kopijyvä Oy
Kuopio, 2013
Editors: Prof. Pertti Pasanen, Prof. Kai Peiponen,
Prof. Matti Vornanen, Prof. Pekka Kilpeläinen

Distribution:
University of Eastern Finland Library / Sales of publications
P.O. Box 107, FI-80101 Joensuu, Finland
tel. +358-50-3058396
http://www.uef.fi/kirjasto

ISBN: 978-952-61-1248-0 (printed)
ISSNL: 1798-5668
ISSN: 1798-5668
ISBN:978-952-61-1249-7 (pdf)
ISSNL: 1798-5668
ISSN: 1798-5668

Author's address:
University of Eastern Finland
Department of Applied Physics
P.O.Box 1627
70211 KUOPIO
FINLAND
email: Teemu.Luostari@uef.fi

Supervisors:
Docent Tomi Huttunen, Ph.D.
University of Eastern Finland
Department of Applied Physics
email: Tomi.Huttunen@uef.fi

Professor Peter Monk, Ph.D.
University of Delaware
Department of Mathematical Sciences
NEWARK, DE 19716
USA
email: Peter.Monk@math.udel.edu

Professor Jari Kaipio, Ph.D.
University of Auckland
Department of Mathematics
Private Bag 92019
AUCKLAND 1142
NEW ZEALAND
email: J.Kaipio@math.auckland.ac.nz

Reviewers:
Professor Jens Markus Melenk, Ph.D.
Institut für Analysis und Scientific Computing, E101
TU Wien
Wiedner Hauptstrasse 8-10
A-1040 Wien
AUSTRIA
email: Melenk@tuwien.ac.at

Senior Research Engineer Radek Tezaur, Ph.D.
Department of Aeronautics and Astronautics
Stanford University
STANFORD, CA 94305
USA
email: RTezaur@stanford.edu

Opponent:
Professor Jeremy Astley, Ph.D.
Engineering and the Environment
University of Southampton
Highfield
SOUTHAMPTON
SO17 1BJ
GREAT BRITAIN
email: rja@isvr.soton.ac.uk

ABSTRACT

Acoustic and elastic wave models are often encountered in engineering. Examples include seismic imaging, medical applications and the automotive industry. Such wave models are challenging to solve and sometimes require a great deal of computer resources. Therefore, efficient, robust and accurate numerical methods are needed to attack these problems.

This thesis focuses on simulating time-harmonic wave propagation problems occuring in acoustics and elasticity. A non-polynomial numerical method called the ultra weak variational formulation (UWVF) will be extended in several directions. The UWVF is a volume based method and it traditionally uses a finite element mesh of triangles or tetrahedra. Unlike the standard polynomial basis functions of the finite element method (FEM), the original UWVF uses propagating plane wave basis functions. The main drawback of the plane wave basis is ill-conditioning that occurs when too many plane waves are used on an element. Part of this thesis will focus on improving the performance of the UWVF in situations where the plane wave basis does not approximate the solution efficiently. These problems include cases where singular or rapidly decaying fields are present. A particular concern is the choice of basis functions in the acoustic UWVF.

The UWVF is a discontinuous method (DGM) and therefore techniques from the theory of the discontinuous Galerkin schemes can be applied to derive error estimates. In particular, new error estimates for the elastic UWVF will be presented.

Finally, a new UWVF will be introduced to solve vibration problems in thin elastic plates. Numerical results and basic error estimate will show that the UWVF can be used to solve thin clamped plate problems.

Universal Decimal Classification: 534, 534.8, 534.2, 534.12 519.6
INSPEC Thesaurus: acoustic waves; elastic waves; wave propagation; vibrations; acoustics; elasticity; numerical analysis; harmonics;

harmonic analysis; simulation; modeling; Galerkin method; error analysis
Yleinen suomalainen asiasanasto: akustiikka; aaltoliike; värähtelyt; numeeriset menetelmät; numeerinen analyysi; matemaattinen analyysi; matemaattiset menetelmät; simulointi

Acknowledgements

This work was mainly carried out in the Department of Applied Physics at the University of Eastern Finland, during the years 2007-2013. In addition, part of this work has been done in the Department of Mathematical Sciences at the University of Delaware, USA.

I am very grateful to my principal supervisor Docent Tomi Huttunen, Ph.D., for his invaluable help, guidance, encouragement and support. I would like to thank you for many scientific discussions and the opportunity to work in this interesting research field. I want to express my gratitude to my second supervisor Professor Peter Monk for his tireless guidance, encouragement, interesting scientific discussions and advises in the field of numerical analysis. I would like to thank you for the linguistic revisions concerning our manuscripts and this thesis. In addition, I am grateful that I had the opportunity to visit in the Department of Mathematical Sciences, University of Delaware, USA, during these years. I would also like to thank my third supervisor Professor Jari Kaipio for your support, guidance and the opportunity to work in the Inverse Problems Group.

I want to thank the reviewers Professor Markus Melenk and Senior Research Engineer Radek Tezaur, Ph.D., for your excellent advises and suggestions for improving the quality of this thesis.

I would like to express my gratitude to the staff of the Department of Applied Physics for the support, great and inspiring athmosphere. In particular, I would like to thank the whole staff of the Inverse Problems Group for support, encouragement and all these memorable years. I have really enjoyed my time with you. I am grateful to my former roommates Ville Rimpiläinen, Ph.D., Ossi Lehtikangas, M.Sc. and Jussi Toivanen, M.Sc., all of the scientific and almost scientific discussions that we have had.

I am very grateful to my parents Erkki and Sirpa for your love,

understanding, encouragement and support during all these year. I would like to thank also my brothers Kai, Jari and Tommi including your families for your support, many discussions and lessons of life. I thank also my relatives and friends for your friendship and support.

Last but not least, I would like to thank my dearest Kaisa for your endless love, support, encouragement and everything. I cannot put into words how much you mean to me.

I would like to acknowledge the Finnish Academy of Science and Letters: Vilho, Yrjö and Kalle Väisälä Foundation, Emil Aaltonen Foundation, Saastamoinen Foundation, Finnish Cultural Foundation: North Savo Regional Fund, Finnish Doctoral Programme in Computational Sciences (FICS) and the Academy of Finland (the Finnish Programme for Centres of Excellence in Research 2006-2011 and 2012-2017) for the financial support.

Kotka, September 19, 2013 *Teemu Luostari*

ABBREVIATIONS

1D	One-dimensional
2D	Two-dimensional
3D	Three-dimensional
ABC	Absorbing boundary condition
AVM	Adjoint variable method
BEM	Boundary element method
DD	Domain decomposition
DDM	Direct differentiation method
DEM	Discontinuous enrichment method
DG	Discontinuous Galerkin
DGM	Discontinuous Galerkin method
DPG	Discontinuous Petrov-Galerkin
DSA	Design sensitivity analysis
EW	Evanescent wave
FDTD	Finite difference time domain
FEM	Finite element method
FMM	Fast multipole method
FOSLS	First order system of least squares
GFEM	Generalized finite element method
GLS	Galerkin least squares
GMRES	Generalized minimum residual method
HIFU	High intensity focused ultrasound
HRTF	Head-related transfer function
IFT	Inverse Fourier transform
ILU	Incomplete Lower-Upper
imDGM	Improved discontinuous Galerkin method
LDGM	Local discontinuous Galerkin method
LED	Light emitting diode
LSM	Least-squares method
mDGM	Modified discontinuous Galerkin method
MFMM	Multilevel fast multipole method
MFS	Methods of fundamental solution
nnz	Number of non-zeros

PDE	Partial differential equation
PML	Perfectly matched layer
PUFEM	Partition of unity finite element method
PW	Plane wave
SDGM	Stable discontinuous Galerkin method
SEA	Statistical energy analysis
SEM	Spectral element method
TDG	Trefftz discontinuous Galerkin
TMM	Transfer matrix method
UWVF	Ultra weak variational formulation
VTCR	Variational theory of complex rays
WBM	Wave based method
WVF	Weighted variational formulation

NOMENCLATURE

A	scalar, satisfies the Helmholtz equation, Section 4.1.3
A	orthogonal matrix, Section 4.3.1
A_j^k	unknown coefficient in PUFEM, Section 3.1
$\boldsymbol{a}$, $\boldsymbol{b}$	vectors, Section 4.1.1
$a_p^{K_k}$	unknown coefficient in LSM, Section 3.2
$\boldsymbol{B}$	vector field satisfying Maxwell equation, Section 4.1.3
$\boldsymbol{b}$	data vector, Section 4.1.2
C	sparse matrix, Section 4.1.2
C	arbitrary constant, Section 4.1.3
$\mathbb{C}$	complex numbers, Section 4.1
c	speed of sound (in fluids), Section 2.3
c_P	speed of pressure wave (P-wave), Section 2.1
c_S	speed of shear wave (S-wave), Section 2.1
D	plate bending stiffness, Section 2.2
D	sparse block diagonal matrix, Section 4.1.2
$\boldsymbol{d}_k$	direction of propagation (unit vector), Section 3.1
$\boldsymbol{d}_{\mathrm{inc}}$	incident direction of propagation (unit vector), Section 5.3.1
E	Young's modulus, Section 2.1
F_k	operator of the UWVF, Section 4.1.1
$\boldsymbol{f}$	body force, Section 2.1
f	frequency, Section 5.2.1
$\boldsymbol{g}$	source term on the boundary, Section 4.1
g_1, g_2	source terms on the boundary, Section 4.2
g	acoustic source term on the boundary, Section 3.1
H	Sobolev space, Section 4.1.3
h	element size, Section 4.1.3
I	identity matrix, Section 2.1
i	imaginary unit, Section 2.1
j	integer, Section 3.1
K_1, K_2	wave numbers, 5.3.2
K_k	element k in the domain, Section 3.2
k	integer, Section 3.1
L^2_η	weighted space, Section 4.1.1

(L_x, L_y)	dimensions (rectangle) bounding the cavity, Section 3.4
l	integer, Section 4.1.3
ℓ	integer, Section 3.5.1
$\tilde{\ell}$	integer, Section 4.3.1
	rational number (modified Bessel basis), Section 4.3.1
M_x	bending moment, Section 2.2
M_y	bending moment, Section 2.2
M_{xy}, M_{yx}	twisting moments, Section 2.2
m	integer, Section 4.1.3
N	number of elements, Section 4.1.1
$\mathbb{N}$	natural numbers, Section 3.3
N_E	integer, Section 3.3
N_k	unknown coefficient, Section 3.1
N_j	solution of a governing PDE, Section 3.1
N_p	integer, $N_p - 1$ is the number of basis functions, Section 3.2
$\boldsymbol{n}$	outward unit normal, Section 3.1
n	index of refraction, Section 3.5.1
n	integer, Section 5.2.1
n_e	integer, Section 3.3
n_k	refraction index of medium, Section 3.5.1
n_n	number of nodes, Section 3.1
$\boldsymbol{P}$	vector, $(\boldsymbol{P} \cdot \boldsymbol{P})^2 = r^4$, Section 3.3
P	time-dependent pressure, Section 2.3
P_0	static state pressure, Section 2.3
P^h	best approximation operator, Section 4.1.3
P_n	mapping, Section 3.3
P_t	mapping, Section 3.3
p	number of basis functions, Section 3.1
p_a	acoustic (time-harmonic) pressure, Section 2.3
p_a^h	approximation for acoustic pressure, Section 3.1
p_a^{ex}	exact solution, Section 5.1.1
p_{inc}	incident wave field, Section 4.3.1
p_k	number of basis functions in element K_k, Section 3.5.1
p^P, p^S	number of basis functions, Section 4.1.2
p_{R}	reflected field, Section 4.3.1

p_{T}	transmitted field, Section 4.3.1
Q	defines the type of the boundary condition, Section 4.1
Q_1, Q_2	defines the type of the boundary condition, Section 4.2
Q_x	shear force, Section 2.2
Q_y	shear force, Section 2.2
q	time-harmonic volume source (loading), Section 2.2
q_P, q_S	integer, Section 4.1.3
q_a	integer, Section 4.3.2
q_b	time-dependent volume source (loading), Section 2.2
q_p	integer, Section 3.5.2
R	reflection coefficient, Section 5.3.2
$\Re$	real part, Section 2.1
r	distance (polar coordinates), Section 3.1
	radius, Section 3.3
r_1, r_2	radius, Section 5.3.3
r_P, r_S	integer, Section 4.1.3
$\tilde{r}_1$	integer, Section 3.4
S	entropy, Section 2.3
S_0	static state entropy, Section 2.3
$\boldsymbol{s}$	tangential unit vector, Section 3.3
	auxiliary variable (in DG scheme), Section 4.2.1
$\boldsymbol{s}_1$, $\boldsymbol{s}_2$	unit vectors (polarization), Section 5.2.1
s	integer, Section 4.3.1
$\tilde{s}_1$	integer, Section 3.4
$\hat{\boldsymbol{s}}$	numerical flux, Section 4.2.1
^{T}	denotes the transpose operator, Section 2.1
$\mathcal{T}_h$	consists of the elements (mesh), Section 4.1.1
$\boldsymbol{t}$	auxiliary variable (in DG scheme), Section 4.2.1
$\hat{\boldsymbol{t}}$	numerical flux, Section 4.2.1
t	thickness of the plate, Section 2.2
$\boldsymbol{U}$	time-dependent displacement (U_x, U_y, U_z), Section 2.1
$\boldsymbol{u}$	time-harmonic displacement (u_x, u_y, u_z), Section 2.1
$\boldsymbol{u}^P$	pressure (or dilatational) P-wave, Section 2.1
$\boldsymbol{u}^{SH}$	horizontal component of shear wave SH-wave, Section 2.1
$\boldsymbol{u}^{SV}$	vertical component of shear wave SV-wave, Section 2.1

$\boldsymbol{u}_h$	approximation for $\boldsymbol{u}$, Section 4.1.3
$\boldsymbol{u}_k$, $\boldsymbol{u}\|_{K_k}$	displacement field on the element K_k
$\boldsymbol{u}_j$, $\boldsymbol{u}\|_{K_j}$	displacement field on the element K_j
$\hat{\boldsymbol{u}}_f$	fundamental solution, Section 3.4
$\hat{\boldsymbol{u}}$	numerical flux, Section 4.1.1
u	general fields satisfying governing PDE, Section 3.1
	auxiliary variable (in DG scheme), Section 4.2.1
$\tilde{u}$	approximation for u (WBM), Section 3.4
$\hat{u}$	numerical flux, Section 4.2.1
u_c	amplitude of an corner mode, Section 3.3
u^E	enrichment part in the DEM, Section 3.5.3
u_e	amplitude of an edge mode, Section 3.3
u^P	polynomial part in the DEM, Section 3.5.3
$\boldsymbol{V}$	time-dependent particle velocity, Section 2.3
$\boldsymbol{V}_0$	static state particle velocity, Section 2.3
$\boldsymbol{v}$	time-harmonic velocity field, Section 2.3
v	test function, Section 3.1
W	time-dependent displacement (U_z), Section 2.2
w	time-harmonic displacement (u_z), Section 2.2
$\hat{w}$	numerical flux, Section 4.2.1
w_{smth}	solution of homogeneous PDE, Section 5.4.1
w_{fund}	fundamental solution, Section 5.4.1
$\boldsymbol{X}$	unknown coefficients to be determined, Section 4.1.2
$\mathcal{X}$	unknown function in the UWVF, Section 4.1.1
X	weighted space, Section 4.1.1
$\boldsymbol{x}$	coordinate vector $\boldsymbol{x} = (x, y, z)$, Section 3.3
$\boldsymbol{x}_{0,k}$	centroid of the element, Section 4.3.1
x_0, y_0	scaling coordinates, Section 4.3.1
$\mathcal{Y}$	functional in the UWVF on ∂K_k, Section 4.1.1
α	integer, Section 4.1.3
$\alpha^P_{k,\ell}$, $\alpha^{SH}_{k,\ell}$, $\alpha^{SV}_{k,\ell}$	amplitudes of basis functions, Section 4.1.2
$\alpha_{k,\tilde{\ell}}$	variable in the evanescent wave basis, Section 4.3.1
β_j	unknown coefficient, Section 3.1
$\beta_{k,\tilde{\ell}}$	variable in the evanescent wave basis, Section 4.3.1
Γ	boundary, Section 3.1

δ	stress tensor (test function), Section 4.1.1
	bounded variable, Section 4.2.3
$\delta(\cdot)$	Dirac's distribution, Section 5.4.1
$\epsilon(\cdot)$	the strain tensor, Section 2.1
η	numerical flux (coupling) parameter, Section 4.1
η_1, η_2	numerical flux (coupling) parameter, Section 4.2
ζ	test function in acoustics, Section 4.3
θ	angle, Section 3.1
θ^{EW}	angle in the evanescent wave basis, Section 4.3.1
θ_{crit}	critical angle, Section 4.3.1
θ_{inc}	incident angle of propagation, Section 4.3.1
θ_{R}	reflection angle, Section 4.3.1
θ_{T}	transmission angle, Section 4.3.1
∂K_k	faces (edges) of the element, Section 4.1.1
κ	acoustic wave number
κ_b	plate bending wave number, Section 2.2
κ_P	pressure wave number (P-wave number), Section 2.1
κ_S	shear wave number (S-wave number), Section 2.1
$(\kappa_{xr}, \kappa_{yr})$	wave numbers in WBM (r-set), Section 3.4
$(\kappa_{xs}, \kappa_{ys})$	wave numbers in WBM (s-set), Section 3.4
$\varkappa$	(auxiliary) variable refers to weighting, Section 4.1.3
Λ	depends on the shape of the element, Section 4.1.3
Λ_l	Lagrange polynomial, Section 3.5.3
λ	Lamé constant, Section 2.1
λ_b	plate bending wavelength, Section 2.2
μ	Lamé constant, Section 2.1
$\boldsymbol{\nu}_{\text{A}}$	unit vector, Section 5.3.3
ν	Poisson ration, Section 2.1
$\boldsymbol{\xi}$	test function, (in DG scheme), Section 4.2.1
$\Sigma_{k,j}$	common interface of K_k and K_j, Section 4.1.1
σ_τ	time-dependent stress tensor, Section 2.1
σ	time-harmonic stress tensor, Section 2.1
$\hat{\sigma}$	numerical flux, Section 4.1.1
ρ	density of medium, Section 2.1
ρ_0	static state density of medium, Section 2.3

$\boldsymbol{\tau}$	auxiliary variable (cf. test function velocity), Section 4.3
$\boldsymbol{\tau}_{\mathrm{A}}$	unit vector, Section 5.3.3
τ	time variable, Section 2.3
Φ_k	wave functions in WBM, Section 3.4
Φ_r	r-set wave functions in WBM, Section 3.4
Φ_s	s-set wave functions in WBM, Section 3.4
$\boldsymbol{\phi}$	smooth vector test function, Section 4.1.1
$\boldsymbol{\phi}^P_{k,\ell}$, $\boldsymbol{\phi}^{SH}_{k,\ell}$, $\boldsymbol{\phi}^{SV}_{k,\ell}$	P-, SH- and SV-wave basis functions, Section 4.1.2
ϕ	piecewise linear nodal basis function 3.1
ϕ	test function, (in DG scheme), Section 4.2.1
φ	angle, Section 3.3
$\varphi_{k,\ell}$	basis functions in the UWVF, Section 3.5.1
$\varphi^{PW}_{k,\ell}$, $\varphi^{EW}_{k,\ell}$	PW and EW basis functions, Section 4.2.2
$\boldsymbol{\varphi}$	test function, (in DG scheme), Section 4.2.1
ψ	test function, (in DG scheme), Section 4.2.1
Ω	computational domain, Section 3.1
ω	angular frequency, Section 2.1
$\{\!\{\cdot\}\!\}$	the average across common interface, Section 4.1.1
$[\![\cdot]\!]$	the jump across common interface, Section 4.1.1
$\otimes$	outer product i.e. $\boldsymbol{a} \otimes \boldsymbol{b} = \boldsymbol{a}\boldsymbol{b}^T$, Section 4.1.1

LIST OF PUBLICATIONS

This thesis consists of the present review of the author's work in the field of computational physics and the following selection of the author's publications:

I T. Luostari, T. Huttunen and P. Monk, "The ultra weak variational formulation using Bessel basis functions," *Communications in Computational Physics* **11,** 400–414 (2012).

II T. Luostari, T. Huttunen and P. Monk, "Error estimates for the ultra weak variational formulation in linear elasticity," *ESAIM: Mathematical Modelling and Numerical Analysis* **47,** 183–211 (2013).

III T. Luostari, T. Huttunen and P. Monk, "Improvements for the ultra weak variational formulation," *International Journal for Numerical Methods in Engineering* **94,** 598–624 (2013).

IV T. Luostari, T. Huttunen and P. Monk, "The ultra weak variational formulation in thin clamped plates problems," Submitted for publication: *Journal of Computational Physics*

Throughout the overview, these papers will be referred to by Roman numerals.

AUTHOR'S CONTRIBUTION

All articles have been written as a collaboration of the author and his supervisors. The author of this thesis has been the corresponding author in all of the publications but the help, guidance and contribution of the co-authors has been significant. The author has also been responsible for the numerical results.

The author of this thesis has extended, applied and further developed existing ultra weak variational formulation (UWVF) codes, and all codes have been implemented using MATLAB®. New basis functions in acoustics have been implemented by the author.

The author has been responsible for the majority of the work on linear elasticity. Error estimates for the UWVF for linear elasticity were derived by the author with advice from the co-authors. An existing 2D linear elasticity code has been extended to 3D by the author.

The author suggested the topic of vibration of plates and has been responsible for that work. In particular, the author has implemented the new UWVF for plate vibration problems building on previously developed codes.

Some of the meshes used in simulations have been constructed using MATLAB®, COMSOL Multiphysics® and NETGEN. Meshes with square elements have been constructed by the author and hexahedral elements have been constructed in collaboration between the author and his supervisors.

Contents

1 Introduction

Simulation of propagating acoustic or elastic waves is needed in various fields of industry ranging from remote sensing to noise control. These involve frequencies across the broad spectrum of sounds. For instance, high frequency sound is used in medical applications, audible frequencies in automotive industries and low frequencies are used in seismology. Not only the frequency range but also geometrical properties of the computational domain such as fine detailed structures, big computational regions or multiscale structures generate challenges and impose limitations on modeling. Therefore, it is important to improve current solvers and develop new efficient numerical modeling methods. Even though, computing power has increased over the years, numerical wave simulation often remains a challenging and time intensive task.

Polynomial methods such as the finite element method (FEM) or the boundary element method (BEM) are commonly used to solve wave problems in acoustics and elasticity. In the FEM, the computational domain is divided into small elements, a weak form of the problem is discretized and locally supported polynomial test and basis functions are used to approximate the problem. As a result, the FEM is a flexible method that can be applied to complex geometries and a wide variety of physical problems. In the BEM, an integral representation of the solution is used and only the boundary of the domain is discretized. Low order FEM or BEM need at least 10 degrees of freedom per wavelength in order to achieve a tolerable accuracy. At higher wave numbers the number of degrees of freedom per wavelength needed is even larger due to pollution error [1] (or for BEM [2]). At very high frequencies statistical energy analysis (SEA) [3] is widely used, but statistical methods will not be considered here.

In order to overcome the disadvantages of low order FEM, other polynomial based methods have been developed such as the Galer-

kin/least-squares method (GLS) [4], very high order finite element method called the spectral element method (SEM) [5], the *hp* finite element method (*hp* FEM) [6–8] and the discontinuous Galerkin method (DGM) [9]. Recently, the focus has been on developing a stable polynomial method suitable for large wave numbers [10–14] or optimizing the test functions to obtain better stability [15–17]. In particular, the discontinuous Petrov-Galerkin (DPG) method with optimal test functions has been developed by Demkowicz and Gopalakrishnan et al. [15–17]. In acoustics, numerical tests show that the DPG method with optimal test functions has no pollution error in 1D and small pollution error in 2D [16, 17]. At the same time, Melenk and Sauter [7, 8] have shown that the *hp* FEM can control pollution error provided that the polynomial degree is allowed to grow slowly with frequency.

In acoustics and elasticity, solutions may have singularities. For example, singular solutions are generated near sharp corners, edges, change in boundary condition, or point sources. Polynomial methods, such as the traditional FEM, are not the most suitable to approximate singular problem efficiently. Strategies to improve the accuracy of FEM include mesh refinement (*h*-version) near the singularity, the use of higher order polynomials (*p*-version) or the use of both strategies (*hp*-version). Another natural direction beyond the polynomial based methods is the use of specially chosen non-polynomial basis functions. The idea of using specially designed basis functions is not new. In 1973 [18], non-polynomial basis functions in the FEM were tailored to cope with singularities. In the case of elastic cracks, the accuracy of the FEM was enhanced by using enriched singular functions in [19]. In [20], "cracked elements" were used in order to decrease the error in elastic plate problems. A large literature now exists in this direction.

Another challenge arising from computational wave propagation is that the problem is often posed on an unbounded computational domain. Then the solution needs to satisfy a suitable radiation condition. Although non-polynomial basis functions can help with this aspect of wave propagation (e.g. infinite elements [21, 22]

and wave envelope method [23]), we do not focus on this problem in our studies.

Physical basis functions, in addition to polynomials, can be used on a bounded domain to approximate oscillatory solutions. One of the first such methods is the partition of unity finite element method (PUFEM) developed by Babuška and Melenk [24,25]. The PUFEM is based on the standard weak formulation of FEM for acoustic problems but instead of using polynomial basis functions, it uses plane waves that are multiplied by piecewise polynomial partition of unity functions. Methods similar to PUFEM have been investigated under different names such as the finite ray element method [26], microlocal discretization [27,28] and special wave boundary element method [29]. More general approximations have been introduced in the generalized finite element method (GFEM) [30] where piecewise polynomial finite elements and PUFEM are added (leaving out the FEM part the method reduces to the PUFEM).

Many methods have been developed using physical basis functions alone. These methods which use sums of known solutions of the partial differential equation belong to the class of Trefftz methods [31,32]. To be more specific, in the Trefftz method, the functions which are used in the approximation satisfy the governing partial differential equation (cf. plane waves satisfy the Helmholtz equation) but may violate the boundary conditions. Hence, sums of these functions are then adjusted to satisfy the boundary condition. For example, the method of fundamental solution (MFS) [33] is a Trefftz method using sums of fundamental solutions corresponding to source points outside the computational domain.

In 1994, the ultra weak variational formulation (UWVF) of Després [34] was introduced. Two years later in 1996, both theoretical and the numerical results for acoustics and electromagnetism were considered in Cessenat's thesis [35] (supervised by Després). Originally it uses discontinuous piecewise plane wave basis functions.

Concurrently, in 1996, Ladevèze [36] introduced the variational theory of complex rays (VTCR) to solve elasticity problems. Here

the "complex rays" are solutions of the governing partial differential equation (cf. plane waves, corner and edge evanescent waves). In 1998, Desmet introduced a wave based method (WBM) [37] which uses a weighted residual formulation and sums of wave functions that satisfy the governing equation. The WBM was applied to vibro-acoustic problems in various fields of engineering [37]. In the same year 1998, the least-squares method (LSM) by Stojek [38] was introduced and Bessel and Hankel functions were used in acoustic wave modeling. One year later, Monk and Wang [39] used plane wave and Bessel functions in the LSM for acoustic problems and proved error estimates.

More recently, in 2001, the discontinuous enrichment method (DEM) [40] was introduced. It uses discontinuous basis functions that consist of a polynomial part enriched by non-polynomial functions such as plane waves. The DEM uses a hybrid discontinuous Galerkin formulation and weak continuity between elements is enforced using Lagrange multipliers. Without the polynomial part, the DEM reduces to the DGM with Lagrange multipliers and non-polynomial basis functions.

The aim of this thesis is to investigate and further develop the UWVF. One of the main focuses is on the choice of basis functions of the acoustic UWVF. In particular, it is well-known that plane wave based methods suffer from ill-conditioning when too many basis functions are used on a single element. The UWVF with Bessel basis functions will be studied in order to try to stabilize the method (obtaining a lower condition number and as good accuracy as plane waves).

As in the case of FEM [18], the performance of the UWVF deteriorates in the presence of singular solutions [41]. Therefore, we investigate the use of fractional order Bessel basis functions near corner singularities. Similar kinds of singular problems have also been investigated for other non-polynomial methods such as the non-polynomial FEM [42] and the WBM [43–46].

Another case where accuracy can deteriorate occurs because rapidly decaying interface waves are challenging to approximate

with plane waves [47–50]. Motivated by studies using the DEM [49, 50], the use of evanescent wave basis functions in the UWVF will be examined for a fluid-fluid interface problem with straight or curved interfaces. The focus will be on the cases when rapidly decaying waves are present.

The UWVF will also be developed for linear elasticity in three dimensions. In particular, error estimates for the elastic UWVF will be derived using the equivalence of the UWVF with an upwind discontinuous Galerkin (DG) scheme. The derivation of error estimates for the elastic-UWVF is motivated by [39, 51] and uses new approximation properties of plane waves proved in [52, 53].

Finally, the UWVF will be extended to clamped thin plate problems. This can be considered as a first step towards applications to more general plate problems with free and simply supported boundary conditions. Similar problems have been studied using the WBM [54], DEM [55] and VTCR [56].

The outline of this thesis is as follows: first the governing physical equations are given for linear elasticity, vibration of plates and acoustics. Second, an overview of non-polynomial methods applied to acoustics, electromagnetism, elasticity and vibro-acoustics will be given. We shall discuss aspects of the PUFEM, LSM, UWVF, VTCR, WBM, DEM and DGM. Many of the non-polynomial methods that will be reviewed were introduced in the mid 1990's. Commonly used basis functions, application fields and a summary of the main novelties of each method will be considered. In the third chapter, the UWVFs for linear elasticity, plate vibration and acoustic problems are derived, error estimates are considered and new basis function choices are described. Then the main numerical results are presented based on the contents of the original publications **I**-**IV**. Finally, we draw some conclusions and discuss possible future applications of the UWVF.

2 Governing equations

In this chapter we shall give a short outline of the governing equations in linear elasticity, plate vibration and acoustics. For linear elasticity and acoustics we focus on first order systems because the upcoming derivation of the UWVF follows from the upwind DG scheme applied to an appropriate first order system. For the vibration of plates a simpler first order system will be written in Section 4.

2.1 LINEAR ELASTICITY

Elastic waves are mechanical vibrations that propagate in solid materials. In linear elasticity, the basic goal is to approximate the time-dependent displacement fields $\boldsymbol{U} = (U_x, U_y, U_z)$ in solids. The upcoming derivation of the equations of linear elasticity follows references [57, 58]. The stress tensor can be written as

$$\sigma_\tau = (\lambda \nabla \cdot \boldsymbol{U}) I + 2\mu\epsilon(\boldsymbol{U}) \tag{2.1}$$

where I is the identity matrix, λ and μ are the Lamé constants of the form

$$\mu = \frac{E}{2(1-\nu)} \quad \text{and} \quad \lambda = \frac{E\nu}{(1+\nu)(1-2\nu)}.$$

Here E is the Young's modulus and ν is the Poisson ratio of the solid. In this thesis all these constants are assumed to be real and positive.

The strain tensor $\epsilon(\boldsymbol{U})$ in (2.1) is

$$\epsilon(\boldsymbol{U}) = \frac{1}{2}(\nabla \boldsymbol{U} + (\nabla \boldsymbol{U})^T) \tag{2.2}$$

where the superscript T denotes the transpose operator.

The time-dependent momentum equation is then defined to be

$$\nabla \cdot \sigma_\tau + \rho \boldsymbol{f} = \rho \frac{\partial^2 \boldsymbol{U}}{\partial \tau^2} \tag{2.3}$$

where ρ is the density of the medium, $\boldsymbol{f}$ is the body force and τ denotes time.

Equations (2.3) and (2.1) form the time-dependent first order system in linear elasticity. Assuming now that $\boldsymbol{f} = \boldsymbol{0}$ (no body forces) and that the displacement field and stress tensor are time-harmonic: $\boldsymbol{U} = \Re\{\boldsymbol{u}\exp(-i\omega\tau)\}$, $\sigma_\tau = \Re\{\sigma\exp(-i\omega\tau)\}$ where $\Re\{\cdot\}$ denotes the real part, the angular frequency of the field is ω, the spatially dependent displacement vector is $\boldsymbol{u} = (u_x, u_y, u_z)$ and strain tensor is σ. Then the time-harmonic stress tensor and momentum equation can be written as a first order system

$$\begin{aligned} \sigma &= (\lambda \nabla \cdot \boldsymbol{u}) I + 2\mu\epsilon(\boldsymbol{u}), \\ \nabla \cdot \sigma + \omega^2 \rho \boldsymbol{u} &= \boldsymbol{0}. \end{aligned}$$

Alternatively, combining (2.3), (2.1) and (2.2) and choosing $\boldsymbol{f} = \boldsymbol{0}$, yields the well-known second order equation, known as the Navier equation

$$\mu \Delta \boldsymbol{U} + (\lambda + \mu)\nabla(\nabla \cdot \boldsymbol{U}) = \rho \frac{\partial^2 \boldsymbol{U}}{\partial \tau^2}.$$

Then, the lossless time-harmonic Navier problem is to find the displacement $\boldsymbol{u}$ such that

$$\mu \Delta \boldsymbol{u} + (\lambda + \mu)\nabla(\nabla \cdot \boldsymbol{u}) + \omega^2 \rho \boldsymbol{u} = \boldsymbol{0}. \tag{2.4}$$

In a homogeneous medium, the displacement field $\boldsymbol{u}$ can be decomposed into three wave components: the pressure (or dilatational) P-wave $\boldsymbol{u}^P$, the horizontal component of shear SH-wave $\boldsymbol{u}^{SH}$ and the vertical component of shear SV-wave $\boldsymbol{u}^{SV}$ as follows

$$\boldsymbol{u} = \boldsymbol{u}^P + \boldsymbol{u}^{SH} + \boldsymbol{u}^{SV}$$

such that

$$\Delta \boldsymbol{u}^P + \kappa_P^2 \boldsymbol{u}^P = \boldsymbol{0},$$
$$\Delta \boldsymbol{u}^{SH} + \kappa_S^2 \boldsymbol{u}^{SH} = \boldsymbol{0},$$
$$\Delta \boldsymbol{u}^{SV} + \kappa_S^2 \boldsymbol{u}^{SV} = \boldsymbol{0},$$

where the wave number for P-waves is $\kappa_P = \omega/c_P$, the wave number for S-waves is $\kappa_S = \omega/c_S$ and the following identities hold $\nabla \times \boldsymbol{u}^P = 0$ and $\nabla \cdot \boldsymbol{u}^{SH} = \nabla \cdot \boldsymbol{u}^{SV} = 0$. Wave speeds for the pressure wave (P-wave) and shear waves (S-waves) are

$$c_P = \sqrt{\frac{\lambda + 2\mu}{\rho}} \quad \text{and} \quad c_S = \sqrt{\frac{\mu}{\rho}},$$

respectively.

2.2 PLATE VIBRATION

Many elastic structures (e.g. airplanes, cars) are constructed from thin plates. In plate theory the idea is to take the advantage of the thinness of the plate to reduce the problem from 3D to 2D. We can then investigate deformations/stresses of thin 2D plates. When elastic wave motion is investigated in thin plates, the unknown time dependent out-of-plane displacement is denoted by $W := W(x, y, t)$. This is just the z-component of the displacement field $\boldsymbol{U}$ appearing in the previous section. Suppose the plate is at rest and lies in the (x, y) plane. Then the problem can be formulated using a fourth order Kirchhoff's thin plate partial differential equation. Next we give a short derivation of Kirchhoff's thin plate equations following [57, 59–61], see also the Ph.D. theses [54, 62]. For plate elasticity, the equations of motion are given by

$$\frac{\partial Q_x}{\partial x} + \frac{\partial Q_y}{\partial y} + q_b = \rho t \frac{\partial^2 W}{\partial \tau^2}, \tag{2.5}$$

$$\frac{\partial M_y}{\partial y} - \frac{\partial M_{xy}}{\partial x} - Q_y = 0, \tag{2.6}$$

$$\frac{\partial M_x}{\partial x} - \frac{\partial M_{xy}}{\partial y} - Q_x = 0, \tag{2.7}$$

where Q_x, Q_y are shear forces, M_x and M_y are bending moments, M_{xy} is the twisting moment, q_b is the volume source term (loading), ρ is the density, t is the thickness of the plate and τ refers to time. As discussed in [61], equation (2.5) refers to forces acting along the z-axis, equation (2.6) refers to forces and moments acting on the x-axis and equation (2.7) refers to forces and moments with respect to the y-axis. Due to the fact that the changes in forces Q_y and Q_x and higher order contributions of q_b are small those are neglected in (2.6) and (2.7) [57, 61]. Following [57, 61], a schematic figure of the governing forces and moments is shown in Figure 2.1.

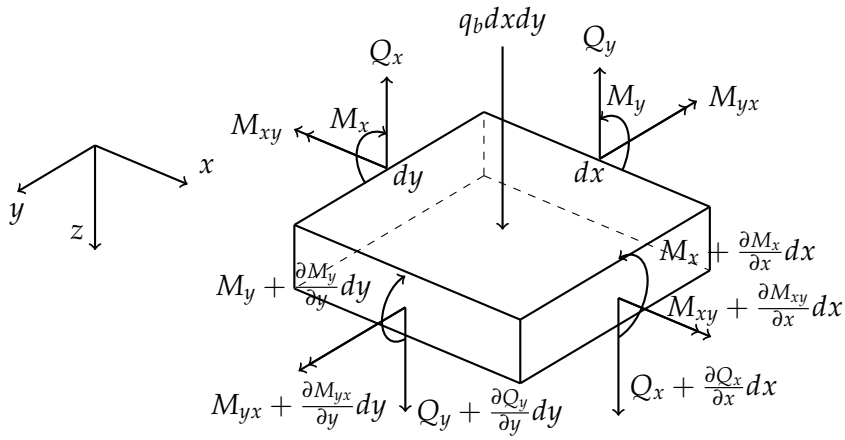

Figure 2.1: Infinitesimal thin elastic plate. Forces acting on the thin elastic plate following [57, 61] (see also [62]).

For the thin plate, the bending moments and twisting moments are given by, (for more details see [57, 59–61]),

$$M_x = -D\left(\frac{\partial^2 W}{\partial x^2} + \nu \frac{\partial^2 W}{\partial y^2}\right), \tag{2.8}$$

$$M_y = -D\left(\frac{\partial^2 W}{\partial y^2} + \nu \frac{\partial^2 W}{\partial x^2}\right), \tag{2.9}$$

$$M_{xy} = -M_{yx} = D(1-\nu)\frac{\partial^2 W}{\partial x \partial y}, \tag{2.10}$$

where $D = Et^3/(12(1-\nu^2))$ is called the plate bending stiffness (or stiffness coefficient of the plate [60]), E is the Young's modulus, t is the thickness of the plate and ν is the Poisson ratio. Combining equations (2.5), (2.6), (2.7), (2.8), (2.9) and (2.10) assuming a time-harmonic displacement $W = \Re\{w(x,y)\exp(-i\omega\tau)\}$ and a force term $q_b = \Re\{q(x,y)\exp(-i\omega\tau)\}$, the time independent biharmonic (fourth order) problem based on Kirchhoff's thin plate theory in 2D is given by

$$\Delta^2 w - \kappa_b^4 w = q, \tag{2.11}$$

where Δ^2 is the bi-Laplacian and $\kappa_b = (\rho t\omega^2/D)^{1/4}$ is the plate bending wave number. The function q is the source term or loading. The Kirchhoff theory is valid for cases when the plate bending wavelength $\lambda_b = \frac{2\pi}{\kappa_b} > 6t$, see [54, 63].

2.3 ACOUSTICS

In acoustics, we want to predict the acoustic pressure P in the fluid. Taking into account viscous effects, the equations for acoustic pressure in a fluid reduce to the Navier equation with a special choice of Lamé constants (see for example [58]). If viscous effects are so small that they can be neglected, we obtain the Helmholtz equation. We now give a brief derivation of the wave equation and Helmholtz equation for an inviscid fluid following mainly the books [64, 65], see also [58].

The continuity equation (conservation of mass) in linear acoustics can be written as

$$\frac{\partial \rho}{\partial \tau} + \nabla \cdot (\rho \boldsymbol{V}) = 0, \tag{2.12}$$

where ρ is the density, τ is time and $\boldsymbol{V}$ is the time-dependent particle velocity vector.

Let now P be the time-dependent pressure that satisfies the state equation $P = P(\rho, S)$ where S denotes the entropy. We assume that the changes for the velocity, pressure, entropy and density around

the equilibrium (static state) are small and the static state values can be written as $\boldsymbol{V}_0 = 0$ and P_0, S_0 and ρ_0 are constant. Then the equation of motion (also known as the linearized Euler equation) can be written as

$$\rho_0 \frac{\partial \boldsymbol{V}}{\partial \tau} = -\nabla P. \tag{2.13}$$

Using the linear material law $P = c^2\rho$, where c is the speed of sound in the continuity equation (2.12), one obtains

$$\frac{1}{c^2}\frac{\partial P}{\partial \tau} + \nabla \cdot (\rho_0 \boldsymbol{V}) = 0. \tag{2.14}$$

In the time-harmonic case, the velocity field is written as $\boldsymbol{V} = \Re\{\boldsymbol{v}\exp(-i\omega\tau)\}$ and the pressure $P = \Re\{p_a \exp(-i\omega\tau)\}$ where the velocity field $\boldsymbol{v}$ and acoustic pressure field p_a are time-independent. Then equations (2.13) and (2.14) can be written as

$$\frac{i\omega}{c^2} p_a = -\nabla \cdot (\rho_0 \boldsymbol{v}), \tag{2.15}$$

$$i\omega\rho_0 \boldsymbol{v} = -\nabla p_a. \tag{2.16}$$

Combining now (2.15) and (2.16), a homogeneous Helmholtz equation is obtained as follows

$$\Delta p_a + \kappa^2 p_a = 0, \tag{2.17}$$

where $\kappa = \omega/c$ is the acoustic wave number.

3 Non-polynomial approximation

This chapter is devoted to a short review of several non-polynomial methods used for the numerical approximation of wave problems. First the main characteristics and applications of non-polynomial methods are discussed. Then the development of these methods is summarized. Emphasizing the physical nature of the non-polynomial methods, the focus is on the basis functions. Hence, the detailed technicalities associated with the mathematical formulation of each method are not considered.

3.1 PARTITION OF UNITY METHOD

The partition of unity finite element method (PUFEM) is due to Melenk and Babuška [24]. The PUFEM uses continuous basis functions and the variational formulation of PUFEM is based on the standard bilinear form of the FEM. To aid the upcoming discussion, we shall write the weak form for the Helmholtz problem (with Neumann boundary condition), for more details see e.g. [24, 58, 64, 66]. Let Ω be a bounded open computational domain with boundary Γ. Then the problem is to find the acoustic pressure p_a such that

$$\Delta p_a + \kappa^2 p_a = 0 \quad \text{in } \Omega, \tag{3.1}$$

$$\frac{\partial p_a}{\partial \boldsymbol{n}} = g \quad \text{on } \Gamma, \tag{3.2}$$

where $\boldsymbol{n}$ is the unit outward normal and g is the source term on the boundary. This problem has a unique solution provided $-\kappa^2$ is not a Neumann eigenvalue of the Laplacian.

In the FEM, the Helmholtz equation (3.1) is multiplied by a test function $v \in H^1(\Omega)$ where this Sobolev space is defined by $H^1(\Omega) = \{v \in L^2(\Omega) \,|\, \|\nabla v\|^2 + \|v\|^2 < \infty\}$ where $\|\cdot\|$ is the L^2

norm. The equation is then integrated over the computational domain Ω and integration by parts can be used to obtain

$$\int_\Omega \nabla p_a \cdot \nabla v \mathrm{d}V - \int_\Omega \kappa^2 p_a v \mathrm{d}V = \int_\Gamma \frac{\partial p_a}{\partial \boldsymbol{n}} v \mathrm{d}A.$$

The boundary condition (3.2) can then be used and the problem becomes: Find the acoustic pressure field $p_a \in H^1(\Omega)$ such that

$$\int_\Omega \nabla p_a \cdot \nabla v \mathrm{d}V - \int_\Omega \kappa^2 p_a v \mathrm{d}V = \int_\Gamma g v \mathrm{d}A,$$

for all $v \in H^1(\Omega)$. This is the weak or variational formulation of the problem. In the FEM, the computational domain is divided into non-overlapping elements meeting at edges and element vertices (commonly called nodes). Then the FEM approximation for the unknown approximate pressure field p_a can be written as

$$p_a^h = \sum_{j=1}^{n_n} \beta_j \phi_j$$

where n_n is the number of nodes, β_j are unknown coefficients and ϕ_j are the piecewise linear nodal basis functions. Test functions are chosen to be $v = \phi_l$.

Unlike the traditional FEM, the PUFEM approximation for an unknown field p_a is constructed so that the piecewise linear polynomial partition of unity basis functions $\{\phi_j\}_{j=1}^{n_n}$ are multiplied by functions N_j satisfying the governing partial differential equation (PDE), i.e.

$$p_a = \sum_{j=1}^{n_n} N_j \phi_j, \tag{3.3}$$

where again ϕ_j are the piecewise linear nodal basis functions, n_n is the number of nodes and N_j is a solution of the governing PDE, see e.g. [24]. The PUFEM was first applied to Laplace's equation and the Helmholtz equation [24] with a basis built from harmonic polynomials or plane waves, respectively. For example, in

the Helmholtz problem plane waves are used so that

$$N_j = \sum_{k=1}^{p_j} A_j^k \exp(i\kappa \boldsymbol{d}_k \cdot \boldsymbol{x}), \tag{3.4}$$

where A_j^k are unknown coefficients, p_j is the number of basis functions[1] on patch j and $\boldsymbol{d}_k = (\cos(\theta_k), \sin(\theta_k))$ is the direction of propagation where $\theta_k = 2\pi k/p_j$, $k = 1, \ldots, p_j$, see e.g. [24,25,67].

An alternative to plane wave functions are the wave-band functions that have been investigated in [68]. The wave-band functions can be written as [68,69]

$$\int_{\theta_k}^{\theta_{k+1}} \exp(i\kappa \boldsymbol{d} \cdot \boldsymbol{x}) \, \mathrm{d}\theta, \tag{3.5}$$

where $\boldsymbol{d} = (\cos(\theta), \sin(\theta))$, $k = 0, \ldots, p-1$ and $\theta_k = \frac{2\pi k - \pi}{p}$ (p is the number of directions). In [68], the accuracy of this approximation and p-version convergence of PUFEM was investigated. It was shown that the accuracy of the wave-band PUFEM is similar to plane wave PUFEM.

Recently [70], the PUFEM has been investigated in 2D acoustic problems with Bessel basis functions. The Bessel basis functions can be written as [70]

$$J_k(\kappa r) e^{ik\theta},$$

where $k = 0, \ldots, p_j - 1$, r and θ are polar coordinates. Numerical tests focused on scattering from a rigid cylinder in an unbounded domain. These results suggest that near the scatterer the plane wave basis functions give better accuracy than Bessel basis and away from the scatterer the Bessel basis gives more accurate solutions than plane waves.

The PUFEM has been successfully used to approximate 2D and 3D time-harmonic problems in acoustics and elasticity, see for instance [24, 25, 67, 71–79]. In [71, 72] square elements were used,

[1] In this thesis p refers to the number of basis functions (since it is common in numerical methods to consider p-convergence) and p_a refers to acoustic pressure.

in [67] quadrilateral elements were used and triangular elements have also been used in the PUFEM, e.g. [80–82]. In the case of jumps in the wave speeds between different subdomains of the computational domain, the continuity conditions can be enforced using Lagrange multipliers, see [83–85].

The PUFEM is a more accurate method (e.g. in terms of the number of degrees of freedom needed for a given accuracy [72]) than the piecewise linear FEM when solving oscillatory problems but it suffers from ill-conditioning when too many plane wave functions are used on a patch [74]. The ill-conditioning is a well-known and common drawback of plane wave methods. A strategy for controlling the ill-conditioning was introduced in [41] where the number of basis functions varies from element to element based on heuristic formulae using local wave number and element size information (cf. equation (5.2)).

Another drawback of PUFEM is the requirement to use high-order numerical quadratures (integration) in the assembly of system matrices [67]. This has been the focus of much recent work and many improvements are available: nearly analytical integration [73], fast integration [86] and analytical integration [87,88] techniques.

Beyond acoustic and elasticity problems, the PUFEM has been studied to solve 1D convection/diffusion problems in [89] and time dependent diffusion problems in [90]. In [89] the performance of the PUFEM with exponential and polynomial local bases was investigated. The results show that the exponential basis functions give more accurate results than polynomial based schemes.

The PUFEM belongs to the class of generalized finite element methods (GFEM). The GFEM was introduced by Strouboulis, Babuška and Copps in [30] and uses the bilinear form of the FEM. However, in the GFEM the approximation includes the PUFEM part and polynomial FEM part so that

$$u = \sum_{j=1}^{n_n} N_j \phi_j + \sum_{k=1}^{n_n} \beta_k \phi_k, \tag{3.6}$$

where the second term on the right hand side is the traditional FEM part (ϕ is a polynomial basis function) and the first term is the PUFEM. Obviously, when the second sum in (3.6) is zero the PUFEM is recovered. In [91], the PUFEM and Trefftz methods are called "knowledge-based FEM" because they use functions which satisfy the PDE.

A similar method to PUFEM is the "finite ray element method" by Mayer and Mandel [26]. In [26] the Galerkin FEM and the first order system of least squares (FOSLS) with the plane wave basis functions were investigated. Later, the idea of PUFEM with local plane wave basis has also been applied to BEM [29]. The BEM with plane waves has been successfully used to model wave problems in acoustics and elasticity, see for example, [29, 77, 92–95]. Furthermore, theoretical studies of the boundary integral method (related to BEM with plane waves) were presented in [27, 28] where the method was termed microlocal discretization.

3.2 LEAST-SQUARES METHOD

The non-polynomial least-squares method (LSM) was introduced in the late 90s by Stojek [38] and Monk and Wang [39]. The LSM uses a finite element mesh and it belongs to the class of Trefftz methods. In the LSM [39] weak continuity over the element edges is enforced by minimizing a quadratic functional defined on element edges and on the boundary. The LSM can also be derived via a DG scheme with different choices of numerical fluxes [96].

In [38], T-elements (Trefftz elements) consisting of Bessel and Hankel basis functions that satisfy the Helmholtz equation were used. Numerical tests included p-convergence and h-convergence studies. In [39], an error estimate for the LSM was derived and both plane waves and Bessel basis functions were investigated for 2D acoustic problems. The results suggest that plane waves are more practical to use than the Bessel functions (in the case of Bessel functions quadrature needs to be used whereas using plane waves integrals can be analytically derived). In the LSM [39], the approxi-

mation for the solution is written as

$$u = \sum_{K_k} \sum_{p=0}^{N_p} a_p^{K_k} \phi_p^{K_k},$$

where K_k is an element in the domain Ω, $a_p^{K_k}$ are the unknowns and $\{\phi^{K_k}\}_{p=0}^{N_p}$ are functions satisfying the PDE locally on K_k, for example, plane wave or Bessel functions.

The LSM has been extended to diffraction problems using T-elements that satisfy the Sommerfeld radiation condition and in the same study vertex singularities were also approximated with T-elements [97]. Barnett and Betcke [42] developed a non-polynomial FEM to tackle singular solutions using fractional order Fourier-Bessel functions in acoustic problems. This method belongs to the general class of LSM. Motivated by the work of [39, 42], fractional order Fourier-Bessel functions were used in the LSM for polygonal-line grating problems and an L^2 error estimate for the method was provided in [98].

3.3 VARIATIONAL THEORY OF COMPLEX RAYS

The variational theory of complex rays (VTCR) was first implemented for elasticity problems [36] in the mid 90s. The variational formulation of the VTCR is based on satisfying the boundary conditions and interface conditions and leads to a non-symmetric variational formulation. The VTCR uses a finite element mesh and integrals in the variational form are then defined along the boundaries and element interfaces.

In elasticity [99, 100] use of VTCR over a range of frequencies is investigated and in [101] the VTCR was extended to 3D curved shells. For elasticity problems, the VTCR uses plane waves (cf. (3.15)), evanescent corner waves and evanescent edge waves basis functions. These are termed "complex rays". For example, following [56, 100], for the dynamic Kirchhoff plate equation (2.11)

without damping, an edge mode could be written as

$$u_e \exp(\sqrt{\omega} P_n \boldsymbol{n} \cdot \boldsymbol{x} + i\sqrt{\omega} P_s \boldsymbol{s} \cdot \boldsymbol{x}), \tag{3.7}$$

where u_e is an unknown amplitude, $\boldsymbol{n}$ and $\boldsymbol{s}$ refer to the normal vector and tangential vector, respectively on the edge and

$$P_n = r\sqrt{1 + \sin^2(\theta)} \quad \text{and} \quad P_t = r\sin(\theta),$$

where r is a radius and θ is an angle. The corner modes can be written, see again [56, 100], as

$$u_c \exp(\sqrt{\omega} \boldsymbol{P} \cdot \boldsymbol{x}), \tag{3.8}$$

where u_c is an amplitude, $(\boldsymbol{P} \cdot \boldsymbol{P})^2 = r^4$ and $r^4 = 12\rho(1-\nu^2)/(t^2 E)$. Both edge mode (3.7) and corner mode (3.8) satisfy the dynamic Kirchhoff's equation ($\Delta^2 u - \kappa_b^4 u = 0$ where $\kappa_b^4 = (\rho t \omega^2 / D)$).

Recently, the VTCR has been extended to wave modeling problems in time-harmonic acoustics. In 2008, the VTCR was introduced for the 2D time-harmonic acoustic problems [69] using the plane wave and wave band (cf. (3.5)) basis functions. Numerical tests include modeling car cavity noise, scattering and acoustic cavity problem in an L-shaped domain. The results show that the VTCR error converges more rapidly as a function of the number of degrees of freedom than linear or quadratic finite elements (using square elements).

Basis functions obtained using Fourier series were used in [102, 103] for solving 2D acoustic wave problems. The Fourier series functions in [102, 103] are defined by

$$\int_{-\pi}^{\pi} \exp(i n_e \theta) \exp(i\kappa \boldsymbol{d} \cdot \boldsymbol{x}) \, \mathrm{d}\theta, \tag{3.9}$$

where $n_e = -N_E, \ldots, N_E$, $n_e \in \mathbb{N}$. Fourier series basis functions are related via the Jacobi-Anger expansion to Bessel functions cf. [103, 104]. In [102] the results show that the Fourier based VTCR has slightly smaller errors than the wave band based VTCR. Furthermore, the condition number was slightly greater using wave bands than Fourier series.

Unbounded 2D acoustic problems were considered in [103] so that in the unbounded part of the domain the basis functions were of the form

$$\exp(in_e\theta)H^{(2)}_{|n_e|}(\kappa r), \tag{3.10}$$

where $n_e = -N_E, \ldots, N_E$, $H^{(2)}_{|n_e|}(\cdot)$ is the Hankel function of second kind and order $|n_e|$ and r is the distance apart of source and measurement points. These basis functions satisfy the Sommerfeld radiation condition. In bounded cavities Fourier basis functions were used. It was shown that the convergence rate of the VTCR is better than that of a fixed order BEM. Spherical harmonics expansion (Herglotz) wave functions were used in 3D acoustic problems in [104]. A strategy beyond the static choice of different basis function is the adaptive approach of choosing the number of basis functions based on estimates of local error. The adaptive version of the VTCR was introduced in [105].

A new technique for solving time domain elasticity problems was introduced in [106, 107]. The FEM was used at low frequencies and the VTCR at medium frequencies and then the inverse Fourier transform (IFT) was computed to obtain a time dependent solution. It was suggested that this is a more efficient strategy than computation in the time domain only. In addition to elasticity and acoustic problems, the VTCR with exponential functions has been successfully used in 2D advection-diffusion problems at high Péclet numbers with constant parameters in [108], cf. [109]. Both *h*- and *p*-convergences was investigated.

3.4 WAVE BASED METHOD

Unlike the FEM, where the computational domain is divided into a large number of small elements, the computational domain of the wave based method (WBM), is split into large convex subdomains [37]. The WBM uses a weighted residual formulation defined on the boundary and along the subdomain interfaces and its basis functions are chosen to be of Trefftz type [37]. As discussed

in [110], the WBM is similar in spirit to the LSM but differs in the choice of basis functions and variational form.

In [37,111,112], the WBM has been used to solve vibro-acoustics and generally problems that arise from automotive engineering applications. The WBM has been successfully applied to both homogeneous and inhomogeneous PDEs. In the case of inhomogeneous PDEs, a particular solution is taken into account in the WBM approximation. Considering the inhomogeneous case with a point source, see [37,113], let Ω denote the domain, then the field u is approximated (herein for the sake of simplicity on the whole domain Ω) by $\tilde{u}$ given as follows

$$u \approx \tilde{u} = \sum_{k=1}^{N_k} u_k \Phi_k + \hat{u}_f, \tag{3.11}$$

where N_k is the number of wave functions, Φ_k are the wave functions and $\hat{u}_f$ is the particular solution of the inhomogeneous PDE. It is suggested that for 2D acoustic problems, two sets of functions should be considered (r and s sets) as follows

$$\sum_{k=1}^{N_k} u_k \Phi_k = \sum_{r=1}^{N_r} u_r \Phi_r + \sum_{s=1}^{N_s} u_s \Phi_s, \tag{3.12}$$

where $N_k = N_r + N_s$ is the number of wave functions [37], see also [110]. The wave functions in (3.12), that satisfy the Helmholtz equation, are defined as follows

$$\Phi_r = \cos(\kappa_{xr} x) \exp(-i\kappa_{yr} y), \tag{3.13}$$

$$\Phi_s = \exp(-i\kappa_{xs} x) \cos(\kappa_{ys} y). \tag{3.14}$$

The wave number components in wave functions (3.13) and (3.14) are [37]

$$(\kappa_{xr}, \kappa_{yr}) = \left(\frac{\tilde{r}_1 \pi}{L_x}, \pm \sqrt{\kappa^2 - (\kappa_{xr})^2} \right),$$

$$(\kappa_{xs}, \kappa_{ys}) = \left(\pm \sqrt{\kappa^2 - (\kappa_{ys})^2}, \frac{\tilde{s}_1 \pi}{L_y} \right),$$

where $\kappa_{xr}^2 + \kappa_{yr}^2 = \kappa_{xs}^2 + \kappa_{ys}^2 = \kappa^2$, $\tilde{r}_1 = 0, 1, \ldots$, $\tilde{s}_1 = 0, 1, \ldots$. The parameters L_x and L_y give the dimensions of the smallest rectangular domain (bounding the cavity).

The convexity of the domain is a sufficient condition for the convergence of the WBM and non-convex domains are split into convex subdomains [37]. However, the convexity assumption sets a limit for the use of WBM decreasing its geometric flexibility. Hence, the WBM is coupled with the FEM, in order to cope with complex domains in acoustics [114, 115]. The WBM is used in simpler and larger regions and FEM elements are used in order to handle complex shapes of the domain. This approach has better convergence and is more efficient than using the FEM alone. The hybrid FEM-WBM was applied for 2D structural-acoustics [116], for 3D vibro-acoustics [117] and 3D acoustics [118]. Furthermore, the WBM has been coupled with the statistical energy analysis (SEA) approach in vibro-acoustics in [119]. The WBM was used in the acoustic domain and SEA was used in the (plate) elasticity domain.

Unbounded (fluid) problems in 2D vibro-acoustics were considered in [120]. In the unbounded fluid, functions which satisfy the Sommerfeld radiation condition were used. The WBM has been extended to unbounded 2D scattering acoustics [113]. In addition, 3D semi-infinite acoustics radiation problems have been considered in [121] and unbounded 3D problems have been investigated in [122].

The WBM has been applied to Kirchhoff thin elastic plate problems [123] where the clamped, free and simply supported plate boundary conditions were used. However, it was observed that the stress singularities hamper the accuracy of WBM. For corner stress singularities a new approach was introduced using specially chosen corner functions [43]. In particular, the corner functions are derived as the solutions of an infinite wedge domain problem. These new corner functions improve the accuracy of the WBM in the presence of corner singularities. This approach, introduced in [43], has been adapted to singular problems in 2D elasticity [44], in acoustics [45] and in poroelasticity [46].

Finally, the WBM has also been used to approximate the poroelastic Biot models in [46, 124]. The Biot equation was written as three decoupled Helmholtz equations in order to derive the wave functions used in the WBM.

3.5 DISCONTINUOUS GALERKIN METHODS

The discontinuous Galerkin methods (DGM) include a wide class of finite element type methods. Unlike the FEM, the basis functions in the DGM are discontinuous and the required continuity across the element interfaces is enforced weakly using numerical fluxes or Lagrange multipliers. We next give an overview of non-polynomial discontinuous Galerkin methods including the ultra weak variational formulation, the discontinuous Galerkin method (with and without Lagrange multipliers) and the discontinuous enrichment method.

3.5.1 The ultra weak variational formulation

The ultra weak variational formulation (UWVF) [34, 35, 125] is a method tailored to linear elliptic wave problems. The computational domain is divided into non-overlapping finite elements. In the original UWVF coupling between elements is based on the "Isometry lemma". The UWVF then gives a sesquilinear form and the integrals are defined along the boundary and element edges in 2D (or faces in 3D). Because local solutions are used on each element, the UWVF belongs to the class of Trefftz methods, see e.g. [126]. On the other hand, the UWVF can be derived via a DG scheme [51, 127, 128] using different choices of fluxes.

The traditional acoustic UWVF uses plane wave basis functions [35, 125] , i.e.

$$\varphi_{k,\ell} = \begin{cases} \exp\left(i\overline{\kappa} n_k \boldsymbol{d}_{k,\ell} \cdot \boldsymbol{x}\right) & \text{in an element } K_k \\ 0 & \text{elsewhere} \end{cases} \tag{3.15}$$

where overline denotes complex conjugation, K_k is the element in the domain $\Omega = \cup_{k=1}^{N} K_k$, n_k is the index of refraction in K_k and the

direction of propagation is given by

$$\boldsymbol{d}_{k,\ell} = \left(\cos\left(2\pi\frac{\ell-1}{p_k}\right), \sin\left(2\pi\frac{\ell-1}{p_k}\right)\right), \quad 1 \leq \ell \leq p_k,$$

where p_k is the number of basis functions. It can be seen that the plane wave basis (3.15) satisfies the adjoint Helmholtz equation $\Delta\overline{\varphi} + n^2\kappa^2\overline{\varphi} = 0$. However, any other basis functions that satisfy the adjoint of the governing equation can be used in the UWVF. For example, wave-band functions (3.5) and the basis functions in (3.10) could also be used in the UWVF (but have not been to date).

The UWVF with Bessel basis functions was considered for time-harmonic electromagnetic and elastic wave equations in [129]. In the article **I**, Bessel functions were investigated in the acoustic UWVF. The UWVF with generalized plane waves is introduced in order to handle (smoothly) varying coefficients in the governing PDE in [130]. Recently, the use of Hankel function basis functions in the UWVF has been investigated in [131].

Originally [35, 125], the acoustic UWVF used a fixed number of basis functions per element. However, this is neither the most efficient nor robust strategy when the element size is not constant in the computational domain. Ill-conditioning may occur if too many plane waves are used in a small element. The UWVF was improved by varying the number of basis functions from element to element (based on the condition number) to improve the stability of the method [132]. In [41] the number of basis functions per element was derived efficiently based on a simple ad hoc formula using information on the local wave number and element size (see equation (5.2) below).

Another strategy to reduce the computational burden and memory requirements associated with unbounded problems was discussed in [133, 134] where the UWVF was coupled with the fast multipole method (FMM) and multilevel fast multipole method (MFMM). Numerical tests focused on electromagnetic scattering problems and the results showed that the use of FMM and MFMM reduces memory requirements.

In [41,126] it was shown that the performance of the UWVF was hampered in the case of problems with singular solutions. The results suggest that mesh refinement near the singularity instead of increasing the number of basis functions improves the accuracy. In practice, away from the singularity, it is generally more efficient to increase the number of basis functions rather than refine the mesh. Based on the numerical results in [41, 126], the plane wave basis does not approximate singular solutions efficiently. In a different approach to improving the accuracy for singular problems, the acoustic UWVF was coupled with classical Raviart-Thomas finite elements in [135]. In the original publication **I**, fractional order Bessel basis functions were used to improve the accuracy of the UWVF when singular solution is present.

The UWVF was examined for 2D linear elasticity in [48]. The (P-wave and S-wave) basis functions used in the 2D linear elasticity problem were obtained using the Helmholtz decomposition. Hence, the P-wave and S-wave basis functions satisfy vectorial Helmholtz equations. Numerical tests included the investigation of the effects of varying the number of P-wave and S-wave basis functions and also the modeling of Rayleigh waves that decay rapidly away from a free surface. It was observed [48] that it is more challenging to approximate rapidly decaying Rayleigh waves than propagating plane waves using the UWVF. In addition, numerical results suggest that the "optimal" ratio for P- and S-wave basis functions is roughly the ratio of P-wave number to S-wave number. In 2008 [136], the UWVF was extended to 2D fluid-solid problems. Subsequently, the UWVF was applied extensively to medical ultrasound problems [48,132,137,138].

In addition to ultrasound problems, the UWVF has been successfully applied to model the head-related transfer function (HRTF) on audible frequencies [139] and modeling of porous traffic noise barriers in [140]. Modeling of light emitting diode (LED) in optoelectronics was considered in [141]. The UWVF has also been used to investigate inverse problems arising in electromagnetism [142,143], fluid-solid interface problems [144] and in particular, ul-

trasound control problems [145–148].

The UWVF has also been investigated for different scattering problems where the unbounded computational domain is truncated by using a suitable absorbing boundary condition or artificial layer. The perfectly matched layer (PML) was adapted to 3D acoustic UWVF in [137]. The numerical results show that the UWVF with PML had smaller errors compared to the case when a simple absorbing boundary condition (ABC) is used. The low order ABC and PML were compared in 3D electromagnetism in [127]. The electromagnetic UWVF with PML has also been extended to 2D anisotropic problems in [149].

More details concerning the UWVF such as its derivation via DG schemes, error estimates and new choices for basis functions will be given in the next chapter.

3.5.2 Discontinuous Galerkin method

The UWVF can be derived as an upwind DG scheme [51, 127, 128] and therefore the UWVF shares similar properties with the DGM. Once the UWVF has been shown to be an upwind DGM [51, 127, 128], the error analysis of the traditional DGM can be used to obtain results for the UWVF as well. We now focus on the non-polynomial discontinuous Galerkin methods without Lagrange multipliers and enforce weak continuity across element interfaces using numerical fluxes.

It was shown in [150] that the acoustic DGM includes the UWVF with a suitable choice of numerical fluxes (cf. below the elastic UWVF fluxes in (4.6) and (4.7)). The theoretical properties of the general DGM (and also of the UWVF) have been investigated recently very actively by Gittelson, Hiptmair, Moiola and Perugia [53, 150–155].

For the acoustic UWVF a global error estimate was derived in [51]. Error estimates for the acoustic DGM h-version were developed in [150] and for the p-version in [53]. The theory of the DGM (as well as the UWVF) in acoustics has been further extended

by taking into account the approximation properties of plane waves [151,152]. An error estimate for the p-version of DGM for Maxwell's equation was developed in [153]. A recent study [154] reported the dispersion analysis of the acoustic DGM (as well as the UWVF) with numerical results. Results suggest that in 2D relative dispersion grows as $\mathcal{O}(\kappa^{2q_p})$ for $\kappa \to 0$ where $q_p := \lfloor \frac{p-1}{2} \rfloor$ (p is the number of basis functions and $\lfloor \cdot \rfloor$ is the floor function). In addition, in [155] the error analysis of a numerical scheme for approximating scattering by a sound soft scatterer with locally refined meshes was considered. The DGM with plane wave basis is sometimes called the Trefftz discontinuous Galerkin method (TDG method) [151, 155].

In [128], the DGM (with numerical fluxes) was studied for 2D aero-acoustics and the UWVF was shown to be a special form of the DGM (concurrently with [127]). Numerical tests include an investigation of the condition number and convergence studies for aero-acoustic problems. In the case of an inhomogeneous PDE, a modified variational formulation was presented (the volume source was imposed on element interfaces). This improves the robustness of the DGM.

The DGM and the local discontinuous Galerkin method (LDGM) with the non-polynomial basis functions for time-dependent and steady-state problems were introduced by Yuan and Shu [156]. Their formulations of DGM and LDGM followed from [157, 158] but they chose exponential and trigonometric basis functions. Numerical tests included 1D and 2D problems with hyperbolic, parabolic and elliptic partial differential equations such as Burgers equation, boundary layer problems and the Helmholtz equation. The DGM with non-polynomial approximation basis has been used to approximate 1D elliptic partial differential equations in [159] and in particular for 1D Schrödinger equation in [160]. The latest research in [161] investigates the use of Trefftz basis functions in the DGM and gives results for the time-dependent 1D Maxwell equation. The performance was compared with the finite difference time domain (FDTD) method and DGM with leapfrog time stepping.

3.5.3 Discontinuous enrichment method

In the previous section, the weak continuity between elements was enforced using numerical fluxes. In the discontinuous enrichment method (DEM), weak continuity across the element edges (or faces) is enforced via Lagrange multipliers. Although, the variational formulation of DEM differs from the FEM, the DEM uses finite element meshes (commonly quadrilaterals and hexahedra).

In the DEM, the piecewise polynomial basis is enriched by functions (generally plane waves or exponentials) that satisfy the governing homogeneous PDE. Unlike PUFEM, the enriched basis is added to the polynomial part so that

$$u = u^P + u^E, \tag{3.16}$$

where u^P is the polynomial part (cf. FEM) and u^E is the enriched part (e.g. plane waves) [40]. Clearly, the representation of the solution in (3.16) is the same as that used in the GFEM (3.6). Without the polynomial part u^P, the DEM is the DGM with Lagrange multipliers [162, 163]. Therefore, we include the DGM with Lagrange multipliers under the DEM category.

The DEM was first introduced to solve acoustic and advection-diffusion problems [40]. The DEM/DGM has been successfully used in 2D and 3D acoustic problems in [162–166]. In the acoustic case, error estimates and the well-posedness of the DGM with Lagrange multipliers was analyzed in [167]. In 2006, Gabard [168] extended the DGM for displacement based acoustics (that is the vector valued Helmholtz equation). The results included comparisons of DGM and the mixed finite element method. The DGM needs less degrees of freedom to have more accurate results than the mixed finite element method. The DEM was introduced for 2D elasticity problems in [169] where both DEM and DGM elements were used and the results were compared with FEM. The dispersion analysis of the DEM has been investigated in [162, 170] for acoustics and in elasticity in [171].

In acoustics [162–166] and elasticity [169] plane waves have been used in the enrichment function u^E. However, as shown in [47] it is

challenging to capture rapidly decaying waves using plane waves. Hence, the plane wave and new evanescent wave basis functions were used [49,50] for fluid-fluid and fluid-solid interface problems in cases when the rapidly decaying evanescent fields were present (when total internal reflection occurs). The new evanescent wave enrichment in addition to plane waves improved the accuracy of DEM. In addition, in [49,50] non-matching meshes with quadrilateral and hexahedral elements were used.

Traditionally the DEM uses quadrilateral elements in 2D [40] and hexahedral elements in 3D [166]. However, Grosu and Harari implemented the DEM with new triangular 2D elements [172] and new 3D tetrahedral elements (in addition to new hexahedral elements) [173]. Both dispersion and conditioning issues were investigated. The results in [172,173] show that the new elements in DEM have little dispersion at higher order.

The DEM was studied for the Kirchhoff plate problem in [174]. Numerical tests included homogeneous and inhomogeneous problems using DEM and DGM elements. The DEM was formulated so that free, clamped and simply supported plate boundary conditions can be imposed. In addition, additional Lagrange multipliers were used at element corners. The non-polynomial basis was chosen to be plane wave and evanescent wave functions.

Beyond acoustics and elasticity, the DEM for the 1D advection-diffusion problem has been investigated in [40,162]. In [109], the DEM was extended to 2D advection-diffusion problems with high Péclet number (advection dominated) with constant parameters and structured meshes. In [175], the DEM for diffusion-advection equation were considered with unstructured meshes and in [176] with non-constant parameters in the advection-diffusion equation. In these problems the enrichment functions are exponentials (that satisfy the homogeneous advection-diffusion equation). Recently, the DGM has been applied to 3D advection-diffusion problems [177]. An unusual application was introduced in [178] where the DEM was applied to solve 3D Bose-Einstein condensation problems (Gross-Pitaevskii equation). In this study, the enrichment functions

were plane waves.

Different variational formulations for the DGM have been investigated in [179–182]. A very similar method to DGM with Lagrange multipliers is a mixed hybrid formulation by Gillman, Djellouli and Amara [179]. Their method uses Lagrange multipliers and oscillated polynomials (the shape functions are of the form $\exp(-i\kappa h_l \Lambda_l)$ where h_l is the length of the element edge, Λ_l is the Lagrange polynomial on the vertex and $1 \leq l \leq 3$ (triangular element)). In [181] the modified discontinuous Galerkin method (mDGM) with discontinuous Lagrange multipliers was developed aiming to a more robust method. The mDGM was improved further in [182] and is called the stable discontinuous Galerkin method (SDGM). The SDGM shares similarities with the LSM and the DGM (with Lagrange multipliers). Both mDGM and SDGM (or improved modified discontinuous Galerkin method (imDGM)) were first introduced in the Ph.D. thesis by Grigoroscuta-Strugaru [180].

3.6 COMPARISON STUDIES

In general, the performance of new modeling methods is usually compared to traditional low order FEM or BEM approximations that are computed using commercial software, for example, Nastran®, Ansys® or Comsol Multiphysics®. However, due to the popularity and attractive features of non-polynomial methods, some of these methods have also been compared with each other.

Equations (3.4)-(3.16) show that the methods share similar strategies in choosing the non-polynomial approximation functions but the methods use different variational formulations.

In 2D acoustics, the LSM and the UWVF were compared in [126], the UWVF, DGM (without Lagrange multipliers) and LSM in [96] and the UWVF and PUFEM were investigated in [41]. These studies show that all methods perform similarly at lower frequencies but at higher frequencies the UWVF and DGM perform better (having better accuracy). The recent study in [183] compared the performances of the DEM, UWVF and PUFEM at mid-frequencies.

The comparison highlights the DEM and investigates error convergence with respect to the number of degrees of freedom, the condition numbers, the number of non-zeros in LU decomposition and time for the LU decomposition of the global matrix. The results show more differences between the UWVF and PUFEM than found in the article by Huttunen et al. [41].

The difference between the DGM (without Lagrange multipliers) and UWVF is in the definitions of fluxes [150]. The *h*-version of the DGM and UWVF were investigated in [150] for 2D acoustics. The numerical results showed similar behavior for both methods, and the choice of numerical flux does not drastically affect the accuracy. In [53], the UWVF and the DGM were compared in 2D acoustic problems increasing the number of basis functions per elemenet (*p*-version). The results showed that both methods behave rather similarly from the point of view of convergence. Generally, the DGM has slightly smaller errors compared to the UWVF. The (theoretical) stability properties of PUFEM, LSM, UWVF and DGM are reviewed in [184].

In [162] condition number comparisons between the DEM and PUFEM were investigated and the results showed that the DEM has significantly smaller condition numbers. In [81] the performance of the PUFEM in 1D was compared with DEM (and GFEM). The results show that all methods perform similarly. For 2D duct flow (rigid walls) the PUFEM was compared with FEM. The PUFEM error converges more rapidly as a function of the number of degrees of freedom per square wavelength than the low order FEM.

The mDGM and DGM (with Lagrange multipliers) were compared in [181] and the results suggested the mDGM to be a more accurate and stable method. Furthermore, the SDGM, LSM and DGM (with Lagrange multipliers) were investigated in [182] and the results suggest that the SDGM is more robust than the DGM and it has better convergence behavior than the LSM.

The weighted variational formulation (WVF) was developed in [185] and is similar to the VTCR. The performance of the WVF was compared with the UWVF and the VTCR. The results suggest that

the WVF performed better than the VTCR but similar to the UWVF.

Even though there have been several comparison studies it is difficult to declare a clear winner amongst the non-polynomial methods because different model problems have been considered.

3.7 SUMMARY OF NON-POLYNOMIAL METHODS

An overview of non-polynomial methods is given in Table 3.1 that consists mainly of journal articles. In Table 3.1, the DEM category includes the DGM with Lagrange multipliers but the UWVF and the DGM (without Lagrange multipliers) are shown separately.

Table 3.1: Summary of non-polynomial methods.

Method	Authors/ref	year	field	novelty
DEM	Farhat, Harari & Franca [40]	2001	acoustics/advection-diffusion	the DEM introduced and compared with FEM and PUFEM
	Farhat, Harari & Hetmaniuk [162]	2003	acoustics	mid-frequency problems, dispersion analysis, different DGM elements
	Farhat, Harari & Hetmaniuk [163]	2003	acoustics/advection-diffusion	the DEM used in 2D acoustics and 1D inhomogeneous advection-diffusion equation, DEM/DGM elements
	Farhat, Wiedemann-Goiran & Tezaur [164]	2004	acoustics	DGM using unstructured and structured meshes
	Farhat, Tezaur & Wiedemann-Goiran [165]	2004	acoustics	higher-order (quadrilateral) elements used in DGM
	Harari, Tezaur & Farhat [170]	2006	acoustics	dispersion analysis, comparison with DEM, biquadratic Galerkin and GLS methods
	Tezaur & Farhat [166]	2006	acoustics	the DGM used in 3D acoustic simulations
	Zhang, Tezaur & Farhat [169]	2006	elasticity	2D elasticity, plane wave propagation, DEM and DGM elements
	Gabard [168]	2006	acoustics	displacement based Helmholtz equation considered
	Tezaur, Zhang & Farhat [49]	2008	acoustics-elasticity	evanescent wave basis in DEM introduced for 2D fluid-fluid and fluid-solid problems, matching and non-matching meshes used
	Massimi, Tezaur & Farhat [50]	2008	acoustics-elasticity	evanescent wave basis in DEM introduced for 3D fluid-fluid and fluid-solid problems, matching and non-matching meshes used
	Grosu & Harari [172]	2009	acoustics	2D quadrilateral and triangular DEM elements
	Kalashnikova, Farhat & Tezaur [109]	2009	advection-diffusion	2D advection-diffusion equation at high Péclet numbers (advection dominated) with constant parameters
	Amara, Djellouli & Farhat [167]	2009	acoustics	convergence analysis of the DGM, a priori error estimate for the R-4-1 element, well-posedness of DGM
	Farhat, Tezaur & Toivanen [186]	2009	acoustics	an iterative domain decomposition (DD) method used with DGM
	Petersen, Farhat & Tezaur [187]	2009	acoustics	the DGM was developed to 1D time-dependent wave equation
	Grosu & Harari [173]	2009	acoustics	3D hexahedral and tetrahedral DEM elements
	Harari & Makmel [171]	2009	elasticity	dispersion analysis of the DEM in the plane-strain elasticity
	Massimi, Tezaur & Farhat [174]	2010	plate elasticity	the DEM introduced to plate vibration problems
	Farhat, Kalashnikova & Tezaur [175]	2010	advection-diffusion	unstructured meshes at high Péclet numbers
	Gabard, Gamallo & Huttunen [96]	2011	acoustics	comparison studies of the DGM, UWVF and LSM
	Kalashnikova, Tezaur & Farhat [176]	2011	advection-diffusion	variable (advection field) coefficient, high Péclet numbers in 2D
	Grigoroscuta-Strugaru et al. [181]	2012	acoustics	mDGM, more stable than DGM, two step strategy
	Amara et al. [182]	2012	acoustics	SDGM, two step strategy, more stable than mDGM
	Wang et al. [183]	2012	acoustics	comparison of DEM, UWVF and PUFEM
	Farhat & Toivanen [178]	2012	quantum mechanics	the DEM introduced for Bose-Einstein condensation problems
	Brogniez, Farhat & Hachem [177]	2013	advection-diffusion	DGM used for solving 3D advection-diffusion problems, unstructured meshes
DGM	Yuan & Shu	2006	multi-field	exponential and trigonometric functions, time-dependent and steady-state problems, DGM/LDGM
	Gabard [128]	2007	aero-acoustics	the connection between the UWVF and an upwind DGM

Table 3.1 – *(Continued) Summary of non-polynomial methods.*

Method	Authors/ref	year	field	novelty
	Yuan & Shu [159]	2008	2nd order PDE	DGM with non-polynomial approximation spaces, error estimate, 1D numerical tests
	Wang & Shu [160]	2009	quantum mechanics	DGM used to solve 1D Shrödinger equation
	Gittelson, Hiptmair & Perugia [150]	2009	acoustics	*h*-version of the error estimates of the DGM
	Hiptmair, Moiola & Perugia [53]	2011	acoustics	error analysis of the *p*-version of DGM
	Betcke & Phillips [188]	2012	acoustics	DGM with dominant wave directions
	Gittelson & Hiptmair [154]	2012	acoustics	dispersion analysis of the DGMs and the UWVF of 2D Helmholtz equation
	Hiptmair et al. [189]	2012	Laplacian equation	error estimates, *hp*-version, harmonic polynomials
	Hiptmair, Moiola & Perugia [153]	2013	electromagnetism	error analysis, *p*-version (see also [53])
	Hiptmair, Moiola & Perugia [155]	2013	acoustics	error analysis, locally refined elements, sound soft scatterer
	Kretzschmar et al. [161]	2013	electrodynamics	the Trefftz type basis used in time-dependent electrodynamics
LSM	Stojek [38]	1998	acoustics	T-elements, *p*- and *h*-convergence studies
	Monk & Wang [39]	1999	acoustics	Bessel and plane wave basis
	Stojek, Markiewicz & Mahrenholtz [97]	2000	acoustics	T-elements, diffraction problems
	Barnett & Betcke [42]	2010	acoustics	fractional Fourier-Bessel functions used, few elements
	Zheng, Ma & Zhang [98]	2013	acoustics	L^2 error estimate, fractional Fourier-Bessel functions
PUFEM	Melenk [24]	1995	acoustics	the PUFEM developed with theoretical error estimates
	Melenk & Babuška [25]	1996	acoustics	theory introduced, including 1D and 2D numerical results
	Melenk & Babuška [71]	1997	acoustics/Laplace	approximation properties of harmonic and generalized harmonic polynomials, theory of PUFEM presented
	Babuška & Melenk [72]	1997	acoustics	convergence proof, a posteriori error estimates
	Babuška & Zhang [190]	1998	beam elasticity	mathematical analysis, Timoshenko beam, error estimates, shows that the PUFEM is free of locking and no numerical boundary layer
	Laghrouche & Bettess [67]	2000	acoustics	quadrilateral elements, investigations of the number of integration points
	Ortiz & Sanchez [73]	2001	acoustics	integration method proposed (nearly analytical) and generalized conjugate gradient method used
	Laghrouche, Bettess & Astley [74]	2002	acoustics	the PUFEM tested to 2D scattering problems integration and ill-conditioning issues considered
	Sugimoto & Bettess [191]	2003	acoustics	hybrid method, coupling of PUFEM and wave infinite elements
	Bettess et al. [80]	2003	acoustics	semi-analytical integration
	Laghrouche et al. [76]	2003	acoustics	the PUFEM introduced to 3D acoustic scattering problems
	Munts, Hulshoff & de Borst [89]	2003	diffusion/convection	convection and diffusion problems in 1D, comparison of the exponential enrichment and the polynomial enrichment
	Perrey-Debain et al. [77]	2004	acoustics	PUFEM and plane wave based BEM used in 3D scattering problems
	Ortiz [192]	2004	acoustics	PUFEM used in diffraction and refraction problems
	Astley & Gamallo [81]	2005	flow acoustics	PUFEM examined in flow acoustics (uniform flows)
	Li & Zhou [75]	2005	elasticity	PUFEM tested in elasticity, one wave number were considered

Table 3.1 – *(Continued) Summary of non-polynomial methods.*

Method	Authors/ref	year	field	novelty
	Laghrouche et al. [83]	2005	acoustics	Lagrange multipliers to enforce continuity between media
	De Bel, Villon & Bouillard [78]	2005	elasticity	plate elasticity, PUFEM with exact basis vs. polynomial basis
	Gamallo & Astley [82]	2006	flow acoustics	PUFEM studied in short wavelength flow acoustics (in particular, non-uniform potential flows)
	Strouboulis & Hidajat [68]	2006	acoustics	comparison of plane wave and wave-band bases with PUFEM
	Kechroud, Soulaimani & Antoine [193]	2009	acoustics	Padé type boundary condition, conjugated and unconjugated PUFEM
	El Kacimi & Laghrouche [79]	2009	elasticity	the PUFEM introduced to 2D elastic scattering problems
	El Kacimi & Laghrouche [86]	2010	elasticity	a fast integration approach introduced, unstructured meshes, integrals computed in closed form
	El Kacimi & Laghrouche [194]	2010	elasticity	two different plane wave element types: 4- and 9-noded
	Laghrouche, El-Kacimi & Trevelyan [195]	2010	acoustics	PUFEM with different non-reflecting boundary conditions
	Mohamed, Laghrouche & El-Kacimi [196]	2010	acoustics	convergence studies, scattering problems (multiple scatterers)
	Laghrouche & Mohamed [70]	2010	acoustics	PUFEM with Bessel basis functions
	El Kacimi & Laghrouche [197]	2011	elasticity	PUFEM investigated using Generalized Minimum RESidual method (GMRES) with Incomplete Lower-Upper (ILU) preconditioner based on wavelets, Gibbs reordering algorithm applied
	Laghrouche, El-Kacimi & Trevelyan [84]	2012	elasticity	layered media (solid-solid), Lagrange multipliers
	Essahbi et al. [198]	2011	vibro-acoustics	plane wave based method (PWBM) applied to vibro-acoustics
	Essahbi et al. [87]	2012	acoustics	plane wave based finite element method examined in 2D acoustics, analytical integration technique introduced
	Mohamed et al. [90]	2012	diffusion	the "extended" PUFEM used to 2D time-dependent diffusion problems, included single and multiple heat sources
	Facco et al. [85]	2012	acoustics	non-conforming elements
	Chazot, Nennig & Perrey-Debain [199]	2013	acoustics	the PUFEM investigated in 2D acoustics with absorbing materials
	Mohamed et al. [200]	2013	heat transfer	time-dependent radiative heat-transfer problems
UWVF	Després [34]	1994	analysis	the UWVF was introduced and theoretical aspects were investigated
	Cessenat & Després [125]	1998	acoustics	the acoustic UWVF introduced with theoretical error estimate and numerical results
	Cessenat & Després [201]	2003	electromagnetism	the electromagnetic UWVF introduced
	Huttunen, Monk & Kaipio [132]	2002	acoustics	basis functions varied from element to element, curved elements
	Huttunen, Kaipio & Hynynen [202]	2003	ultrasound acoustics	the UWVF tailored to the focused ultrasound applications
	Huttunen et al. [48]	2004	elasticity	2D elastic-UWVF was introduced
	Huttunen, Monk & Kaipio [137]	2004	acoustics	the 3D acoustic UWVF with PML introduced
	Huttunen et al. [138]	2005	ultrasound acoustics	UWVF used in inverse problems
	Huttunen, Malinen & Monk [127]	2007	electromagnetism	UWVF derived as an upwind discontinuous Galerkin method
	Gamallo & Astley [126]	2007	acoustics	the comparison of the UWVF and the LSM
	Huttunen & Monk [149]	2007	electromagnetism	UWVF for anisotropic media
	Huttunen et al. [139]	2007	acoustics	the HRTF was modeled, audio acoustics
	Darrigrand & Monk [133]	2007	electromagnetism	an efficient integral representation for the UWVF was introduced and different FMM approaches were tested

Table 3.1 – *(Continued) Summary of non-polynomial methods.*

Method	Authors/ref	year	field	novelty
	Huttunen, Kaipio & Monk [136]	2008	acoustics-elasticity	UWVF for fluid-solid interactions
	Buffa & Monk [51]	2008	acoustics	a global error estimate for the UWVF derived, 2D numerical results
	Badics & Matsumoto [129]	2008	electromagnetism/elasticity	stable basis, Bessel basis functions, used in the UWVF
	Luostari, Huttunen & Monk [203]	2009	acoustics	different numerical flux parameters
	Huttunen, Gamallo & Astley [41]	2009	acoustics	the performances of the PUFEM and UWVF were compared
	Loeser & Witzigmann [141]	2009	optoelectronics	the UWVF tested in optoelectronics, LED source
	Monk, Schöberl & Sinwel [135]	2010	acoustics	hybridizing the UWVF and the Raviart-Thomas elements
	Ding, Van Renterghem & Botteldooren [140]	2011	acoustics	the UWVF was used in the traffic noise barrier simulations, different porous barriers investigated
	Imbert-Gérard & Després [130]	2011	electromagnetism	the UWVF with non-constant coefficient
	Darrigrand & Monk [134]	2012	electromagnetism	hybrid method, the UWVF were coupled with the MFMM
	Melenk, Parsania & Sauter [204]	2012	acoustics	convergence, stability, highly indefinite Helmholtz equation
VTCR	Ladevèze [36]	1996	elasticity	VTCR introduced
	Ladevèze et al. [56]	2001	elasticity	the VTCR developed for plate vibration problems
	Ladevèze et al. [205]	2003	plate elasticity	the VTCR with heterogeneous plates
	Ladevèze et al. [99]	2003	plate elasticity	the VTCR used to calculate vibrations in a frequency range, 3D, three strategies used in computations: averaging over the frequency range, Newton algorithm and quasi-Newton algorithm
	Rouch & Ladevèze [206]	2003	plate elasticity	VTCR examined in 3D elastic plate problems
	Riou, Ladevèze & Rouch [101]	2004	shell elasticity	the VTCR used in curved shell problems (3D)
	Ladevèze & Riou [100]	2005	plate elasticity	the VTCR used to predict the response within a frequency range, the Taylor series expansion used
	Blanzé & Rouch [207]	2005	plate elasticity	VTCR studied in 3D plates with stochastic interfaces (connections between plates), the uncertainties in the connections modeled using polynomial chaos expansion
	Ladevèze & Chevreuil [106]	2005	elasticity	3D beam, low-frequency range modeled using FEM and medium frequency range using VTCR then the IFT
	Dorival, Rouch & Allix [208]	2006	plate elasticity	substructured version of the VTCR introduced
	Chevreuil, Ladevèze & Rouch [107]	2007	elasticity	low frequency range computed using FEM and medium frequency range using VTCR in 3D complex structures and then taking the IFT
	Blanc, Blancé & Rouch [209]	2007	plate-elasticity	the VTCR studied in heterogeneous plates with uncertainties (sensitivity analysis)
	Riou, Ladevèze & Sourcis [69]	2008	acoustics	the VTCR introduced to acoustic problems
	Kovalevsky, Ladevèze & Riou [102]	2012	acoustics	functions based on the Fourier series were used in the VTCR
	Kovalevsky et al. [104]	2012	acoustics	the VTCR extended to 3D medium frequency acoustic problems, Herglotz wave functions used in the VTCR
	Riou & Ladevèze [108]	2012	advection-diffusion	VTCR introduced in high-Peclet advection-diffusion problems in 2D
	Riou et al. [105]	2012	acoustics	VTCR with adaptive approach (angular directions) introduced for 2D Helmholtz problems

Table 3.1 – *(Continued) Summary of non-polynomial methods.*

Method	Authors/ref	year	field	novelty
	Kovalevsky, Riou & Ladevèze [103]	2013	acoustics	the VTCR examined in unbounded scattering problems
WBM	Desmet [37]	1998	vibro-acoustics	the WBM introduced for vibro-acoustic problems
	Desmet, Sas & Vandepitte [111]	2001	vibro-acoustics	the WBM investigated in 2D vibro-acoustic problems
	Desmet et al. [112]	2002	vibro-acoustics	the WBM tested in 3D vibro-acoustic problems
	Van Hal et al. [114,115]	2003	acoustics	hybrid method: finite element-wave based method (FEM-WBM), 2D
	Pluymers et al. [120]	2004	vibro-acoustics	WBM used in the vibro-acoutics with unbounded domains
	Pluymers et al. [210]	2005	vibro-acoustics	structural acoustics, bass-reflex loudspeaker
	Van Hal, Desmet & Vandepitte [116]	2005	structural-acoustics	hybrid method mid-frequency range, FEM-WBM
	Vanmaele, Vandepitte & Desmet [123]	2007	plate elasticity	the WBM introduced for plate bending vibrations, steady-state, Kirchhoff plate equation, convex domains
	He, Huang & Peng [211]	2008	vibro-acoustic	the WBM applied to 2D vibro-acoustic problem with sensitivity analysis (using direct differentiation method (DDM))
	Rejlek et al. [121]	2008	acoustics	WBM applied to semi-infinite acoustic radiation problems in 3D
	Lanoye et al. [212]	2008	acoustics	porous acoustics, WBM vs. measurements
	Vanmaele, Vandepitte & Desmet [43]	2009	plate elasticity	the accuracy of the WBM improved when stress singularities are present at corners, corner functions
	Van Genechten et al. [118]	2009	acoustics	hybrid method, WBM with modally reduced FEM
	Jegorovs [213]	2009	diffusion	the WBM used in the light diffusion approximation, see also [214]
	Van Genechten et al. [113]	2010	acoustics	WBM studied in multiple scattering problems (multi-level approach), unbounded domains
	Van Genechten et al. [215]	2010	acoustics/elasticity	multi-level approach used in order to cope better with multiple (circular) objects bounded models
	Bergen et al. [122]	2010	acoustics	3D acoustics, unbounded domains
	Dijckmans, Vermeir & Lauriks [216]	2010	vibro-acoustics	WBM used in multilayered structures, comparison with measurements and transfer matrix method (TMM)
	Koo et al. [217]	2011	vibro-acoustics	the WBM tested in 2D vibro-acoustics with design sensitivity analysis (DSA), adjoint variable method (AVM) used in the DSA that is more efficient than the DDM
	Vergote et al. [119]	2011	vibro-acoustics	hybrid method, WBM and SEA combined (WBM-SEA),
	Deckers et al. [218]	2011	acoustics	WBM with B-splines on the boundaries (curved boundaries), Gauss-Legendre and Romberg quadrature were investigated
	Deckers et al. [46]	2011	poroelasticity	the efficiency of the WBM improved using corner functions, cf. [43]
	Van Genechten, Vandepitte & Desmet [117]	2011	vibro-acoustics	hybrid method of the WBM and FEM in 3D vibro-acoustics
	Vanmaele et al. [44]	2012	elasticity	the WBM with the strategy introduced in [43], Navier's equation
	Bergen et al. [219]	2012	acoustics	the WBM examined in 2D acoustic semi-infinite domain (semi-unbounded) problems
	Deckers et al. [124]	2012	poroelasticity	WBM investigated in poroelasticity (Biot equations)
	Deckers et al. [45]	2012	acoustics	the WBM with corner functions in 2D acoustics cf. [43]
	Vergote et al. [220]	2013	plate elasticity	the WBM used to solve 3D plate problems

Table 3.1 – *(Continued) Summary of non-polynomial methods.*

Method	Authors/ref	year	field	novelty
	Deckers, Vandepitte & Desmet [221]	2013	acoustics/poroelasticity	the WBM with axisymmetric problems
	Dijckmans & Vermeir [222]	2013	vibro-acoustics	hybrid method: wave based-transfer matrix method (WB-TMM)
	Jonckheere et al. [223]	2013	acoustics/poroelasticity	hybrid method, FEM used for solving Biot and WBM Helmholtz equation

4 The ultra weak variational formulation

In this chapter we shall discuss the UWVF applied to linear elasticity, vibration of plates and acoustics. In particular, in the first two cases the UWVF will be derived via a DG scheme. For acoustics, only the final form of the UWVF will be given due to the fact that it is better known than the elastic UWVF. We also summarize error estimates for each problem.

4.1 THE UWVF IN LINEAR ELASTICITY

The derivation of the elastic UWVF will follow the strategy shown in the original publication **II**.

Let $\Omega \subset \mathbb{R}^3$ denote the bounded open computational domain. The boundary of the domain Ω is denoted by Γ and the unit outward normal is $\boldsymbol{n}$. For convenience, we recall the time-harmonic stress tensor

$$\sigma = (\lambda \nabla \cdot \boldsymbol{u}) I + 2\mu\epsilon(\boldsymbol{u}) \quad \text{in } \Omega \tag{4.1}$$

where the strain tensor $\epsilon(\boldsymbol{u})$ in (4.1) is

$$\epsilon(\boldsymbol{u}) = \frac{1}{2}(\nabla \boldsymbol{u} + (\nabla \boldsymbol{u})^T).$$

Then the time-harmonic momentum equation is

$$\nabla \cdot \sigma + \omega^2 \rho \boldsymbol{u} = \boldsymbol{0} \quad \text{in } \Omega. \tag{4.2}$$

For the UWVF we assume that the parameters λ, μ and ρ are piecewise constant and real.

The boundary condition is assumed to be

$$(\sigma \boldsymbol{n} - i\eta \boldsymbol{u}) = Q\,(-\sigma \boldsymbol{n} - i\eta \boldsymbol{u}) + \boldsymbol{g} \quad \text{on } \Gamma \tag{4.3}$$

where η is a real positive definite numerical flux matrix, $Q \in \mathbb{C}$ with $|Q| \leq 1$ gives the boundary conditions and $\boldsymbol{g}$ is the source term on the boundary Γ. Note in particular $Q = -1$ gives a standard displacement boundary condition and $Q = 1$ gives a standard traction boundary condition. In the article **II**, $Q = 0$ was considered.

In linear elasticity, the problem is to find the displacement field $\boldsymbol{u}$ that satisfies equations (4.1), (4.2) and (4.3).

4.1.1 Derivation of the UWVF via a DG scheme

The computational domain Ω is divided into non-overlapping regular elements $\Omega = \cup_{k=1}^{N} K_k$ where N is the number of elements. The element face is denoted by ∂K_k and the unit outward normal is $\boldsymbol{n}_k$. The derivation of the elastic UWVF starts by applying Betti's third identity, e.g. [48, 224, 225]. For sufficiently smooth vector functions $\boldsymbol{u}$ and $\overline{\boldsymbol{\phi}}$ which satisfy equations (4.1) and (4.2), the volume integral in Betti's identity vanishes, so that

$$\begin{aligned} &\int_{\partial K_k} [\sigma \boldsymbol{n}_k \cdot \overline{\boldsymbol{\phi}} - \overline{\delta} \boldsymbol{n}_k \cdot \boldsymbol{u}] \, \mathrm{d}S \\ &\qquad = \underbrace{\int_{K_k} [(\nabla \cdot \sigma) \cdot \overline{\boldsymbol{\phi}} - (\nabla \cdot \overline{\delta}) \cdot \boldsymbol{u}] \, \mathrm{d}V}_{=0} \end{aligned} \tag{4.4}$$

where the stress tensor σ is given by (4.1) and $\overline{\delta} = (\lambda \nabla \cdot \overline{\boldsymbol{\phi}}) I + 2\mu\epsilon(\overline{\boldsymbol{\phi}})$. Following the standard approach to deriving a DG scheme the displacement field $\boldsymbol{u}$ is replaced by a numerical flux $\hat{\boldsymbol{u}}$ and the stress tensor σ is replaced a numerical flux $\hat{\sigma}$ on the faces of the mesh, so equation (4.4) can be written as

$$\int_{\partial K_k} (\hat{\boldsymbol{u}} \cdot \overline{\delta} \boldsymbol{n}_k - \hat{\sigma} \boldsymbol{n}_k \cdot \overline{\boldsymbol{\phi}}) \, \mathrm{d}S = 0. \tag{4.5}$$

Equation (4.5) can be split in two parts: an integral over the interior interfaces between elements and an integral over the boundary faces. The interior interfaces will be considered first and second the boundary faces. The common face between K_k and K_j is denoted

by $\Sigma_{k,j}$. Obviously, it will be assumed that $\Sigma_{k,j} \neq \emptyset$. The following notation will be used from now on $\boldsymbol{u}_k = \boldsymbol{u}|_{K_k}$, $\boldsymbol{u}_j = \boldsymbol{u}|_{K_j}$ and the outer product is defined so that $\boldsymbol{a} \otimes \boldsymbol{b} = \boldsymbol{a}\boldsymbol{b}^T$ where $\boldsymbol{a}$ and $\boldsymbol{b}$ are column vectors. Following strategies in [226], over a common face $\Sigma_{k,j}$ the averages and jumps are defined to be

$$\{\!\{\boldsymbol{u}\}\!\} = \frac{\boldsymbol{u}_k + \boldsymbol{u}_j}{2}, \qquad \{\!\{\sigma\}\!\} = \frac{\sigma_k + \sigma_j}{2},$$
$$[\![\boldsymbol{u}]\!] = \boldsymbol{u}_k \otimes \boldsymbol{n}_k + \boldsymbol{u}_j \otimes \boldsymbol{n}_j, \qquad [\![\sigma]\!] = \sigma_k \boldsymbol{n}_k + \sigma_j \boldsymbol{n}_j,$$

where $\boldsymbol{n}_k$ is the unit outward normal to K_k and $\boldsymbol{n}_j$ is the unit outward normal to K_j. The numerical flux functions are defined face by face (in particular on $\Sigma_{k,j}$) as follows

$$\hat{\boldsymbol{u}} = \{\!\{\boldsymbol{u}\}\!\} - \frac{i\eta^{-1}}{2}[\![\sigma]\!], \tag{4.6}$$
$$\hat{\sigma} = \{\!\{\sigma\}\!\} + \frac{i\eta}{2}[\![\boldsymbol{u}]\!]. \tag{4.7}$$

In order to derive the particular form of the UWVF (same form as in [48]), equation (4.5) is multiplied by i and equations (4.6) and (4.7) are substituted into equation (4.5). Then

$$\begin{aligned}
&\int_{\sum_{k,j}} i[\overline{\delta}_k \boldsymbol{n}_k \cdot \hat{\boldsymbol{u}}_k - \hat{\sigma}_k \boldsymbol{n}_k \cdot \overline{\boldsymbol{\phi}}_k]\,\mathrm{d}S \\
&\quad = \int_{\sum_{k,j}} i\left[\frac{1}{2}(\boldsymbol{u}_k + \boldsymbol{u}_j) - \frac{i\eta^{-1}}{2}(\sigma_k \boldsymbol{n}_k + \sigma_j \boldsymbol{n}_j)\right] \cdot \overline{\delta}_k \boldsymbol{n}_k \,\mathrm{d}S \\
&\qquad - \int_{\sum_{k,j}} i\left[\frac{1}{2}(\sigma_k + \sigma_j)\boldsymbol{n}_k + \frac{i\eta}{2}(\boldsymbol{u}_k \otimes \boldsymbol{n}_k + \boldsymbol{u}_j \otimes \boldsymbol{n}_j)\boldsymbol{n}_k\right] \cdot \overline{\boldsymbol{\phi}}_k \,\mathrm{d}S.
\end{aligned}$$

Using now the relation (see the original publication **II**) $(\boldsymbol{u}_k \otimes \boldsymbol{n}_k + \boldsymbol{u}_j \otimes \boldsymbol{n}_j)\boldsymbol{n}_k = \boldsymbol{u}_k - \boldsymbol{u}_j$ it can be deduced that

$$\begin{aligned}
&\int_{\sum_{k,j}} i[\overline{\delta}_k \boldsymbol{n}_k \cdot \hat{\boldsymbol{u}}_k - \hat{\sigma}_k \boldsymbol{n}_k \cdot \overline{\boldsymbol{\phi}}_k]\,\mathrm{d}S \\
&\quad = \int_{\sum_{k,j}} i\left[\frac{1}{2}(\boldsymbol{u}_k + \boldsymbol{u}_j) - \frac{i\eta^{-1}}{2}(\sigma_k \boldsymbol{n}_k + \sigma_j \boldsymbol{n}_j)\right] \cdot \overline{\delta}_k \boldsymbol{n}_k \,\mathrm{d}S \\
&\qquad - \int_{\sum_{k,j}} i\left[\frac{1}{2}(\sigma_k + \sigma_j)\boldsymbol{n}_k + \frac{i\eta}{2}(\boldsymbol{u}_k - \boldsymbol{u}_j)\right] \cdot \overline{\boldsymbol{\phi}}_k \,\mathrm{d}S.
\end{aligned} \tag{4.8}$$

Rearranging terms and taking into account the complex conjugation, equation (4.8) can be simplified to

$$\begin{aligned}
&\int_{\sum_{k,j}} i[\overline{\delta}_k \boldsymbol{n}_k \cdot \hat{\boldsymbol{u}}_k - \hat{\sigma}_k \boldsymbol{n}_k \cdot \overline{\boldsymbol{\phi}}_k]\,\mathrm{d}S \\
&\quad = \int_{\sum_{k,j}} \frac{\eta^{-1}}{2}(-\sigma_k \boldsymbol{n}_k - i\eta \boldsymbol{u}_k) \cdot \overline{(-\delta_k \boldsymbol{n}_k - i\eta \boldsymbol{\phi}_k)}\,\mathrm{d}S \\
&\qquad - \int_{\sum_{k,j}} \frac{\eta^{-1}}{2}(-\sigma_j \boldsymbol{n}_j - i\eta \boldsymbol{u}_j) \cdot \overline{(\delta_k \boldsymbol{n}_k - i\eta \boldsymbol{\phi}_k)}\,\mathrm{d}S. \qquad (4.9)
\end{aligned}$$

Furthermore, equation (4.9) can be written as

$$\begin{aligned}
&\int_{\sum_{k,j}} i[\overline{\delta}_k \boldsymbol{n}_k \cdot \hat{\boldsymbol{u}}_k - \hat{\sigma}_k \boldsymbol{n}_k \cdot \overline{\boldsymbol{\phi}}_k]\,\mathrm{d}S \\
&\quad = \frac{1}{2}\left[\int_{\sum_{k,j}} \eta^{-1}\mathcal{X}_k \cdot \overline{\mathcal{Y}}_k\,\mathrm{d}S - \int_{\sum_{k,j}} \eta^{-1}\mathcal{X}_j \cdot \overline{F_k(\mathcal{Y}_k)}\,\mathrm{d}S\right], \qquad (4.10)
\end{aligned}$$

where the new functions $\{\mathcal{X}_k\}$ are given by

$$\mathcal{X}_k = (-\sigma_k \boldsymbol{n}_k - i\eta \boldsymbol{u}_k), \qquad (4.11)$$

$\mathcal{Y}_k = (-\delta_k \boldsymbol{n}_k - i\eta \boldsymbol{\phi}_k)$, and $F_k(\mathcal{Y}_k) = (\delta_k \boldsymbol{n}_k - i\eta \boldsymbol{\phi}_k)$.

Now we turn to the boundary faces. On the boundary $\Gamma_k = \Gamma \cap \partial K_k$ the numerical fluxes $\hat{\boldsymbol{u}}_k$ and $\hat{\sigma}_k$ are defined by

$$\hat{\boldsymbol{u}}_k = \boldsymbol{u}_k, \qquad (4.12)$$

$$\hat{\sigma}_k = \sigma_k. \qquad (4.13)$$

Equation (4.5) can then be written using numerical fluxes (4.12) and (4.13) as

$$\begin{aligned}
&\int_{\Gamma_k} i[\overline{\delta}_k \boldsymbol{n}_k \cdot \hat{\boldsymbol{u}}_k - \hat{\sigma}_k \boldsymbol{n}_k \cdot \overline{\boldsymbol{\phi}}_k]\,\mathrm{d}S \\
&\quad = \int_{\Gamma_k} \eta^{-1}[-i\eta\sigma_k \boldsymbol{n}_k \cdot \overline{\boldsymbol{\phi}}_k + i\eta\overline{\delta}_k \boldsymbol{n}_k \cdot \boldsymbol{u}_k]\,\mathrm{d}S
\end{aligned}$$

where η^{-1} is taken as a common factor. Adding and subtracting terms $\sigma_k \boldsymbol{n}_k \cdot \overline{\delta}_k \boldsymbol{n}_k/2$ and $\eta^2 \boldsymbol{u}_k \cdot \overline{\boldsymbol{\phi}}_k/2$ and dividing the above equation

into two parts, and rearranging terms, it can be written as

$$\begin{aligned}
&\int_{\Gamma_k} i[\overline{\delta}_k \boldsymbol{n}_k \cdot \hat{\boldsymbol{u}}_k - \hat{\sigma}_k \boldsymbol{n}_k \cdot \overline{\boldsymbol{\phi}}_k] \mathrm{d}S \\
&= \int_{\Gamma_k} \frac{1}{2}\eta^{-1} \big[\sigma_k \boldsymbol{n}_k \cdot \overline{\delta}_k \boldsymbol{n}_k - i\eta \sigma_k \boldsymbol{n}_k \cdot \overline{\boldsymbol{\phi}}_k \\
&\qquad\qquad + i\eta \boldsymbol{u}_k \cdot \overline{\delta}_k \boldsymbol{n}_k + \eta^2 \boldsymbol{u}_k \cdot \overline{\boldsymbol{\phi}}_k \big] \mathrm{d}S \\
&- \int_{\Gamma_k} \frac{1}{2}\eta^{-1} \big[\sigma_k \boldsymbol{n}_k \cdot \overline{\delta}_k \boldsymbol{n}_k + i\eta \sigma_k \boldsymbol{n}_k \cdot \overline{\boldsymbol{\phi}}_k \\
&\qquad\qquad - i\eta \boldsymbol{u}_k \cdot \overline{\delta}_k \boldsymbol{n}_k + \eta^2 \boldsymbol{u}_k \cdot \overline{\boldsymbol{\phi}}_k \big] \mathrm{d}S. \qquad (4.14)
\end{aligned}$$

Rearranging terms more and taking into account the complex conjugation, equation (4.14) can be simplified to obtain

$$\begin{aligned}
&\int_{\Gamma_k} i[\overline{\delta}_k \boldsymbol{n}_k \cdot \hat{\boldsymbol{u}}_k - \hat{\sigma}_k \boldsymbol{n}_k \cdot \overline{\boldsymbol{\phi}}_k] \, \mathrm{d}S \\
&= \int_{\Gamma_k} \frac{1}{2}\eta^{-1} (-\sigma_k \boldsymbol{n}_k - i\eta \boldsymbol{u}_k) \cdot \overline{(-\delta_k \boldsymbol{n}_k - i\eta \boldsymbol{\phi}_k)} \, \mathrm{d}S \\
&\quad - \int_{\Gamma_k} \frac{1}{2}\eta^{-1} (\sigma_k \boldsymbol{n}_k - i\eta \boldsymbol{u}_k) \cdot \overline{(\delta_k \boldsymbol{n}_k - i\eta \boldsymbol{\phi}_k)} \, \mathrm{d}S. \qquad (4.15)
\end{aligned}$$

Taking into account the boundary condition (4.3), equation (4.15) can now be written as

$$\begin{aligned}
&\int_{\Gamma_k} i[\overline{\delta}_k \boldsymbol{n}_k \cdot \hat{\boldsymbol{u}}_k - \hat{\sigma}_k \boldsymbol{n}_k \cdot \overline{\boldsymbol{\phi}}_k] \, \mathrm{d}S \\
&= \int_{\Gamma_k} \frac{1}{2}\eta^{-1} (-\sigma_k \boldsymbol{n}_k - i\eta \boldsymbol{u}_k) \cdot \overline{(-\delta_k \boldsymbol{n}_k - i\eta \boldsymbol{\phi}_k)} \, \mathrm{d}S \\
&\quad - \int_{\Gamma_k} \frac{1}{2}\eta^{-1} Q \, (-\sigma_k \boldsymbol{n}_k - i\eta \boldsymbol{u}_k) \cdot \overline{(\delta_k \boldsymbol{n}_k - i\eta \boldsymbol{\phi}_k)} \, \mathrm{d}S \\
&\quad - \int_{\Gamma_k} \frac{1}{2}\eta^{-1} \boldsymbol{g} \cdot \overline{(\delta_k \boldsymbol{n}_k - i\eta \boldsymbol{\phi}_k)} \, \mathrm{d}S.
\end{aligned}$$

Using the definitions of $\mathcal{X}_k$, $\mathcal{Y}_k$ and $F_k(\mathcal{Y}_k)$, we can obtain the iden-

tity

$$\begin{aligned}&\int_{\Gamma_k} i[\overline{\delta}_k \boldsymbol{n}_k \cdot \hat{\boldsymbol{u}}_k - \hat{\sigma}_k \boldsymbol{n}_k \cdot \overline{\boldsymbol{\phi}}_k]\,\mathrm{d}S \\ &= \frac{1}{2}\Big[\int_{\Gamma_k} \eta^{-1}\mathcal{X}_k \cdot \overline{\mathcal{Y}}_k\,\mathrm{d}S - \int_{\Gamma_k} Q\eta^{-1}\mathcal{X}_k \cdot \overline{F_k(\mathcal{Y}_k)}\,\mathrm{d}S \\ &\quad - \int_{\Gamma_k} \eta^{-1}\boldsymbol{g} \cdot \overline{F_k(\mathcal{Y}_k)}\,\mathrm{d}S\Big]. \end{aligned} \tag{4.16}$$

Combining now equations (4.5), (4.10) and (4.16) and summing over all elements, we have that $\mathcal{X}_k$, $1 \leq k \leq N$, satisfies

$$\begin{aligned}&\sum_{k=1}^{N}\Big[\int_{\partial K_k} \eta^{-1}\mathcal{X}_k \cdot \overline{\mathcal{Y}}_k\,\mathrm{d}S - \sum_{j=1, j\neq k}^{N}\int_{\Sigma_{k,j}} \eta^{-1}\mathcal{X}_j \cdot \overline{F_k(\mathcal{Y}_k)}\,\mathrm{d}S \\ &\quad - \int_{\Gamma_k} Q\eta^{-1}\mathcal{X}_k \cdot \overline{F_k(\mathcal{Y}_k)}\,\mathrm{d}S\Big] = \sum_{k=1}^{N}\int_{\Gamma_k} \eta^{-1}\boldsymbol{g} \cdot \overline{F_k(\mathcal{Y}_k)}\,\mathrm{d}S. \end{aligned} \tag{4.17}$$

for all suitable $\mathcal{Y}_k$, $1 \leq k \leq N$. We now provide details of the functional framework behind this equation. Following the strategy used in [51] and in the paper **II**, we introduce the weighted space $L^2_\eta(\partial K_k)$ with the weighted norm defined by

$$\|\boldsymbol{u}\|^2_{L^2_\eta(\partial K_k)} = \int_{\partial K_k} (\eta^{-1}\boldsymbol{u}) \cdot \overline{\boldsymbol{u}}\,\mathrm{d}S.$$

Let $X = \Pi_{K_k \in \mathcal{T}_h} L^2_\eta(\partial K_k)$ have the norm

$$\|\mathcal{X}\|^2_X = \sum_{k=1}^{N}\int_{\partial K_k} \frac{1}{2}\left(\eta^{-1}\mathcal{X}_k\right) \cdot \overline{\mathcal{X}}_k\,\mathrm{d}S = \frac{1}{2}\sum_{k=1}^{N}\|\mathcal{X}_k\|^2_{L^2_\eta(\partial K_k)} \tag{4.18}$$

with the inner product

$$(\mathcal{X}, \mathcal{Y})_X = \sum_{k=1}^{N}\int_{\partial K_k} \frac{1}{2}\left(\eta^{-1}\mathcal{X}_k\right) \cdot \overline{\mathcal{Y}}_k\,\mathrm{d}S.$$

The left hand side of equation (4.17) is the sesquilinear form $a(\mathcal{X}, \mathcal{Y})$

defined by

$$
\begin{aligned}
a(\mathcal{X},\mathcal{Y}) = &\sum_{k=1}^{N}\int_{\partial K_k}\frac{1}{2}\eta^{-1}\mathcal{X}_k\cdot\overline{\mathcal{Y}}_k\,\mathrm{d}S\\
&-\sum_{k=1}^{N}\sum_{j=1,j\neq k}^{N}\int_{\Sigma_{k,j}}\frac{1}{2}\eta^{-1}\mathcal{X}_j\cdot\overline{F_k(\mathcal{Y}_k)}\,\mathrm{d}S\\
&-\sum_{k=1}^{N}\int_{\Gamma_k}\frac{1}{2}Q\eta^{-1}\mathcal{X}_k\cdot\overline{F_k(\mathcal{Y}_k)}\,\mathrm{d}S
\end{aligned}
\tag{4.19}
$$

and the boundary data functional can be obtained from

$$
b(\mathcal{Y}) = \sum_{k=1}^{N}\int_{\Gamma_k}\frac{1}{2}\eta^{-1}\boldsymbol{g}\cdot\overline{F_k(\mathcal{Y}_k)}\,\mathrm{d}S. \tag{4.20}
$$

Combining now (4.19) and (4.20) the DG scheme becomes the problem of finding $\mathcal{X}\in X$ so that

$$
a(\mathcal{X},\mathcal{Y}) = b(\mathcal{Y}) \quad \text{for all } \mathcal{Y}\in X. \tag{4.21}
$$

Equation (4.21) is the UWVF for the Navier equation (see the article **II** and [48]).

4.1.2 Basis functions and the discretization

In 2D linear elasticity the basis functions of the UWVF were P- and S-waves that were obtained by using the Helmholtz decomposition [48]. In 3D linear elasticity, the solution of the adjoint Navier equation is separated into three wave components as follows

$$
\boldsymbol{\phi}_k = \boldsymbol{\phi}_k^P + \boldsymbol{\phi}_k^{SH} + \boldsymbol{\phi}_k^{SV} \quad \text{in } K_k,
$$

where $\boldsymbol{\phi}_k^P$ is a P-wave (pressure wave), $\boldsymbol{\phi}^{SH}$ is a SH-wave (horizontal component of S-wave) and $\boldsymbol{\phi}^{SV}$ is a SV-wave (vertical component of S-wave). On each element K_k the number of basis functions is chosen as p_k^P for P-wave and p_k^S for S-waves. Each P-wave basis function is given by

$$
\boldsymbol{\phi}_{k,\ell}^P = \begin{cases} \alpha_k^P \boldsymbol{d}_{k,\ell}^P \exp(i\overline{\kappa}_P \boldsymbol{d}_{k,\ell}^P\cdot\boldsymbol{x}) & \text{in } K_k \\ 0 \quad \text{elsewhere} \end{cases}, \tag{4.22}
$$

where $1 \leq \ell \leq p_k^P$, α_k^P is the amplitude and the direction of propagation $\boldsymbol{d}_{k,\ell}^P$ is a unit vector. In particular, the P-wave satisfies the Helmholtz equation so that $\Delta\overline{\boldsymbol{\phi}}_{k,\ell}^P + \kappa_P^2\overline{\boldsymbol{\phi}}_{k,\ell}^P = \mathbf{0}$ in K_k and $\nabla \times \boldsymbol{\phi}_k^P = 0$. The S-wave basis functions are given by

$$\boldsymbol{\phi}_{k,\ell}^{SH} = \begin{cases} \alpha_k^{SH}\boldsymbol{d}_{k,\ell}^{S\perp}\exp(i\overline{\kappa}_S\boldsymbol{d}_{k,\ell}^S\cdot\boldsymbol{x}) & \text{in } K_k \\ 0 \quad \text{elsewhere} \end{cases}, \tag{4.23}$$

$$\boldsymbol{\phi}_{k,\ell}^{SV} = \begin{cases} \alpha_k^{SV}\boldsymbol{d}_{k,\ell}^{S\perp}\times\boldsymbol{d}_{k,\ell}^{S}\exp(i\overline{\kappa}_S\boldsymbol{d}_{k,\ell}^S\cdot\boldsymbol{x}) & \text{in } K_k \\ 0 \quad \text{elsewhere} \end{cases}, \tag{4.24}$$

where $1 \leq \ell \leq p_k^S$, $\boldsymbol{d}_{k,\ell}^{S\perp} \perp \boldsymbol{d}_{k,\ell}^S$ are unit vectors and α_k^{SH}, α_k^{SV} are the amplitudes. Similarly to P-wave basis functions, the S-wave basis functions satisfy the adjoint Helmholtz equations

$$\begin{aligned} \Delta\overline{\boldsymbol{\phi}}_{k,\ell}^{SH} + \kappa_S^2\overline{\boldsymbol{\phi}}_{k,\ell}^{SH} &= \mathbf{0}, \quad \text{in } K_k, \\ \Delta\overline{\boldsymbol{\phi}}_{k,\ell}^{SV} + \kappa_S^2\overline{\boldsymbol{\phi}}_{k,\ell}^{SV} &= \mathbf{0}, \quad \text{in } K_k, \end{aligned}$$

with the following relations $\nabla\cdot\boldsymbol{\phi}_k^{SH} = \nabla\cdot\boldsymbol{\phi}_k^{SV} = 0$ and $\boldsymbol{d}_{k,\ell}^S \perp \boldsymbol{d}_{k,\ell}^{S\perp} \perp (\boldsymbol{d}_{k,\ell}^{S\perp}\times\boldsymbol{d}_{k,\ell}^S)$. The directions in the basis functions (4.22), (4.23) and (4.24) are chosen following [227, 228].

Following the original article **II**, the subspaces can be defined as $X_k^h \subset L_\eta^2(\partial K_k)$ with $X^h = \Pi_{k=1}^N X_k^h$ and $1 \leq k \leq N$. Using now the basis functions (4.22), (4.23) and (4.24) in (4.11), then $\mathcal{X}_k^h \in X_k^h$ can be written as

$$\begin{aligned} \mathcal{X}_k^h = &\sum_{\ell=1}^{p_k^P} \mathcal{X}_{k,\ell}^P\left(-\sigma_{k,\ell}^P\boldsymbol{n}_k - i\eta\boldsymbol{\phi}_{k,\ell}^P\right) \\ &+ \sum_{\ell=1}^{p_k^S} \mathcal{X}_{k,\ell}^{SH}\left(-\sigma_{k,\ell}^{SH}\boldsymbol{n}_k - i\eta\boldsymbol{\phi}_{k,\ell}^{SH}\right) \\ &+ \sum_{\ell=1}^{p_k^S} \mathcal{X}_{k,\ell}^{SV}\left(-\sigma_{k,\ell}^{SV}\boldsymbol{n}_k - i\eta\boldsymbol{\phi}_{k,\ell}^{SV}\right) \end{aligned}$$

where $\{\mathcal{X}_{k,\ell}^P\}_{\ell=1}^{p_k^P}$, $\{\mathcal{X}_{k,\ell}^{SH}\}_{\ell=1}^{p_k^S}$, $\{\mathcal{X}_{k,\ell}^{SV}\}_{\ell=1}^{p_k^S}$ are unknown expansion coefficients and $\sigma_{k,\ell}^\bullet = (\lambda\nabla\cdot\boldsymbol{\phi}_{k,\ell}^\bullet)I + 2\mu\epsilon(\boldsymbol{\phi}_{k,\ell}^\bullet)$ where $\bullet$ =P, SH or SV.

Similarly $\mathcal{Y}_k^h \in X_k^h$ is of the form

$$\begin{aligned}\mathcal{Y}_k^h = &\sum_{\ell=1}^{p_k^P} \mathcal{Y}_{k,\ell}^P \left(-\sigma_{k,\ell}^P \boldsymbol{n}_k - i\eta \boldsymbol{\phi}_{k,\ell}^P\right) \\ &+ \sum_{\ell=1}^{p_k^S} \mathcal{Y}_{k,\ell}^{SH} \left(-\sigma_{k,\ell}^{SH} \boldsymbol{n}_k - i\eta \boldsymbol{\phi}_{k,\ell}^{SH}\right) \\ &+ \sum_{\ell=1}^{p_k^S} \mathcal{Y}_{k,\ell}^{SV} \left(-\sigma_{k,\ell}^{SV} \boldsymbol{n}_k - i\eta \boldsymbol{\phi}_{k,\ell}^{SV}\right)\end{aligned}$$

where $\{\mathcal{Y}_{k,\ell}^P\}_{\ell=1}^{p_k^P}$, $\{\mathcal{Y}_{k,\ell}^{SH}\}_{\ell=1}^{p_k^S}$, $\{\mathcal{Y}_{k,\ell}^{SV}\}_{\ell=1}^{p_k^S}$ are the expansion coefficients. In addition $F_k(\mathcal{Y}_k^h)$ can be easily computed as

$$\begin{aligned}F_k(\mathcal{Y}_k^h) = &\sum_{\ell=1}^{p_k^P} \mathcal{Y}_{k,\ell}^P \left(\sigma_{k,\ell}^P \boldsymbol{n}_k - i\eta \boldsymbol{\phi}_{k,\ell}^P\right) \\ &+ \sum_{\ell=1}^{p_k^S} \mathcal{Y}_{k,\ell}^{SH} \left(\sigma_{k,\ell}^{SH} \boldsymbol{n}_k - i\eta \boldsymbol{\phi}_{k,\ell}^{SH}\right) \\ &+ \sum_{\ell=1}^{p_k^S} \mathcal{Y}_{k,\ell}^{SV} \left(\sigma_{k,\ell}^{SV} \boldsymbol{n}_k - i\eta \boldsymbol{\phi}_{k,\ell}^{SV}\right).\end{aligned}$$

Indeed one reason for choosing a basis for $\mathcal{X}_k^h$ is that in the way described above F is trivial to compute. In summary, the space X_k^h is spanned by the basis functions that is

$$\begin{aligned}X_k^h = \operatorname{span}\Big\{ &\sigma_{k,\ell}^P \boldsymbol{n}_k + i\eta \boldsymbol{\phi}_{k,\ell}^P, \quad 1 \le \ell \le p_k^P, \\ &\sigma_{k,\ell}^{SH} \boldsymbol{n}_k + i\eta \boldsymbol{\phi}_{k,\ell}^{SH}, \quad 1 \le \ell \le p_k^S, \\ &\sigma_{k,\ell}^{SV} \boldsymbol{n}_k + i\eta \boldsymbol{\phi}_{k,\ell}^{SV}, \quad 1 \le \ell \le p_k^S \Big\}\end{aligned}$$

for $k = 1, \ldots, N$ and $X^h = \Pi_{k=1}^N X_k^h$. Then the discretized form of the UWVF can be obtained by replacing $\mathcal{X}$ by $\mathcal{X}^h$ and replacing $\mathcal{Y}$ by $\mathcal{Y}^h$ in (4.21): we seek $\mathcal{X}^h \in X^h$ such that

$$a(\mathcal{X}^h, \mathcal{Y}^h) = b(\mathcal{Y}^h) \quad \text{for all } \mathcal{Y}^h \in X^h.$$

In matrix form, the discrete UWVF can be written as

$$(\mathrm{D}-\mathrm{C})\boldsymbol{X}=\boldsymbol{b} \tag{4.25}$$

where $\boldsymbol{X}=(x_{11}^{P},\ldots,x_{1p_1^P}^{P},x_{11}^{SH},\ldots,x_{1p_1^S}^{SH},x_{11}^{SV},\ldots,x_{1p_1^S}^{SV},\ldots)^T$ consists of the unknown coefficients (to be determined), D is a block diagonal, Hermitian positive definite matrix and the sparse matrix C has both off-diagonal and diagonal blocks (when $Q\neq 0$).

The originators of the UWVF [35, 125] have suggested that the linear system (4.25) should be solved in preconditioned form as

$$(I-\mathrm{D}^{-1}\mathrm{C})\boldsymbol{X}=\mathrm{D}^{-1}\boldsymbol{b}$$

where I is the identity matrix. In order to reduce the computational burden, the matrix D can be efficiently inverted blockwise as in [132].

4.1.3 Error estimates

In this section the main error estimates for the elastic UWVF are outlined following the paper **II**. Strategies for obtaining these estimates follow [35, 39, 51, 52, 125, 151, 152].

The physical parameters are assumed to be real and constant and our theory is applicable for $|Q|<1$ but it cannot handle the case $|Q|=1$. Paper **II** considered the case $Q=0$. The domain Ω is assumed to be a convex polygon or smooth. For a smooth domain the subdomains $\{K_k\}$ in the mesh may need to have curvilinear faces. In addition, the mesh is supposed to be quasi-uniform by which we mean that if h is the maximum diameter of all the elements in the mesh then diameter h_{K_k} of K_k is bounded so that $h_{K_k}^{-1}\leq Ch^{-1}$ for some C that is independent of h and the element K_k. Since we are interested in frequency dependent estimates, we make the specific assumption that the numerical flux matrix is bounded so that $\|\eta\|_\infty<C\omega$ and $\|\eta^{-1}\|_\infty<C\omega^{-1}$ for some C.

The basic error estimate on the boundary Γ, cf. [35, 125] and Corollary 3.10 in **II**, can be written as

$$\|\mathcal{X}-\mathcal{X}^h\|_{L^2_\eta(\Gamma)}\leq 2\|(I-P^h)\mathcal{X}\|_X$$

where the X-norm is defined in (4.18),

$$\|\mathcal{X} - \mathcal{X}^h\|^2_{L^2_\eta(\Gamma)} = \sum_{k=1}^{N} \int_{\Gamma_k} \frac{1}{2} \left(\eta^{-1}(\mathcal{X} - \mathcal{X}^h)\right) \cdot \overline{(\mathcal{X} - \mathcal{X}^h)}\, \mathrm{d}S,$$

and P^h is the orthogonal projection from X onto X^h.

The derivation of a global error estimate for the UWVF in $L^2(\Omega)$ uses the dual problem approach from [39], the regularity estimates from [229] and the assumed quasi-uniformity of the mesh.

Because the elasticity parameters are assumed to be real, the piecewise defined local solution $\boldsymbol{u}_h$ approximating $\boldsymbol{u}$ can be computed from $\mathcal{X}^h$ by

$$\boldsymbol{u}_h|_{K_k} = \sum_{\ell=1}^{p^P} \mathcal{X}^P_{k,\ell} \phi^P_{k,\ell} + \sum_{\ell=1}^{p^S} (\mathcal{X}^{SH}_{k,\ell} \phi^{SH}_{k,\ell} + \mathcal{X}^{SV}_{k,\ell} \phi^{SV}_{k,\ell}).$$

Then, see Theorem 3.14 in **II**, assuming that the domain Ω is convex and polyhedral and the mesh is regular and quasi-uniform, the $L^2(\Omega)$ norm error estimate can be written as follows

$$\|\boldsymbol{u} - \boldsymbol{u}_h\|_{0,\Omega} \leq C h^{-1/2} \left(\omega^{\frac{3}{2}} + \omega^{-\frac{5}{2}}\right) \|(I - P^h)\mathcal{X}\|_X.$$

Using the Helmholtz decomposition, the displacement $\boldsymbol{u}$ can be written as

$$\boldsymbol{u} = \nabla A + \nabla \times \boldsymbol{B}$$

so that

$$\nabla \cdot \boldsymbol{u} = \nabla^2 A,$$
$$\nabla \times \boldsymbol{u} = \nabla \times \nabla \times \boldsymbol{B},$$

and we assume the regularity: $A \in H^{r_P+1}(K_k)$ is a scalar field and $\boldsymbol{B} \in H^{r_S+1}(K_k)^3$ is a vector field so that $\nabla \cdot \boldsymbol{B} = 0$ and $\nabla \times (\nabla A) = 0$ and $r_P \in \mathbb{N}$ and $r_S \in \mathbb{N}$. The scalar field A satisfies the Helmholtz equation $\Delta A + \kappa_P^2 A = 0$ and vector field $\boldsymbol{B}$ satisfies the Maxwell equation $\nabla \times \nabla \times \boldsymbol{B} - \kappa_S^2 \boldsymbol{B} = \boldsymbol{0}$.

Following [153], we define the $\varkappa$-weighted norm $\|\boldsymbol{u}\|_{r,\varkappa,K_k}$ for real $\varkappa > 0$ as follows

$$\|\boldsymbol{u}\|_{r,\varkappa,K_k} := \left(\sum_{j=0}^{r} \varkappa^{2(r-j)} |\boldsymbol{u}|_{j,K_k}^2 \right)^{\frac{1}{2}},$$

where the seminorm is given by

$$|\boldsymbol{u}|_{\alpha,K_k}^2 = \sum_{\substack{j,l,m \\ j+l+m=\alpha}} \left\| \frac{\partial^j}{\partial x_1^j} \frac{\partial^l}{\partial x_2^l} \frac{\partial^m}{\partial x_3^m} \boldsymbol{u} \right\|_{0,K_k}^2$$

where j, l, m and $\alpha \in \mathbb{N}_0$.

Let the number of P-wave basis functions be $p^P = (q_P + 1)^2$ such that $q_P \geq 2r_P + 1$ (and $q_P \geq 2(1 + 2^{1/\Lambda_k})$ where Λ_k depends only on the shape of the element K_k). The number of SV-wave (and SH-wave) basis functions is similarly defined as $p^S = (q_S + 1)^2$ such that $q_S \geq 2r_S + 1$ (and $q_S \geq 2(1 + 2^{1/\Lambda_k})$ where Λ_k depends only on the shape of the element K_k). Using the approximation properties of plane waves (motivated by [52, 151–153]) and assuming $\kappa_S h \leq C$ for some fixed C, we obtain the global estimate

$$\|\boldsymbol{u} - \boldsymbol{u}_h\|_{0,\Omega} \leq C \left(\omega^{-1} + \omega^{-5}\right)(1+\omega) \Big(h^{r_P - 2} \|\nabla \cdot \boldsymbol{u}\|_{r_P+1,\kappa_P,\Omega} + h^{r_S-2} \|\nabla \times \boldsymbol{u}\|_{r_S+1,\kappa_S,\Omega} \Big). \tag{4.26}$$

4.2 THE UWVF IN PLATE VIBRATION PROBLEMS

The UWVF for fourth order problems will be derived using the DG scheme following the strategies in [230]. Here $\Omega \subset \mathbb{R}^2$ is a bounded polygonal open set. We want to approximate the displacement of the plate occupying Ω. The thin plate problem is to find the displacement w such that

$$\Delta^2 w - \kappa_b^4 w = 0 \quad \text{in } \Omega \tag{4.27}$$

where the plate bending wave number $\kappa_b = (\rho t \omega^2 / D)^{1/4}$, ρ is the density of the medium, ω is the circular frequency, t is the plate thickness and the plate bending stiffness is $D = Et^3/(12(1-\nu^2))$, modulus of the elasticity E and ν is the Poisson ratio. The plate bending wave number κ_b is now on assumed to be real and constant.

The fourth order PDE (4.27) requires that two boundary conditions be imposed. We assume that the boundary conditions are given by

$$\frac{\partial \Delta w}{\partial \boldsymbol{n}} - i\eta_1 w = Q_1 \left(-\frac{\partial \Delta w}{\partial \boldsymbol{n}} - i\eta_1 w \right) + g_1, \quad \text{on } \Gamma, \tag{4.28}$$

$$\frac{\partial w}{\partial \boldsymbol{n}} - i\eta_2 \Delta w = Q_2 \left(-\frac{\partial w}{\partial \boldsymbol{n}} - i\eta_2 \Delta w \right) + g_2, \quad \text{on } \Gamma, \tag{4.29}$$

where $\boldsymbol{n}$ is the outward normal, $Q_1 \in \mathbb{C}$, $Q_2 \in \mathbb{C}$, $|Q_1| \leq 1$ and $|Q_2| \leq 1$ defines the boundary conditions, η_1 and η_2 are the flux parameters and g_1 and g_2 are the source terms on the boundary Γ. While η_1 and η_2 can be chosen arbitrarily, for simplicity and to balance dimensions we will make the specific choice $\eta_1 = \kappa_b^3$ and $\eta_2 = \kappa_b^{-1}$.

In particular, the boundary conditions (4.28)-(4.29) are tailored to clamped plate boundary conditions (when $Q_1 = -1$ and $Q_2 = 1$). Unfortunately, free plate or simply supported boundary conditions can not be obtained and so this formulation is only a first step towards developing a UWVF for more general plate problems. The existence and uniqueness of the solution of problem (4.27)-(4.29) is proved in the original publication **IV**.

4.2.1 Derivation of the UWVF via a DG scheme

In the original publication **IV** the UWVF for Kirchhoff plate equation was derived following the strategies in [35, 125] using the so-called "Isometry Lemma". However, to be more consistent with the linear elasticity derivations in the previous section, the UWVF for the plate equation will now be derived via an upwind DG scheme

cf. [230]. Therefore, the equation (4.27) will be written as a first order system, using new variables[1] $\boldsymbol{s}$, u and $\boldsymbol{t}$ such that

$$i\kappa_b \boldsymbol{s} = \nabla w, \tag{4.30}$$

$$i\kappa_b u = \nabla \cdot \boldsymbol{s}, \tag{4.31}$$

$$i\kappa_b \boldsymbol{t} = \nabla u, \tag{4.32}$$

$$\nabla \cdot \boldsymbol{t} = i\kappa_b w. \tag{4.33}$$

Now the boundary conditions (4.28) and (4.29) can be written as

$$-i\kappa_b^3 \boldsymbol{t} \cdot \boldsymbol{n} - i\eta_1 w = Q_1(i\kappa_b^3 \boldsymbol{t} \cdot \boldsymbol{n} - i\eta_1 w) + g_1, \quad \text{on } \Gamma, \tag{4.34}$$

$$i\kappa_b \boldsymbol{s} \cdot \boldsymbol{n} + i\eta_2 \kappa_b^2 u = Q_2(-i\kappa_b \boldsymbol{s} \cdot \boldsymbol{n} + i\eta_2 \kappa_b^2 u) + g_2, \quad \text{on } \Gamma. \tag{4.35}$$

The first part of the derivation follows the strategies given in [230] and [51]. The computational domain Ω is now divided into regular non-overlapping elements so that $\Omega = \cup_{k=1}^{N} K_k$ where $k = 1, \ldots, N$ and N is the number of elements. Again, the following notation will be used $w_k = w|_{K_k}$, $u_k = u|_{K_k}$, $\boldsymbol{s}_k = \boldsymbol{s}|_{K_k}$ and $\boldsymbol{t}_k = \boldsymbol{t}|_{K_k}$. Equations (4.30), (4.31), (4.32) and (4.33) are multiplied by test functions $\overline{\boldsymbol{\xi}}$, $\overline{\phi}$, $\overline{\boldsymbol{\varphi}}$ and $\overline{\psi}$, respectively followed by integration over the element K_k. Then using integration by parts, we obtain

$$\int_{K_k} i\kappa_b \boldsymbol{s}_k \cdot \overline{\boldsymbol{\xi}}_k \,\mathrm{d}V = -\int_{\partial K_k} w_k \nabla \cdot \overline{\boldsymbol{\xi}}_k \,\mathrm{d}A + \int_{\partial K_k} w_k \boldsymbol{n}_k \cdot \overline{\boldsymbol{\xi}}_k \,\mathrm{d}A, \tag{4.36}$$

$$\int_{K_k} i\kappa_b u_k \overline{\phi}_k \,\mathrm{d}V = -\int_{\partial K_k} \boldsymbol{s}_k \cdot \nabla \overline{\phi}_k \,\mathrm{d}A + \int_{\partial K_k} \overline{\phi}_k \boldsymbol{n}_k \cdot \boldsymbol{s}_k \,\mathrm{d}A, \tag{4.37}$$

$$\int_{K_k} i\kappa_b \boldsymbol{t}_k \cdot \overline{\boldsymbol{\varphi}}_k \,\mathrm{d}V = -\int_{\partial K_k} u_k \nabla \cdot \overline{\boldsymbol{\varphi}}_k \,\mathrm{d}A + \int_{\partial K_k} u_k \boldsymbol{n}_k \cdot \overline{\boldsymbol{\varphi}}_k \,\mathrm{d}A, \tag{4.38}$$

$$\int_{K_k} i\kappa_b w_k \overline{\psi}_k \,\mathrm{d}V = -\int_{\partial K_k} \boldsymbol{t}_k \cdot \nabla \overline{\psi}_k \,\mathrm{d}A + \int_{\partial K_k} \overline{\psi}_k \boldsymbol{n}_k \cdot \boldsymbol{t}_k \,\mathrm{d}A. \tag{4.39}$$

Summing equations (4.36), (4.37), (4.38) and (4.39), one obtains

$$\begin{aligned} &\int_{K_k} \big\{ \boldsymbol{s}_k \cdot (i\kappa_b \overline{\boldsymbol{\xi}}_k + \nabla \overline{\phi}_k) + u_k (i\kappa_b \overline{\phi}_k + \nabla \cdot \overline{\boldsymbol{\varphi}}_k) \\ &\quad + \boldsymbol{t}_k \cdot (i\kappa_b \overline{\boldsymbol{\varphi}}_k + \nabla \overline{\psi}_k) + w_k (i\kappa_b \overline{\psi}_k + \nabla \cdot \overline{\boldsymbol{\xi}}_k) \big\} \,\mathrm{d}V \\ &= \int_{\partial K_k} \left\{ w_k \boldsymbol{n}_k \cdot \overline{\boldsymbol{\xi}}_k + \boldsymbol{s}_k \cdot \boldsymbol{n}_k \overline{\phi}_k + u_k \boldsymbol{n}_k \cdot \overline{\boldsymbol{\varphi}}_k + \boldsymbol{t}_k \cdot \boldsymbol{n}_k \overline{\psi}_k \right\} \mathrm{d}A. \end{aligned} \tag{4.40}$$

[1] The variable u is not the same variable than in Chapter 3. Variables $\boldsymbol{t}$ or $\boldsymbol{s}$ are not tangential vectors.

Taking into account complex conjugation, equation (4.40) simplifies to

$$\begin{aligned}\int_{K_k} \{ & \boldsymbol{s}_k \cdot \overline{(-i\kappa_b \boldsymbol{\xi}_k + \nabla \phi_k)} + u_k \overline{(-i\kappa_b \phi_k + \nabla \cdot \boldsymbol{\varphi}_k)} \\ & + \boldsymbol{t}_k \cdot \overline{(-i\kappa_b \boldsymbol{\varphi}_k + \nabla \psi_k)} + w_k \overline{(-i\kappa_b \psi_k + \nabla \cdot \boldsymbol{\xi}_k)} \} \, \mathrm{d}V \\ = & \int_{\partial K_k} \left\{ w_k \boldsymbol{n}_k \cdot \overline{\boldsymbol{\xi}}_k + \boldsymbol{s}_k \cdot \boldsymbol{n}_k \overline{\phi}_k + u_k \boldsymbol{n}_k \cdot \overline{\boldsymbol{\varphi}}_k + \boldsymbol{t}_k \cdot \boldsymbol{n}_k \overline{\psi}_k \right\} \mathrm{d}A. \end{aligned} \tag{4.41}$$

Similarly to [51], new variables $\boldsymbol{\xi}$, ϕ, $\boldsymbol{\varphi}$ and ψ are chosen such that

$$i\kappa_b \boldsymbol{\xi} = \nabla \phi, \tag{4.42}$$
$$i\kappa_b \phi = \nabla \cdot \boldsymbol{\varphi}, \tag{4.43}$$
$$i\kappa_b \boldsymbol{\varphi} = \nabla \psi, \tag{4.44}$$
$$i\kappa_b \psi = \nabla \cdot \boldsymbol{\xi}, \tag{4.45}$$

equivalently $\Delta^2 \psi = \kappa_b^4 \psi$. Hence, the volume integral in equation (4.41) vanishes and it can be written as follows

$$\int_{\partial K_k} \left\{ w_k \boldsymbol{n}_k \cdot \overline{\boldsymbol{\xi}}_k + \boldsymbol{s}_k \cdot \boldsymbol{n}_k \overline{\phi}_k + u_k \boldsymbol{n}_k \cdot \overline{\boldsymbol{\varphi}}_k + \boldsymbol{t}_k \cdot \boldsymbol{n}_k \overline{\psi}_k \right\} \mathrm{d}A = 0. \tag{4.46}$$

As for the DG scheme w, $\boldsymbol{s}$, u and $\boldsymbol{t}$ on ∂K_k are now replaced by numerical fluxes $\hat{w}$, $\hat{\boldsymbol{s}}$, $\hat{u}$ and $\hat{\boldsymbol{t}}$, respectively.

Again the equation (4.46) can be split into boundary integrals and integrals on the element interfaces. First the boundary edges will be investigated and then the interior interfaces. On the boundary edge Γ, the fluxes are defined as $\hat{w} = w$, $\hat{\boldsymbol{s}} = \boldsymbol{s}$, $\hat{u} = u$ and $\hat{\boldsymbol{t}} = \boldsymbol{t}$. In order to derive the similar form of the plate UWVF as in the original publication **IV**, equation (4.46) is multiplied by κ_b^3.

Then

$$\begin{aligned}
&\int_{\Gamma_k} \kappa_b^3 (w_k \boldsymbol{n}_k \cdot \overline{\boldsymbol{\xi}}_k + \boldsymbol{s}_k \cdot \boldsymbol{n}_k \overline{\phi}_k + u_k \boldsymbol{n}_k \cdot \overline{\boldsymbol{\varphi}}_k + \boldsymbol{t}_k \cdot \boldsymbol{n}_k \overline{\psi}_k)\, \mathrm{d}A \\
&= -\int_{\Gamma_k} \frac{1}{2\eta_1} (i\kappa_b^3 \boldsymbol{t}_k \cdot \boldsymbol{n}_k - i\eta_1 w_k) \overline{(i\kappa_b^3 \boldsymbol{\xi}_k \cdot \boldsymbol{n}_k - i\eta_1 \psi_k)}\, \mathrm{d}A \\
&\quad + \int_{\Gamma_k} \frac{1}{2\eta_1} (-i\kappa_b^3 \boldsymbol{t}_k \cdot \boldsymbol{n}_k - i\eta_1 w_k) \overline{(-i\kappa_b^3 \boldsymbol{\xi}_k \cdot \boldsymbol{n}_k - i\eta_1 \psi_k)}\, \mathrm{d}A \\
&\quad - \int_{\Gamma_k} \frac{1}{2\eta_2} (-i\kappa_b \boldsymbol{s}_k \cdot \boldsymbol{n}_k + i\eta_2 \kappa_b^2 u_k) \overline{(-i\kappa_b \boldsymbol{\varphi}_k \cdot \boldsymbol{n}_k + i\eta_2 \kappa_b^2 \phi_k)}\, \mathrm{d}A \\
&\quad + \int_{\Gamma_k} \frac{1}{2\eta_2} (i\kappa_b \boldsymbol{s}_k \cdot \boldsymbol{n}_k + i\eta_2 \kappa_b^2 u_k) \overline{(i\kappa_b \boldsymbol{\varphi}_k \cdot \boldsymbol{n}_k + i\eta_2 \kappa_b^2 \phi_k)}\, \mathrm{d}A, \quad (4.47)
\end{aligned}$$

where $\eta_1 = \kappa_b^3$ and $\eta_2 = \kappa_b^{-1}$ are chosen.

Now we turn to element interfaces. Let K_k and K_j share a common face $\Sigma_{k,j}$. Then, the averages and jumps across the interface $\Sigma_{k,j}$ can be written as

$$\begin{aligned}
\{\!\{w\}\!\} &= \frac{w_k + w_j}{2}, \quad [\![w]\!] = w_k \boldsymbol{n}_k + w_j \boldsymbol{n}_j, \\
\{\!\{\boldsymbol{s}\}\!\} &= \frac{\boldsymbol{s}_k + \boldsymbol{s}_j}{2}, \quad [\![\boldsymbol{s}]\!] = \boldsymbol{s}_k \cdot \boldsymbol{n}_k + \boldsymbol{s}_j \cdot \boldsymbol{n}_j, \\
\{\!\{u\}\!\} &= \frac{u_k + u_j}{2}, \quad [\![u]\!] = u_k \boldsymbol{n}_k + u_j \boldsymbol{n}_j, \\
\{\!\{\boldsymbol{t}\}\!\} &= \frac{\boldsymbol{t}_k + \boldsymbol{t}_j}{2}, \quad [\![\boldsymbol{t}]\!] = \boldsymbol{t}_k \cdot \boldsymbol{n}_k + \boldsymbol{t}_j \cdot \boldsymbol{n}_j,
\end{aligned}$$

where the lower index k refers to the element K_k and j refers to the element K_j. Using these definitions, the fluxes on the interior faces $\Sigma_{k,j}$ are now taken to be

$$\hat{w} = \{\!\{w\}\!\} - \frac{1}{2}[\![\boldsymbol{t}]\!], \quad \hat{\boldsymbol{t}} = \{\!\{\boldsymbol{t}\}\!\} - \frac{1}{2}[\![w]\!], \tag{4.48}$$

$$\hat{u} = \{\!\{u\}\!\} - \frac{1}{2}[\![\boldsymbol{s}]\!], \quad \hat{\boldsymbol{s}} = \{\!\{\boldsymbol{s}\}\!\} - \frac{1}{2}[\![w]\!]. \tag{4.49}$$

For the sake of clarity, the left hand side of equation (4.46) is divided in two parts. Using now (4.48) the first and the last term on the left

hand side of equation (4.46) can be written as

$$\begin{aligned}
&\int_{\Sigma_{k,j}} \kappa_b^3 (\hat{w}_k \boldsymbol{n}_k \cdot \overline{\boldsymbol{\xi}}_k + \hat{\boldsymbol{t}}_k \cdot \boldsymbol{n}_k \overline{\psi}_k)\, \mathrm{d}A \\
&\quad = \int_{\Sigma_{k,j}} \kappa_b^3 \Bigg\{ \left(\frac{w_k + w_j}{2} - \frac{1}{2}(\boldsymbol{t}_k \cdot \boldsymbol{n}_k + \boldsymbol{t}_j \cdot \boldsymbol{n}_j) \right) \boldsymbol{n}_k \cdot \overline{\boldsymbol{\xi}}_k \\
&\qquad + \left(\frac{\boldsymbol{t}_k + \boldsymbol{t}_j}{2} - \frac{1}{2}(w_k \boldsymbol{n}_k + w_j \boldsymbol{n}_j) \right) \cdot \boldsymbol{n}_k \overline{\psi}_k \Bigg\}\, \mathrm{d}A. \qquad (4.50)
\end{aligned}$$

On the right hand side of equation (4.50), taking w_k and $\boldsymbol{t}_k$ terms first and w_j and $\boldsymbol{t}_j$ terms last, one obtains

$$\begin{aligned}
&\int_{\Sigma_{k,j}} \kappa_b^3 (\hat{w}_k \boldsymbol{n}_k \cdot \overline{\boldsymbol{\xi}}_k + \hat{\boldsymbol{t}}_k \cdot \boldsymbol{n}_k \overline{\psi}_k)\, \mathrm{d}A \\
&\quad = \int_{\Sigma_{k,j}} \kappa_b^3 \Bigg\{ \left(\frac{w_k}{2} - \frac{1}{2}(\boldsymbol{t}_k \cdot \boldsymbol{n}_k) \right) \boldsymbol{n}_k \cdot \overline{\boldsymbol{\xi}}_k + \left(\frac{\boldsymbol{t}_k}{2} - \frac{1}{2}(w_k \boldsymbol{n}_k) \right) \cdot \boldsymbol{n}_k \overline{\psi}_k \\
&\quad + \left(\frac{w_j}{2} - \frac{1}{2}(\boldsymbol{t}_j \cdot \boldsymbol{n}_j) \right) \boldsymbol{n}_k \cdot \overline{\boldsymbol{\xi}}_k + \left(\frac{\boldsymbol{t}_j}{2} - \frac{1}{2}(w_j \boldsymbol{n}_j) \right) \cdot \boldsymbol{n}_k \overline{\psi}_k \Bigg\}\, \mathrm{d}A. \qquad (4.51)
\end{aligned}$$

Using the fact that $\boldsymbol{n}_k = -\boldsymbol{n}_j$ on the interface $\Sigma_{k,j}$, equation (4.51) can be written as

$$\begin{aligned}
&\int_{\Sigma_{k,j}} \kappa_b^3 (\hat{w}_k \boldsymbol{n}_k \cdot \overline{\boldsymbol{\xi}}_k + \hat{\boldsymbol{t}}_k \cdot \boldsymbol{n}_k \overline{\psi}_k)\, \mathrm{d}A \\
&\qquad = \int_{\Sigma_{k,j}} \frac{\kappa_b^3}{2} \Big(w_k \boldsymbol{n}_k \cdot \overline{\boldsymbol{\xi}}_k - \boldsymbol{t}_k \cdot \overline{\boldsymbol{\xi}}_k + \boldsymbol{t}_k \cdot \boldsymbol{n}_k \overline{\psi}_k - w_k \overline{\psi}_k \\
&\qquad\qquad + w_j \boldsymbol{n}_k \cdot \overline{\boldsymbol{\xi}}_k + \boldsymbol{t}_j \cdot \overline{\boldsymbol{\xi}}_k - \boldsymbol{t}_j \cdot \boldsymbol{n}_j \overline{\psi}_k + w_j \overline{\psi}_k \Big)\, \mathrm{d}A. \qquad (4.52)
\end{aligned}$$

Requiring that $\eta_1 = \kappa_b^3$, equation (4.52) is then

$$\begin{aligned}
&\int_{\Sigma_{k,j}} \kappa_b^3 (\hat{w}_k \boldsymbol{n}_k \cdot \overline{\boldsymbol{\xi}}_k + \hat{\boldsymbol{t}}_k \cdot \boldsymbol{n}_k \overline{\psi}_k)\, \mathrm{d}A \\
&\qquad = -\int_{\Sigma_{k,j}} \frac{1}{2\eta_1} \Big(\kappa_b^6 \boldsymbol{t}_k \cdot \boldsymbol{n}_k \overline{\boldsymbol{\xi}}_k \cdot \boldsymbol{n}_k - \kappa_b^3 \eta_1 \boldsymbol{t}_k \cdot \boldsymbol{n}_k \overline{\psi}_k \\
&\qquad\qquad - \eta_1 w_k \overline{\boldsymbol{\xi}}_k \cdot \boldsymbol{n}_k + \eta_1 w_k \eta_1 \overline{\psi}_k \Big)\, \mathrm{d}A \\
&\qquad\quad + \int_{\Sigma_{k,j}} \frac{1}{2\eta_1} \Big(- \kappa_b^6 \boldsymbol{t}_j \cdot \boldsymbol{n}_j \overline{\boldsymbol{\xi}}_k \cdot \boldsymbol{n}_k - \kappa_b^3 \boldsymbol{t}_j \cdot \boldsymbol{n}_j \eta_1 \overline{\psi}_k \\
&\qquad\qquad + \eta_1 w_j \kappa_b^3 \overline{\boldsymbol{\xi}}_k \cdot \boldsymbol{n}_k + \eta_1 w_j \eta_1 \overline{\psi}_k \Big)\, \mathrm{d}A.
\end{aligned}$$

Rearranging terms and taking into account the complex conjugation, gives

$$\begin{aligned}
&\int_{\Sigma_{k,j}} \kappa_b^3 (\hat{w}_k \boldsymbol{n}_k \cdot \overline{\boldsymbol{\xi}}_k + \hat{\boldsymbol{t}}_k \cdot \boldsymbol{n}_k \overline{\psi}_k)\, \mathrm{d}A \\
&\quad = -\int_{\Sigma_{k,j}} \frac{1}{2\eta_1} \left(i\kappa_b^3 \boldsymbol{t}_k \cdot \boldsymbol{n}_k - i\eta_1 w_k \right) \overline{\left(i\kappa_b^3 \boldsymbol{\xi}_k \cdot \boldsymbol{n}_k - i\eta_1 \psi_k \right)}\, \mathrm{d}A \\
&\quad + \int_{\Sigma_{k,j}} \frac{1}{2\eta_1} \left(i\kappa_b^3 \boldsymbol{t}_j \cdot \boldsymbol{n}_j - i\eta_1 w_j \right) \overline{\left(-i\kappa_b^3 \boldsymbol{\xi}_k \cdot \boldsymbol{n}_k - i\eta_1 \psi_k \right)}\, \mathrm{d}A. \quad (4.53)
\end{aligned}$$

Similarly, using the definitions of the fluxes in (4.49), the second and the third term in equation (4.46) can be written as

$$\begin{aligned}
&\int_{\Sigma_{k,j}} \kappa_b^3 (\hat{\boldsymbol{s}}_k \cdot \boldsymbol{n}_k \overline{\phi}_k + \hat{u}_k \boldsymbol{n}_k \cdot \overline{\boldsymbol{\varphi}}_k)\, \mathrm{d}A \\
&\quad = \int_{\Sigma_{k,j}} \kappa_b^3 \Big\{ \left(\frac{\boldsymbol{s}_k + \boldsymbol{s}_j}{2} - \frac{1}{2}(u_k \boldsymbol{n}_k + u_j \boldsymbol{n}_j) \right) \cdot \boldsymbol{n}_k \overline{\phi} \\
&\qquad + \left(\frac{u_k + u_j}{2} - \frac{1}{2}(\boldsymbol{s}_k \cdot \boldsymbol{n}_k + \boldsymbol{s}_j \cdot \boldsymbol{n}_j) \right) \boldsymbol{n}_k \cdot \overline{\boldsymbol{\varphi}}_k \Big\}\, \mathrm{d}A.
\end{aligned}$$

Rearranging terms in a similar manner as before (taking u_k and $\boldsymbol{s}_k$

terms first and u_j and $\boldsymbol{s}_j$ terms last), one obtains

$$\begin{aligned}
&\int_{\Sigma_{k,j}} \kappa_b^3(\hat{\mathbf{s}}_k \cdot \boldsymbol{n}_k\overline{\phi}_k + \hat{u}_k\boldsymbol{n}_k \cdot \overline{\boldsymbol{\varphi}}_k)\,\mathrm{d}A \\
&\quad= \int_{\Sigma_{k,j}} \kappa_b^3\Bigg\{ \left(\frac{\boldsymbol{s}_k}{2} - \frac{1}{2}u_k\boldsymbol{n}_k\right)\cdot \boldsymbol{n}_k\overline{\phi}_k + \left(\frac{u_k}{2} - \frac{1}{2}\boldsymbol{s}_k\cdot\boldsymbol{n}_k\right)\boldsymbol{n}_k\cdot\overline{\boldsymbol{\varphi}}_k \\
&\qquad + \left(\frac{\boldsymbol{s}_j}{2} - \frac{1}{2}u_j\boldsymbol{n}_j\right)\cdot \boldsymbol{n}_k\overline{\phi}_k + \left(\frac{u_j}{2} - \frac{1}{2}\boldsymbol{s}_j\cdot\boldsymbol{n}_j\right)\boldsymbol{n}_k\cdot\overline{\boldsymbol{\varphi}}_k\Bigg\}\,\mathrm{d}A. \quad (4.54)
\end{aligned}$$

Equation (4.54) can be simplified some more to get

$$\begin{aligned}
&\int_{\Sigma_{k,j}} \kappa_b^3(\hat{\mathbf{s}}_k \cdot \boldsymbol{n}_k\overline{\phi}_k + \hat{u}_k\boldsymbol{n}_k \cdot \overline{\boldsymbol{\varphi}}_k)\,\mathrm{d}A \\
&\quad= \int_{\Sigma_{k,j}} \frac{\kappa_b^3}{2}\Bigg\{ \boldsymbol{s}_k\cdot\boldsymbol{n}_k\overline{\phi}_k - u_k\boldsymbol{n}_k\cdot\boldsymbol{n}_k\overline{\phi}_k \\
&\qquad + u_k\boldsymbol{n}_k\cdot\overline{\boldsymbol{\varphi}}_k - \boldsymbol{s}_k\cdot\boldsymbol{n}_k\boldsymbol{n}_k\cdot\overline{\boldsymbol{\varphi}}_k + \boldsymbol{s}_j\cdot\boldsymbol{n}_k\overline{\phi}_k \\
&\qquad - u_j\boldsymbol{n}_j\cdot\boldsymbol{n}_k\overline{\phi}_k + u_j\boldsymbol{n}_k\cdot\overline{\boldsymbol{\varphi}}_k - \boldsymbol{s}_j\cdot\boldsymbol{n}_j\boldsymbol{n}_k\cdot\overline{\boldsymbol{\varphi}}_k\Bigg\}\,\mathrm{d}A.
\end{aligned}$$

Requiring that $\eta_2 = \kappa_b^{-1}$ and using the fact that $\boldsymbol{n}_k = -\boldsymbol{n}_j$ on the interface $\Sigma_{k,j}$, to have

$$\begin{aligned}
&\int_{\Sigma_{k,j}} \kappa_b^3(\hat{\mathbf{s}}_k \cdot \boldsymbol{n}_k\overline{\phi}_k + \hat{u}_k\boldsymbol{n}_k \cdot \overline{\boldsymbol{\varphi}}_k)\,\mathrm{d}A \\
&\quad= \int_{\Sigma_{k,j}} \frac{1}{2\eta_2}\Bigg\{ \kappa_b\boldsymbol{s}_k\cdot(\eta_2\kappa_b^2\boldsymbol{n}_k\overline{\phi}_k) - \eta_2\kappa_b^2u_k(\eta_2\kappa_b^2\overline{\phi}_k) \\
&\qquad + \eta_2\kappa_b^2u_k(\kappa_b\boldsymbol{n}_k\cdot\overline{\boldsymbol{\varphi}}_k) - \kappa_b\boldsymbol{s}_k\cdot\boldsymbol{n}_k(\kappa_b\boldsymbol{n}_k\cdot\overline{\boldsymbol{\varphi}}_k) \\
&\qquad - \kappa_b\boldsymbol{s}_j\cdot\boldsymbol{n}_k(\eta_2\kappa_b^2\overline{\phi}_k) + \eta_2\kappa_b^2u_j(\eta_2\kappa_b^2\overline{\phi}_k) \\
&\qquad + \eta_2\kappa_b^2u_j(\kappa_b\boldsymbol{n}_k\cdot\overline{\boldsymbol{\varphi}}_k) - \kappa_b\boldsymbol{s}_j\cdot\boldsymbol{n}_j(\kappa_b\boldsymbol{n}_k\cdot\overline{\boldsymbol{\varphi}}_k)\Bigg\}\,\mathrm{d}A.
\end{aligned}$$

Rearranging and simplifying terms still further gives

$$\begin{aligned}
&\int_{\Sigma_{k,j}} \kappa_b^3(\hat{\mathbf{s}}_k \cdot \boldsymbol{n}_k\overline{\phi}_k + \hat{u}_k\boldsymbol{n}_k \cdot \overline{\boldsymbol{\varphi}}_k)\,\mathrm{d}A \\
&\quad= -\int_{\Sigma_{k,j}} \frac{1}{2\eta_2}(-i\kappa_b\boldsymbol{s}_k\cdot\boldsymbol{n}_k + i\eta_2\kappa_b^2u_k)(i\kappa_b\overline{\boldsymbol{\varphi}}_k\cdot\boldsymbol{n}_k - i\eta_2\kappa_b^2\overline{\phi}_k)\,\mathrm{d}A \\
&\qquad + \int_{\Sigma_{k,j}} \frac{1}{2\eta_2}(-i\kappa_b\boldsymbol{s}_j\cdot\boldsymbol{n}_j + i\eta_2\kappa_b^2u_j)(-i\kappa_b\overline{\boldsymbol{\varphi}}_k\cdot\boldsymbol{n}_k - i\eta_2\kappa_b^2\overline{\phi}_k)\,\mathrm{d}A.
\end{aligned}$$

Taking into account the complex conjugation and rearranging terms one can deduce that

$$\begin{aligned}
&\int_{\Sigma_{k,j}} \kappa_b^3(\hat{\mathbf{s}}_k \cdot \boldsymbol{n}_k \overline{\phi}_k + \hat{u}_k \boldsymbol{n}_k \cdot \overline{\boldsymbol{\varphi}}_k)\,\mathrm{d}A \\
&\quad = -\int_{\Sigma_{k,j}} \frac{1}{2\eta_2}(-i\kappa_b \boldsymbol{s}_k \cdot \boldsymbol{n}_k + i\eta_2\kappa_b^2 u_k)\overline{(-i\kappa_b \boldsymbol{\varphi}_k \cdot \boldsymbol{n}_k + i\eta_2\kappa_b^2\phi_k)}\,\mathrm{d}A \\
&\quad + \int_{\Sigma_{k,j}} \frac{1}{2\eta_2}(-i\kappa_b \boldsymbol{s}_j \cdot \boldsymbol{n}_j + i\eta_2\kappa_b^2 u_j)\overline{(i\kappa_b \boldsymbol{\varphi}_k \cdot \boldsymbol{n}_k + i\eta_2\kappa_b^2\phi_k)}\,\mathrm{d}A. \quad (4.55)
\end{aligned}$$

Combining equations (4.53) and (4.55), the integral over the element interfaces $\Sigma_{k,j}$ can be written as

$$\begin{aligned}
&\int_{\Sigma_{k,j}} \kappa_b^3(\hat{w}_k \boldsymbol{n}_k \cdot \overline{\boldsymbol{\xi}}_k + \hat{\boldsymbol{t}}_k \cdot \boldsymbol{n}_k \overline{\psi}_k + \hat{\mathbf{s}}_k \cdot \boldsymbol{n}_k \overline{\phi}_k + \hat{u}_k \boldsymbol{n}_k \cdot \overline{\boldsymbol{\varphi}}_k)\,\mathrm{d}A \\
&\quad = -\int_{\Sigma_{k,j}} \frac{1}{2\eta_1}\left(i\kappa_b^3 \boldsymbol{t}_k \cdot \boldsymbol{n}_k - i\eta_1 w_k\right)\overline{\left(i\kappa_b^3 \boldsymbol{\xi}_k \cdot \boldsymbol{n}_k - i\eta_1\psi_k\right)}\,\mathrm{d}A \\
&\quad + \int_{\Sigma_{k,j}} \frac{1}{2\eta_1}\left(i\kappa_b^3 \boldsymbol{t}_j \cdot \boldsymbol{n}_j - i\eta_1 w_j\right)\overline{\left(-i\kappa_b^3 \boldsymbol{\xi}_k \cdot \boldsymbol{n}_k - i\eta_1\psi_k\right)}\,\mathrm{d}A \\
&\quad - \int_{\Sigma_{k,j}} \frac{1}{2\eta_2}(-i\kappa_b \boldsymbol{s}_k \cdot \boldsymbol{n}_k + i\eta_2\kappa_b^2 u_k)\overline{(-i\kappa_b \boldsymbol{\varphi}_k \cdot \boldsymbol{n}_k + i\eta_2\kappa_b^2\phi_k)}\,\mathrm{d}A \\
&\quad + \int_{\Sigma_{k,j}} \frac{1}{2\eta_2}(-i\kappa_b \boldsymbol{s}_j \cdot \boldsymbol{n}_j + i\eta_2\kappa_b^2 u_j)\overline{(i\kappa_b \boldsymbol{\varphi}_k \cdot \boldsymbol{n}_k + i\eta_2\kappa_b^2\phi_k)}\,\mathrm{d}A. \quad (4.56)
\end{aligned}$$

Taking into account the integral equations on the boundary (4.47) and interior interfaces (4.56) the method can be summarized in the

following equation

$$
\begin{aligned}
0 &= \int_{\partial K_k} \kappa_b^3 (\hat{w}_k \boldsymbol{n}_k \cdot \overline{\boldsymbol{\xi}}_k + \hat{\boldsymbol{t}}_k \cdot \boldsymbol{n}_k \overline{\psi}_k + \hat{\boldsymbol{s}}_k \cdot \boldsymbol{n}_k \overline{\phi}_k + \hat{u}_k \boldsymbol{n}_k \cdot \overline{\boldsymbol{\varphi}}_k) \, \mathrm{d}A \\
&= -\int_{\partial K_k} \frac{1}{2\eta_1} \left(i\kappa_b^3 \boldsymbol{t}_k \cdot \boldsymbol{n}_k - i\eta_1 w_k \right) \overline{\left(i\kappa_b^3 \boldsymbol{\xi}_k \cdot \boldsymbol{n}_k - i\eta_1 \psi_k \right)} \, \mathrm{d}A \\
&\quad + \int_{\Sigma_{k,j}} \frac{1}{2\eta_1} \left(i\kappa_b^3 \boldsymbol{t}_j \cdot \boldsymbol{n}_j - i\eta_1 w_j \right) \overline{\left(-i\kappa_b^3 \boldsymbol{\xi}_k \cdot \boldsymbol{n}_k - i\eta_1 \psi_k \right)} \, \mathrm{d}A \\
&\quad - \int_{\partial K_k} \frac{1}{2\eta_2} (-i\kappa_b \boldsymbol{s}_k \cdot \boldsymbol{n}_k + i\eta_2 \kappa_b^2 u_k) \overline{(-i\kappa_b \boldsymbol{\varphi}_k \cdot \boldsymbol{n}_k + i\eta_2 \kappa_b^2 \phi_k)} \, \mathrm{d}A \\
&\quad + \int_{\Sigma_{k,j}} \frac{1}{2\eta_2} (-i\kappa_b \boldsymbol{s}_j \cdot \boldsymbol{n}_j + i\eta_2 \kappa_b^2 u_j) \overline{(i\kappa_b \boldsymbol{\varphi}_k \cdot \boldsymbol{n}_k + i\eta_2 \kappa_b^2 \phi_k)} \, \mathrm{d}A \\
&\quad + \int_{\Gamma_k} \frac{1}{2\eta_1} (-i\kappa_b^3 \boldsymbol{t}_k \cdot \boldsymbol{n}_k - i\eta_1 w_k) \overline{(-i\kappa_b^3 \boldsymbol{\xi}_k \cdot \boldsymbol{n}_k - i\eta_1 \psi_k)} \, \mathrm{d}A \\
&\quad + \int_{\Gamma_k} \frac{1}{2\eta_2} (i\kappa_b \boldsymbol{s}_k \cdot \boldsymbol{n}_k + i\eta_2 \kappa_b^2 u_k) \overline{(i\kappa_b \boldsymbol{\varphi}_k \cdot \boldsymbol{n}_k + i\eta_2 \kappa_b^2 \phi_k)} \, \mathrm{d}A. \quad (4.57)
\end{aligned}
$$

Now using boundary conditions (4.34) and (4.35), equation (4.57) can be written as

$$
\begin{aligned}
&\int_{\partial K_k} \frac{1}{2\eta_1} \left(i\kappa_b^3 \boldsymbol{t}_k \cdot \boldsymbol{n}_k - i\eta_1 w_k \right) \overline{\left(i\kappa_b^3 \boldsymbol{\xi}_k \cdot \boldsymbol{n}_k - i\eta_1 \psi_k \right)} \, \mathrm{d}A \\
&\quad - \int_{\Sigma_{k,j}} \frac{1}{2\eta_1} \left(i\kappa_b^3 \boldsymbol{t}_j \cdot \boldsymbol{n}_j - i\eta_1 w_j \right) \overline{\left(-i\kappa_b^3 \boldsymbol{\xi}_k \cdot \boldsymbol{n}_k - i\eta_1 \psi_k \right)} \, \mathrm{d}A \\
&\quad + \int_{\partial K_k} \frac{1}{2\eta_2} (-i\kappa_b \boldsymbol{s}_k \cdot \boldsymbol{n}_k + i\eta_2 \kappa_b^2 u_k) \overline{(-i\kappa_b \boldsymbol{\varphi}_k \cdot \boldsymbol{n}_k + i\eta_2 \kappa_b^2 \phi_k)} \, \mathrm{d}A \\
&\quad - \int_{\Sigma_{k,j}} \frac{1}{2\eta_2} (-i\kappa_b \boldsymbol{s}_j \cdot \boldsymbol{n}_j + i\eta_2 \kappa_b^2 u_j) \overline{(i\kappa_b \boldsymbol{\varphi}_k \cdot \boldsymbol{n}_k + i\eta_2 \kappa_b^2 \phi_k)} \, \mathrm{d}A \\
&\quad - \int_{\Gamma_k} \frac{Q_1}{2\eta_1} (i\kappa_b^3 \boldsymbol{t}_k \cdot \boldsymbol{n}_k - i\eta_1 w_k) \overline{(-i\kappa_b^3 \boldsymbol{\xi}_k \cdot \boldsymbol{n}_k - i\eta_1 \psi_k)} \, \mathrm{d}A \\
&\quad - \int_{\Gamma_k} \frac{Q_2}{2\eta_2} (-i\kappa_b \boldsymbol{s}_k \cdot \boldsymbol{n}_k + i\eta_2 \kappa_b^2 u_k) \overline{(i\kappa_b \boldsymbol{\varphi}_k \cdot \boldsymbol{n}_k + i\eta_2 \kappa_b^2 \phi_k)} \, \mathrm{d}A \\
&= \int_{\Gamma_k} \frac{1}{2\eta_1} g_1 \overline{(-i\kappa_b^3 \boldsymbol{\xi}_k \cdot \boldsymbol{n}_k - i\eta_1 \psi_k)} \, \mathrm{d}A \\
&\quad + \int_{\Gamma_k} \frac{1}{2\eta_2} g_2 \overline{(i\kappa_b \boldsymbol{\varphi}_k \cdot \boldsymbol{n}_k + i\eta_2 \kappa_b y^2 \phi_k)} \, \mathrm{d}A. \quad (4.58)
\end{aligned}
$$

Using now (4.30)-(4.33) and (4.42)-(4.45), equation (4.58) can be writ-

ten as

$$\begin{aligned}
&\int_{\partial K_k} \frac{1}{2\eta_1}\left(-\frac{\partial \Delta w_k}{\partial \boldsymbol{n}_k} - i\eta_1 w_k\right)\overline{\left(-\frac{\partial \Delta \psi_k}{\partial \boldsymbol{n}_k} - i\eta_1 \psi_k\right)}\,\mathrm{d}A \\
&\quad - \int_{\Sigma_{k,j}} \frac{1}{2\eta_1}\left(\frac{\partial \Delta w_j}{\partial \boldsymbol{n}_k} - i\eta_1 w_j\right)\overline{\left(\frac{\partial \Delta \psi_k}{\partial \boldsymbol{n}_k} - i\eta_1 \psi_k\right)}\,\mathrm{d}A \\
&\quad + \int_{\partial K_k} \frac{1}{2\eta_2}\left(-\frac{\partial w_k}{\partial \boldsymbol{n}_k} - i\eta_2 \Delta w_k\right)\overline{\left(-\frac{\partial \psi_k}{\partial \boldsymbol{n}_k} - i\eta_2 \Delta \psi_k\right)}\,\mathrm{d}A \\
&\quad - \int_{\Sigma_{k,j}} \frac{1}{2\eta_2}\left(\frac{\partial w_j}{\partial \boldsymbol{n}_k} - i\eta_2 \Delta w_j\right)\overline{\left(\frac{\partial \psi_k}{\partial \boldsymbol{n}_k} - i\eta_2 \Delta \psi_k\right)}\,\mathrm{d}A \\
&\quad - \int_{\Gamma_k} \frac{Q_1}{2\eta_1}\left(-\frac{\partial \Delta w_k}{\partial \boldsymbol{n}_k} - i\eta_1 w_k\right)\overline{\left(\frac{\partial \Delta \psi_k}{\partial \boldsymbol{n}_k} - i\eta_1 \psi_k\right)}\,\mathrm{d}A \\
&\quad - \int_{\Gamma_k} \frac{Q_2}{2\eta_2}\left(-\frac{\partial w_k}{\partial \boldsymbol{n}_k} - i\eta_2 \Delta w_k\right)\overline{\left(\frac{\partial \psi_k}{\partial \boldsymbol{n}_k} - i\eta_2 \Delta \psi_k\right)}\,\mathrm{d}A \\
&= \int_{\Gamma_k} \frac{1}{2\eta_1} g_1 \overline{\left(\frac{\partial \Delta \psi_k}{\partial \boldsymbol{n}_k} - i\eta_1 \psi_k\right)}\,\mathrm{d}A + \int_{\Gamma_k} \frac{1}{2\eta_2} g_2 \overline{\left(\frac{\partial \psi_k}{\partial \boldsymbol{n}_k} - i\eta_2 \Delta \psi_k\right)}\,\mathrm{d}A.
\end{aligned} \tag{4.59}$$

Following [35, 48, 125, 132] and defining a new unknown $\mathcal{X}_k \in (L^2(\partial K_k))^2$, $k = 1, \ldots, N$ as

$$\mathcal{X}_k = \begin{pmatrix} -\frac{\partial \Delta w_k}{\partial \boldsymbol{n}_k} - i\eta_1 w_k \\ -\frac{\partial w_k}{\partial \boldsymbol{n}_k} - i\eta_2 \Delta w_k \end{pmatrix} \quad \text{on } \partial K_k, \tag{4.60}$$

and writing $\mathcal{Y}_k \in (L^2(\partial K_k))^2$ and $F_k(\mathcal{Y}_k) \in (L^2(\partial K_k))^2$, $k = 1, \ldots, N$ so that

$$\text{if} \quad \mathcal{Y}_k = \begin{pmatrix} -\frac{\partial \Delta \psi_k}{\partial \boldsymbol{n}_k} - i\eta_1 \psi_k \\ -\frac{\partial \psi_k}{\partial \boldsymbol{n}_k} - i\eta_2 \Delta \psi_k \end{pmatrix} \quad \text{then} \quad F_k(\mathcal{Y}_k) = \begin{pmatrix} \frac{\partial \Delta \psi_k}{\partial \boldsymbol{n}_k} - i\eta_1 \psi_k \\ \frac{\partial \psi_k}{\partial \boldsymbol{n}_k} - i\eta_2 \Delta \psi_k \end{pmatrix}$$

on ∂K_k.

Then the UWVF can be written as finding $\mathcal{X}_k \in (L^2(\partial \Omega_k))^2$, $1 \leq k \leq N$, such that

$$\begin{aligned}
&\sum_{k=1}^{N} \int_{\partial K_k} \eta^{-1} \mathcal{X}_k \cdot \overline{\mathcal{Y}}_k \,\mathrm{d}A - \sum_{k=1}^{N} \sum_{j=1, k\neq j}^{N} \int_{\Sigma_{k,j}} \eta^{-1} \mathcal{X}_j \cdot \overline{F_k(\mathcal{Y}_k)}\,\mathrm{d}A \\
&- \sum_{k=1}^{N} \int_{\Gamma_k} Q\eta^{-1} \mathcal{X}_k \cdot \overline{F_k(\mathcal{Y}_k)}\,\mathrm{d}A = \sum_{k=1}^{N} \int_{\Gamma_k} \eta^{-1} \boldsymbol{g} \cdot \overline{F_k(\mathcal{Y}_k)}\,\mathrm{d}A
\end{aligned} \tag{4.61}$$

for all $\mathcal{Y}_k \in (L^2(\partial K_k))^2$, $1 \leq k \leq N$ where

$$\eta = \begin{pmatrix} \eta_1 & 0 \\ 0 & \eta_2 \end{pmatrix}, \quad Q = \begin{pmatrix} Q_1 & 0 \\ 0 & Q_2 \end{pmatrix} \quad \text{and} \quad \boldsymbol{g} = \begin{pmatrix} g_1 \\ g_2 \end{pmatrix}.$$

4.2.2 Basis functions

In the original UWVF scheme in acoustics, elasticity and electromagnetism [35, 48, 125] propagating plane wave basis functions are used. However, if φ_k satisfies the homogeneous fourth order partial differential equation:

$$\Delta^2 \varphi_k - \kappa_b^4 \varphi_k = 0 \quad \text{in } K_k$$

for all $k = 1, \ldots, N$, the solution φ_k can be decomposed into two parts [231] as follows

$$\varphi_k = \varphi_k^{PW} + \varphi_k^{EW}$$

where

$$\begin{aligned} \Delta \varphi_k^{PW} + \kappa_b^2 \varphi_k^{PW} &= 0 \quad \text{in } K_k, \\ \Delta \varphi_k^{EW} - \kappa_b^2 \varphi_k^{EW} &= 0 \quad \text{in } K_k. \end{aligned}$$

Motivated by this observation, we choose the basis for the discrete UWVF in K_k to consist of evanescent and propagating waves. The basis $\varphi_{k,\ell}^{PW}$ consists of propagating plane waves, $\ell = 1, \ldots, p_k^{PW}$, where p_k^{PW} is the number of basis functions. The plane wave basis $\varphi_{k,\ell}^{PW}$ is thus

$$\varphi_{k,\ell}^{PW} = \begin{cases} \exp(i\overline{\kappa}_{b,k} \boldsymbol{d}_{k,\ell} \cdot \boldsymbol{x}), & \text{in } K_k, \\ 0, & \text{elsewhere}, \end{cases} \tag{4.62}$$

where the direction is given by

$$\boldsymbol{d}_{k,\ell} = \left(\cos\left(2\pi \frac{\ell - 1}{p_k^{PW}} \right), \sin\left(2\pi \frac{\ell - 1}{p_k^{PW}} \right) \right).$$

The basis $\varphi_{k,\ell}^{EW}$ is chosen to be the evanescent wave basis, with $\ell = 1, \ldots, p_k^{EW}$, and is given by

$$\varphi_{k,\ell}^{EW} = \begin{cases} \exp(\overline{\kappa}_{b,k} \boldsymbol{d}_{k,\ell} \cdot (\boldsymbol{x} - \boldsymbol{x}_{k,0})), & \text{in } K_k, \\ 0, & \text{elsewhere,} \end{cases} \tag{4.63}$$

where $x_{k,0}$ is the centroid of the element K_k. The scaling for the basis provided by $\exp(\overline{\kappa}_{b,k} \boldsymbol{d}_{k,\ell} \cdot \boldsymbol{x}_{k,0})$ in (4.63), is intended to help the robustness of the UWVF matrix (control ill-conditioning). The above basis (4.63) is referred to as "corner waves" by Ladevèze et al. (cf. [56]).

After discretization the matrix form can be written as follows

$$(\mathrm{D} - \mathrm{C})\boldsymbol{X} = \boldsymbol{b},$$

where matrix D is Hermitian and block diagonal while block matrix C consists of diagonal ($Q_1 \neq 0$ or $Q_2 \neq 0$) and off-diagonal blocks. For example, first and third integrals on the right hand side of (4.59):

$$\begin{aligned} &\int_{\partial K_k} \frac{1}{2\eta_1} \left(-\frac{\partial \Delta w_k}{\partial \boldsymbol{n}_k} - i\eta_1 w_k \right) \overline{\left(-\frac{\partial \Delta \psi_k}{\partial \boldsymbol{n}_k} - i\eta_1 \psi_k \right)} \, \mathrm{d}A \\ &+ \int_{\partial K_k} \frac{1}{2\eta_2} \left(-\frac{\partial w_k}{\partial \boldsymbol{n}_k} - i\eta_2 \Delta w_k \right) \overline{\left(-\frac{\partial \psi_k}{\partial \boldsymbol{n}_k} - i\eta_2 \Delta \psi_k \right)} \, \mathrm{d}A \end{aligned}$$

forms the D matrix.

4.2.3 Error estimate

The estimates outlined herein are from the original paper **IV** following [35, 125]. The global solution space is $X = \Pi_{k=1}^{N} (L^2(K_k))^2$ and the X inner product is now defined by

$$(u, v)_X = \sum_{k=1}^{N} \int_{\partial K_k} \eta^{-1} u \cdot \overline{v}$$

with the norm $\|u\|_X^2 = (u, u)_X$. Let the best approximation operator be defined as $P^h : X \to X^h$ in the X norm. Choosing $|Q_1| \leq \delta_1 < 1$

and $|Q_2| \leq \delta_2 < 1$ such that $\delta_1 \leq \delta < 1$ and $\delta_2 \leq \delta < 1$, then on the boundary Γ the following basic error estimate holds

$$\|\mathcal{X} - \mathcal{X}^h\|_{(L^2(\Gamma))^2} \leq \frac{2}{\sqrt{1-\delta^2}} \|\mathcal{X} - P^h\mathcal{X}\|_X.$$

For the plate UWVF, the error estimates in the domain Ω with respect to L^2 norm are not yet available. This could be the topic of further research (in particular using the approximation properties of plane wave and evanescent wave functions).

4.3 THE UWVF IN ACOUSTICS

The acoustic UWVF is better known than the UWVFs for linear elasticity and plate vibration problems described earlier in this chapter. Therefore, in this thesis only the final form of the acoustic UWVF will be given. More details about the derivation of the acoustic UWVF can be found from [35, 51, 125, 132] and see also original publications **I,III**. For simplicity we only consider problems in $\mathbb{R}^2$. Let again $\Omega \subset \mathbb{R}^2$ be a bounded computational domain with the boundary Γ.

To allow us to study fluid-fluid interface problems as considered in the article **III**. Let the refractive index n of the media be piecewise constant so that the material properties and the wave number κ are constant on each element in the mesh. Then, the Helmholtz equation (2.17) can be written as

$$\Delta p_a + n^2\kappa^2 p_a = 0 \quad \text{in } \Omega. \tag{4.64}$$

The first order system for this Helmholtz equation is obtained by introducing a vector variable $\boldsymbol{v}$, so that

$$in\kappa p_a = -\nabla \cdot \boldsymbol{v}, \tag{4.65}$$

$$in\kappa \boldsymbol{v} = -\nabla p_a. \tag{4.66}$$

The boundary condition for the first order system (4.65) and (4.66) is

$$(-in\kappa \boldsymbol{v} \cdot \boldsymbol{n} - i\eta p_a) = Q\,(in\kappa \boldsymbol{v} \cdot \boldsymbol{n} - i\eta p_a) + g, \quad \text{on } \Gamma, \tag{4.67}$$

where η is the numerical flux parameter, $Q \in \mathbb{C}$, $|Q| \leq 1$ defines the boundary conditions (Dirichlet: $Q = -1$, Neumann: $Q = 1$ or Robin: $|Q| < 1$) and g is the acoustic source term on the boundary Γ. In our work the numerical flux parameter is chosen to

$$\eta = n_k \kappa_k \quad \text{on } \Gamma_k \quad \text{and} \quad \eta = \frac{n_k \kappa_k + n_j \kappa_j}{2} \quad \text{on } \Sigma_{k,j}$$

where n_k is the refractive index in K_k (and n_j in K_j).

For the test functions $(\boldsymbol{\tau}, \zeta)$ we assume that they satisfy the following equations

$$-in\kappa\boldsymbol{\tau} = \nabla\zeta, \tag{4.68}$$

$$-\nabla \cdot \boldsymbol{\tau} = in\kappa\zeta, \tag{4.69}$$

in K_k, equivalently $\Delta\zeta + n^2\kappa^2\zeta = 0$. From (4.65), (4.66), (4.67), (4.68) and (4.69), the UWVF is to find $\mathcal{X}_k \in L^2(\partial K_k)$, $k = 1, \ldots, N$, so that

$$\begin{aligned}\sum_{k=1}^{N} \int_{\partial K_k} \frac{1}{\eta} \mathcal{X}_k \overline{\mathcal{Y}_k} \mathrm{d}A - \sum_{k=1}^{N} \sum_{j=1, k\neq j}^{N} \int_{\Sigma_{k,j}} \frac{1}{\eta} \mathcal{X}_j \overline{F_k(\mathcal{Y}_k)} \mathrm{d}A \\ - \sum_{k=1}^{N} \int_{\Gamma_k} \frac{Q}{\eta} \mathcal{X}_k \overline{F_k(\mathcal{Y}_k)} \mathrm{d}A = \sum_{k=1}^{N} \int_{\Gamma_k} \frac{1}{\eta} g \overline{F_k(\mathcal{Y}_k)} \mathrm{d}A\end{aligned} \tag{4.70}$$

for all $\mathcal{Y}_k \in L^2(\partial K_k)$, $k = 1, \ldots, N$ where

$$\mathcal{X}_k = \left(in\kappa \boldsymbol{v}_k \cdot \boldsymbol{n}_k - i\eta p_{a,k}\right).$$

Similarly, $\mathcal{Y}_k$ can be written as

$$\mathcal{Y}_k = \left(in\kappa \boldsymbol{\tau}_k \cdot \boldsymbol{n}_k - i\eta \zeta_k\right)$$

and $F_k(\mathcal{Y}_k)$ as

$$F_k(\mathcal{Y}_k) = \left(-in\kappa \boldsymbol{\tau}_k \cdot \boldsymbol{n}_k - i\eta \zeta_k\right).$$

The discretized form of the acoustic UWVF is obtained by replacing in (4.70) $\mathcal{X}_k$ by $\mathcal{X}_k^h$ given by

$$\mathcal{X}_k^h = \sum_{\ell=1}^{p_k} \mathcal{X}_k \left(-\frac{\partial \varphi_{k,\ell}}{\partial \boldsymbol{n}_k} - i\eta \varphi_{k,\ell} \right),$$

where p_k is the number of basis functions in element K_k and $\varphi_{k,\ell}$ satisfies the adjoint Helmholtz equation $\Delta\overline{\varphi}_{k,\ell} + n^2\kappa^2\overline{\varphi}_{k,\ell} = 0$ and can be chosen to be plane wave as in (3.15). New basis function choices for the acoustic UWVF are considered in the Section 4.3.1.

Similarly, $\mathcal{Y}_k$ in (4.70) is replaced by $\mathcal{Y}_k^h$ that is

$$\mathcal{Y}_k^h = \sum_{\ell=1}^{p_k} \mathcal{Y}_k \left(-\frac{\partial \varphi_{k,\ell}}{\partial \boldsymbol{n}_k} - i\eta\varphi_{k,\ell} \right),$$

and $F_k(\mathcal{Y}_k)$ in (4.70) is replaced by $F_k^h(\mathcal{Y}_k^h)$ such that

$$F_k^h(\mathcal{Y}_k^h) = \sum_{\ell=1}^{p_k} \mathcal{Y}_k \left(\frac{\partial \varphi_{k,\ell}}{\partial \boldsymbol{n}_k} - i\eta\varphi_{k,\ell} \right).$$

As for other problems, the acoustic UWVF can be written in the matrix form

$$(\mathrm{D} - \mathrm{C})\boldsymbol{X} = \boldsymbol{b}.$$

4.3.1 Basis functions

In this section, only the new basis functions which are used in articles **I** and **III** will be outlined. Besides the new basis functions, in articles **I** and **III** the traditional plane wave basis (3.15) is also used in the UWVF.

The Bessel basis has been investigated first for the UWVF in [129] for the Maxwell and Navier equations. However, in the original publication **I** the unscaled Bessel basis was introduced for acoustics as

$$\varphi_{k,\ell} = \begin{cases} J_\ell(n_k\overline{\kappa}_k|\boldsymbol{x}_k - \boldsymbol{x}_{0,k}|)e^{i\ell\theta} & \text{in } K_k, \\ 0 & \text{elsewhere.} \end{cases} \tag{4.71}$$

where $J_\ell(\cdot)$ is the Bessel function of first kind and order ℓ, $1 \leq \ell \leq p_k$, the angle (using a local coordinate system centered at the centroid of the element $\boldsymbol{x}_0$) is denoted by θ and $|\cdot|$ is the euclidean norm.

We also consider a basis that is tailored to the L-shaped domain problem and is called the modified Bessel basis. The aim is to improve the accuracy of the UWVF when a singularity occurs in the corner. The modified Bessel basis is given by

$$\varphi_{k,\ell} = \begin{cases} J_{|\ell|}(n_k\overline{\kappa}_k|\boldsymbol{x}_k - \boldsymbol{x}_{0,k}|)e^{i\ell\theta} \text{ in } K_k \text{ and if } \ell = -2/3, \\ J_\ell(n_k\overline{\kappa}_k|\boldsymbol{x}_k - \boldsymbol{x}_{0,k}|)e^{i\ell\theta} \text{ in } K_k \text{ and if } \ell \neq -2/3, \\ 0, \text{ elsewhere,} \end{cases} \tag{4.72}$$

where the order ℓ is chosen as

$$\ell = \begin{cases} s - \frac{p_k-3}{2} - 1, \text{ when } s = 1, \ldots, p_k - 2, \\ \frac{2}{3}, \text{ when } s = p_k - 1, \\ -\frac{2}{3}, \text{ when } s = p_k. \end{cases}$$

In the original publication **III**, a scaled Bessel function basis was considered. The idea is to scale the Bessel functions to help with conditioning. This new Bessel basis also has scaling term and it is given by

$$\varphi_{k,\ell} = \begin{cases} \frac{J_\ell(n_k\overline{\kappa}|\boldsymbol{x}-\boldsymbol{x}_0|)e^{i\ell\theta}}{n_k\overline{\kappa}\sqrt{|J'_\ell(n_k\overline{\kappa}h_k)|^2+|J_\ell(n_k\overline{\kappa}h_k)|^2}} & \text{in } K_k, \\ 0 & \text{elsewhere,} \end{cases} \tag{4.73}$$

where the order is $\ell = -(p_k-1)/2, \ldots, (p_k-1)/2$, $|\cdot|$ denotes the complex modulus, $\boldsymbol{x}_0$ is the centroid of the element, θ is the angle and J'_ℓ is the first derivative of Bessel function J_ℓ. The mesh size h_k in the denominator is chosen to be the longest edge of the element. In the case of Bessel basis functions the number of basis functions p_k needs to be odd.

In the article **III**, the fluid-fluid interface problem and new evanescent wave basis functions were investigated. To motivate this basis, we now consider two subdomains occupied by different fluids. Let n_1 denote the refractive index of fluid 1 in domain Ω^1 and $n_2 < n_1$ be the refractive index of fluid 2 in domain Ω^2. Suppose a wave is incident on domain Ω^2 from Ω^1. Total internal reflection occurs (evanescent waves on Ω^2) if the incidence angle θ_{inc} of the incident plane wave on the fluid-fluid interface is smaller than the

critical angle θ_{crit}. When $\theta_{\text{inc}} > \theta_{\text{crit}}$, plane waves propagates in both domains. This can be seen from Snell's law as

$$n_1 \cos(\theta_{\text{inc}}) = n_2 \cos(\theta_{\text{T}}),$$

where θ_{T} is the transmission angle from fluid-fluid interface, see Figure 4.1. Then the critical angle is

$$\theta_{\text{crit}} = \cos^{-1}\left(\frac{n_2}{n_1}\right).$$

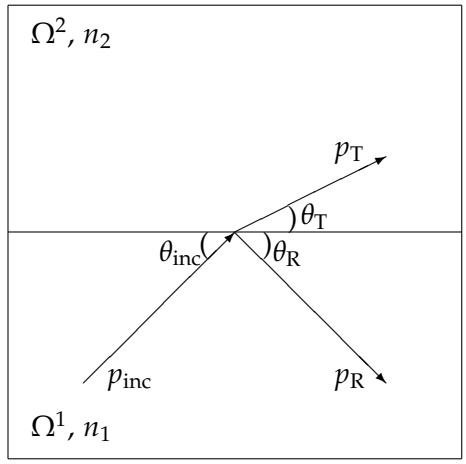

Figure 4.1: Schematic figure of the fluid-fluid interface problem. The incident plane wave is denoted by p_{inc}, reflected wave field is denoted by p_{R} and transmitted wave field is denoted by p_{T}. The angle of incidence wave is denoted by θ_{inc}, angle of reflected wave is θ_{R} and angle of transmitted wave is θ_{T}. The domain Ω^1 has refractive index $n_1 > n_2$ and the domain Ω^2 has refractive index n_2.

In [47] it was observed that in acoustics the plane wave basis does not capture the rapidly decaying wave fields efficiently and in elasticity [48] the same phenomena was revealed for rapidly decaying elastic Rayleigh waves. For the DEM [49, 55] new evanescent wave basis functions were introduced for fluid-fluid and fluid-solid interface problems in order to capture the rapidly decaying evanescent wave modes efficiently. The evanescent wave (EW) basis for

the UWVF in K_k can be written, see the article **III**, as

$$\varphi_{k,\tilde{\ell}}^{EW} = \begin{cases} \exp\left(\left(\mathrm{A}^{-1}\begin{pmatrix} x-x_0 \\ y-y_0 \end{pmatrix}\right)\cdot\begin{pmatrix} i\alpha_{k,\tilde{\ell}} \\ \beta_{k,\tilde{\ell}} \end{pmatrix}\right) & \tilde{\ell} \text{ odd}, \\ \exp\left(\left(\mathrm{A}^{-1}\begin{pmatrix} x-x_0 \\ y-y_0 \end{pmatrix}\right)\cdot\begin{pmatrix} -i\alpha_{k,\tilde{\ell}} \\ \beta_{k,\tilde{\ell}} \end{pmatrix}\right) & \tilde{\ell} \text{ even}, \\ 0 & \text{elsewhere}, \end{cases} \tag{4.74}$$

where the centroid of the element K_k is (x_0, y_0), $\alpha_{k,\tilde{\ell}} = n_1\kappa\cos(\theta_{k,\tilde{\ell}}^{EW})$ and $\beta_{k,\tilde{\ell}} = \sqrt{(n_1\kappa)^2(\cos(\theta_{k,\tilde{\ell}}^{EW}))^2 - (n_2\kappa)^2}$. If $(x_0, y_0) = (0,0)$ is chosen on all elements the basis will be called the unscaled EW basis and if $(x_0, y_0) \neq (0,0)$ it is called a scaled EW basis. The matrix A will be given shortly and is tailored to the direction of evanescent decay in fluid-fluid interface problems. The choices of angles θ^{EW} is used in the evanescent wave basis (4.74) are shown in Table 4.1.

Table 4.1: Angles θ^{EW} in the evanescent wave basis functions (4.74). On the left column is shown the number of evanescent wave basis functions.

EW-basis functions	$\theta^{EW,1}$	$\theta^{EW,2}$	$\theta^{EW,3}$	$\theta^{EW,4}$
2	$\frac{1}{2}\theta_{\text{crit}}$			
4	$\frac{1}{3}\theta_{\text{crit}}$	$\frac{2}{3}\theta_{\text{crit}}$		
6	$\frac{1}{4}\theta_{\text{crit}}$	$\frac{1}{2}\theta_{\text{crit}}$	$\frac{3}{4}\theta_{\text{crit}}$	
8	$\frac{1}{5}\theta_{\text{crit}}$	$\frac{2}{5}\theta_{\text{crit}}$	$\frac{3}{5}\theta_{\text{crit}}$	$\frac{4}{5}\theta_{\text{crit}}$

4.3.2 Error estimates

For the sake of completeness we now recall the basic error estimates of the acoustic UWVF [35, 125]. An L^2 norm estimate is borrowed from [51]. This work has been one of the main motivations for our derivation of the error estimates of the elastic UWVF.

Following [35,125], the global solution space is $X = \Pi_{k=1}^{N} L^2(K_k)$ and the X inner product is defined by

$$(u, v)_X = \sum_{k=1}^{N} \int_{\partial K_k} \eta^{-1} u \cdot \overline{v}$$

with the norm $\|u\|_X^2 = (u, u)_X$. Choosing $|Q| \leq \delta < 1$, then on the boundary Γ the following basic error estimate hold

$$\|\mathcal{X} - \mathcal{X}^h\|_{L^2(\Gamma)} \leq \frac{2}{\sqrt{1-\delta^2}} \|\mathcal{X} - P^h \mathcal{X}\|_X,$$

where P^h is the X-orthogonal projection onto X^h where X^h is the approximation subspace (PW, EW, Bessel, etc.).

The following $L^2(\Omega)$ error estimate in 2D is from Buffa and Monk [51, Theorem 4.1] and can be written as

$$\|p_a - p_a^h\|_{L^2(\Omega)} \leq C h^{-\frac{1}{2}} \|(I - P^h)\mathcal{X}\|_X.$$

In [51, 125] it is observed that in 2D when the number of basis functions is chosen as $p = 2q_a + 1$, the following error estimate holds

$$\|\mathcal{X} - \mathcal{X}^h\|_{L^2(\Gamma)} \leq C h^{q_a - 1/2} \|p_a\|_{\mathcal{C}^{q_a+1}(\Omega)},$$

where $\mathcal{C}^{q_a+1}$ refers to $q_a + 1$ continuously differentiable functions. Then, as discussed in [51], the following estimate holds

$$\|p_a - p_a^h\|_{L^2(\Omega)} \leq C h^{q_a - 1} \|p_a\|_{\mathcal{C}^{q_a+1}(\Omega)}.$$

5 Numerical results

This chapter is devoted to presenting the more significant numerical results from each original paper **I-IV**. The results will be given in chronological order of appearance. Paper **I** discussed a new Bessel basis function (4.71) and problems with singularities. In the second paper **II** numerical results for the 3D elastic UWVF were compared with the theoretical error estimates. The third paper **III** focused on mixed element shapes (triangles and quadrilaterals), rapidly decaying wave fields and the use of Bessel (4.73) and evanescent wave basis functions (4.74). The fourth paper **IV** concerned solving a thin elastic plate problem using the UWVF.

5.1 PAPER I: MODIFIED BESSEL BASIS

Due to the fact that the plane wave based UWVF may suffer from ill-conditioning, in this work we tried to improve the robustness of the UWVF using Bessel basis functions. Bessel function bases have been used in other non-polynomial methods such as in the PUFEM [70], the LSM [39] and the VTCR [102–104].

It is also well-known that the presence of a singularity in the solution hampers the accuracy of numerical approximation methods. Investigations of problems, such as the Helmholtz equation on an L-shaped domain that result in singular solution have been considered using the *hp* cloud FEM [232], GFEM [30], WBM [45], MFS [233], the UWVF [41] and the coupled FEM-UWVF [135]. Strategies to improve the accuracy have included mesh refinement, use of higher degree basis functions or the use of special basis functions. For example, in the FEM the addition of certain singular functions to the approximation spaces was considered by Fix, Gulati and Wakoff [18] who found that this improved the accuracy. Also auxiliary mapping were used by Oh and Babuška [234]. For non-polynomial methods, problems with singular solutions were

approximated by constructing the basis using solutions of an infinite wedge problem [43, 45]. In addition, again for non-polynomial FEM, special functions can be computed in order to improve the accuracy near the corner singularities [42]. In another approach, a hybrid method consisting of the UWVF and the FEM (Raviart-Thomas elements) was introduced in [135] enhancing the approximation near a singularity. In paper **I** the focus was on improving the accuracy of the UWVF using fractional order Bessel basis functions.

5.1.1 Bessel basis function

The use of Bessel basis functions (4.71) for the L-shaped domain problem for the Helmholtz equation was investigated in article **I**. The performance of the Bessel basis functions (4.71) was compared with a standard plane wave basis (3.15).

A singular solution to the homogeneous Helmholtz problem in an L-shaped domain was considered. This is the same test case as in references [41, 126]. The computational domain is denoted by Ω. The boundary is $\Gamma = \Gamma_1 \cup \Gamma_2$ where Γ_1 denotes the two edges that meet at the origin and the other edges are denoted by Γ_2. The problem is to find the acoustic pressure field p_a such that

$$\begin{aligned} \Delta p_a + \kappa^2 p_a &= 0 \text{ in } \Omega, \\ p_a &= 0 \text{ on } \Gamma_1, \\ \frac{\partial p_a}{\partial \boldsymbol{n}} - i\eta p_a &= \frac{\partial p_a^{ex}}{\partial \boldsymbol{n}} - i\eta p_a^{ex} \text{ on } \Gamma_2, \end{aligned}$$

where the Dirichlet condition was chosen by setting $Q = -1$ on Γ_1, and the exact solution is $p_a^{ex}(r,\theta) = J_{\frac{2}{3}}(\kappa r)\sin\left(\frac{2}{3}\theta\right)$ where $r = |\boldsymbol{x}|$. This exact solution $p_a = p_a^{ex}$ has a singular gradient at the origin.

The uniform and non-uniform meshes which were used in the simulations are shown in Figure 5.1. The non-uniform mesh was heavily refined near the origin.

The results for the uniform mesh are shown in Table 5.1. The number of basis functions was chosen so that the relative error is

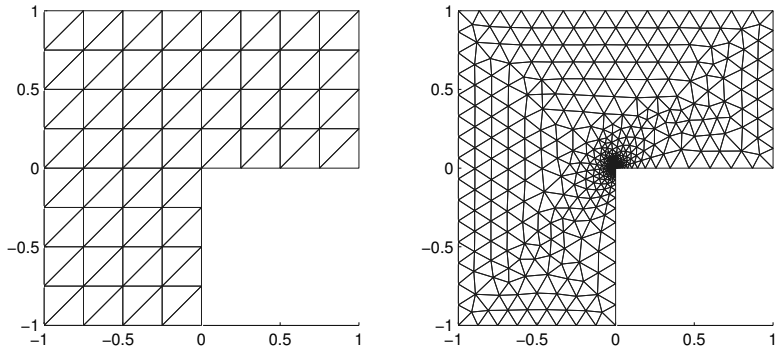

Figure 5.1: Uniform and non-uniform meshes used in the simulations.

roughly the same (1% - 3%) as the wave number κ varies. Relative errors are computed on a dense uniform point grid as follows

$$\text{error}(\%) = \frac{\|p_a^{ex} - p_a^h\|_{\ell^2}}{\|p_a\|_{\ell^2}} \times 100\%, \tag{5.1}$$

where p_a^h is the UWVF approximation and norm is computed as the discrete ℓ^2 norm.

In the case of Bessel functions (4.71) quadrature needs to be used when computing the integrals in the UWVF. Of course, in the case of a plane wave basis (3.15) integrals can be computed in closed form. The condition numbers for the plane wave basis (3.15) are similar to the condition numbers for the unscaled Bessel basis (4.71). In addition, the accuracy is similar for both bases (plane wave basis (3.15) and unscaled Bessel basis (4.71)).

5.1.2 Modified Bessel basis function

In article **I** the use of the modified Bessel basis (4.72) was examined on an L-shaped domain. This modified Bessel basis (4.72) was used in elements that have a vertex at the origin. In the case of a uniform mesh, five elements were enriched by the modified Bessel basis (4.72). In particular, the coupling of a plane wave basis and a modified Bessel basis was investigated. The modified Bessel basis

Table 5.1: Results for the uniform mesh in an L-shaped domain using plane wave (PW) basis (3.15) and unscaled Bessel basis (4.71). The maximum of condition number of block matrix D^k is denoted by max(Dcond).

Basis	κ	Uniform mesh		
		p	error(%)	max(Dcond)
PW	0.05	5	1.52	1.32e6
	0.5	5	1.06	1.31e4
	5	7	1.88	4.78e3
	50	25	2.90	3.35e5
Bessel (4.71)	0.05	5	1.52	1.05e6
	0.5	5	1.06	1.07e4
	5	7	1.85	4.26e3
	50	25	2.89	2.65e5

(4.72) was used again in elements that share an element vertex at the origin and elsewhere the plane wave basis (3.15) was used. This is a practical choice since it speeds up the computations because the use of Bessel basis functions require quadrature to compute the integrals. Results are shown in Table 5.2.

The results in Table 5.2 show that the modified Bessel basis (4.72) improves the accuracy of the UWVF compared to plane wave basis (3.15), especially at higher wave numbers. In addition, the results imply that the coupling of a plane wave basis (3.15) and the modified Bessel basis (4.72) causes no problems and the accuracy is similar to the case when only the modified Bessel basis (4.72) is used.

The results in Tables 5.1 and 5.2 are for a uniform mesh. The unstructured (non-uniform) mesh using the plane wave basis (3.15) and coupled plane wave (3.15) and modified Bessel basis (4.72) was also investigated. The number of basis functions per element was computed using the strategy shown in [41] (see also [235]) as fol-

Table 5.2: Results using uniform mesh in an L-shaped domain. The basis functions are plane wave basis functions (3.15), modified Bessel basis (4.72) and coupled strategy of using plane wave basis functions (3.15) and modified Bessel basis functions (4.72).

Basis	κ	Uniform mesh		
		p	error(%)	max(Dcond)
PW	0.05	5	1.52	1.32e6
	0.5	5	1.06	1.31e4
	5	7	1.88	4.78e3
	50	25	2.90	3.35e5
modified Bessel	0.05	5	1.08	1.05e6
	0.5	5	0.25	1.07e4
	5	7	0.09	4.26e3
	50	25	0.02	2.66e7
PW+modified Bessel	0.05	5	1.08	1.32e6
	0.5	5	0.25	1.31e4
	5	7	0.12	4.78e3
	50	25	0.02	2.66e7

lows

$$p_k = \texttt{round}(\kappa_k h_k + C(\kappa_k h_k)^{1/3}) \tag{5.2}$$

where h_k is the length of the longest edge of the element, C is a constant to be chosen $C = 8$ and if p_k was even then the number of basis functions was reduced by one to obtain an odd number. Again the modified Bessel basis (4.72) was used in elements that share a vertex in the origin coupled with the plane waves used elsewhere. The results are shown in Table 5.3.

The results suggest that at smaller element sizes the effect of the modified Bessel basis is not significant. This seems to be natural since the elements near the singularity are smaller so the modified Bessel basis is active on a smaller region. Therefore it can be concluded that using refined meshes the plane wave basis obtains good accuracy and the modified Bessel basis is not necessar-

Table 5.3: Results for the unstructured mesh in an L-shaped domain using plane wave basis (3.15) and coupling of plane wave basis (3.15) and modified Bessel basis (4.72). The number of basis functions per element was computed using (5.2) with $C = 8$.

Basis	κ	p	error(%)	max(Dcond)
PW	0.05	3	0.19	9.16
	0.5	3	0.19	9.16
	5	3...7	0.08	1.19e6
	50	5...23	0.09	2.45e11
PW+modified Bessel	0.05	3	0.19	2.21e3
	0.5	3	0.19	475.57
	5	3...7	0.09	1.19e6
	50	5...23	0.14	2.45e11

ily needed. On the other hand refining the grid size (h-version) increases the computational burden more (having more degrees of freedom) compared to increasing only the number of basis functions (p-version).

5.2 PAPER II: LINEAR ELASTICITY

The applications of the elastic wave simulations range from medical imaging to seismic exploration. In article **II**, one of the motivations was to extend the 2D elastic UWVF [48] to 3D. In addition another motivation for the linear elasticity article **II** was the derivation of the error estimates, so there were fewer numerical results in that paper. In particular, the aim was to test the convergence of the UWVF numerically and compare results with the theoretical error estimates.

5.2.1 Elastic plane wave in a unit cube

The problem is to find the displacement $\boldsymbol{u}$ such that

$$\begin{aligned} \sigma(\boldsymbol{u}) &= (\lambda \nabla \cdot \boldsymbol{u}) I + 2\mu\epsilon(\boldsymbol{u}) \quad \text{in } \Omega, \\ \nabla \cdot \sigma(\boldsymbol{u}) + \omega^2 \rho \boldsymbol{u} &= \boldsymbol{0} \quad \text{in } \Omega, \\ (\sigma(\boldsymbol{u})\boldsymbol{n} - i\eta\boldsymbol{u}) &= \boldsymbol{g} \quad \text{on } \Gamma \end{aligned} \tag{5.3}$$

where the boundary condition (5.3) can be obtained from (4.3) by setting $Q = 0$. The source term $\boldsymbol{g}$ on the boundary Γ is

$$\boldsymbol{g} = (\sigma(\boldsymbol{u})\boldsymbol{n} - i\eta\boldsymbol{u})$$

where $\boldsymbol{u} = \boldsymbol{d}\exp(i\kappa_P \boldsymbol{d}\cdot\boldsymbol{x}) + \boldsymbol{d}^{\perp}\exp(i\kappa_S \boldsymbol{d}\cdot\boldsymbol{x}) + \boldsymbol{d}\times\boldsymbol{d}^{\perp}\exp(i\kappa_S \boldsymbol{d}\cdot\boldsymbol{x})$ with the incident direction $\boldsymbol{d}$. Following the 2D elastic UWVF [48], the numerical flux η extended to 3D in article **II** was taken to be

$$\eta = \omega\rho(c_P \boldsymbol{n}\otimes\boldsymbol{n} + c_S(\boldsymbol{s}_1\otimes\boldsymbol{s}_1 + \boldsymbol{s}_2\otimes\boldsymbol{s}_2))$$

where $\boldsymbol{n}$ is the outward unit vector on a face, $\boldsymbol{s}_1$ and $\boldsymbol{s}_2$ are the orthogonal tangential unit vectors and $\otimes$ is defined as $\boldsymbol{n}\otimes\boldsymbol{n} = \boldsymbol{n}\boldsymbol{n}^T$, similarly for $\boldsymbol{s}_1\otimes\boldsymbol{s}_1$ and $\boldsymbol{s}_2\otimes\boldsymbol{s}_2$. The following properties hold for polarization vectors $|\boldsymbol{s}_1| = 1$, $|\boldsymbol{s}_2| = 1$ and $\boldsymbol{s}_1 \perp \boldsymbol{n}$, and $\boldsymbol{s}_2 = \boldsymbol{n}\times\boldsymbol{s}_1$.

In the first numerical test case we chose the frequency $f = 0.8\cdot 10^4$, angular frequency $\omega = 2\pi f = 5.0265\cdot 10^4$, Young's modulus $E = 200\cdot 10^9$, Poisson ratio $\nu = 0.3$ and density $\rho = 7800$. The Young's modulus, Poisson ratio and density are close to the material properties of steel. Then the speed of P-wave is $c_P = 5.8751\cdot 10^3$, the speed for S-wave is $c_S = 3.1404\cdot 10^3$, the P-wave number is $\kappa_P = 8.5557$ and the S-wave number is $\kappa_S = 16.0062$.

Following [48], the optimal ratio for p^P and p^S was investigated for 3D linear elasticity. The following ratios were considered[1]: $p^P/p^S = 1$, $p^P/p^S = \mathrm{n}^2/(\mathrm{n}+1)^2$, $p^P/p^S = \mathrm{n}^2/(\mathrm{n}+2)^2$ and $p^P/p^S = \mathrm{n}^2/(\mathrm{n}+3)^2$ where $\mathrm{n}\in\mathbb{N}$. The results are shown in Figure 5.2. The relative errors were computed using an average of the

[1]Note that here n refers to an integer $\mathrm{n}\in\mathbb{N}$ whereas in acoustics n refers to the index of refraction.

errors on chosen x-, y- and z-planes as follows

$$\text{error}(\%) = \frac{1}{3}\left(\frac{\|\boldsymbol{u} - \boldsymbol{u}^h\|_{\ell^2(x=0.3)}}{\|\boldsymbol{u}\|_{\ell^2(x=0.3)}} + \frac{\|\boldsymbol{u} - \boldsymbol{u}^h\|_{\ell^2(y=0.3)}}{\|\boldsymbol{u}\|_{\ell^2(y=0.3)}} + \frac{\|\boldsymbol{u} - \boldsymbol{u}^h\|_{\ell^2(z=0.3)}}{\|\boldsymbol{u}\|_{\ell^2(z=0.3)}} \right) \times 100\%, \tag{5.4}$$

where $\boldsymbol{u}^h$ is the UWVF approximation, norm is computed as the discrete ℓ^2 norm on a planes $x = 0.3$, $y = 0.3$ and $z = 0.3$.

The mesh consists of uniform tetrahedral elements.

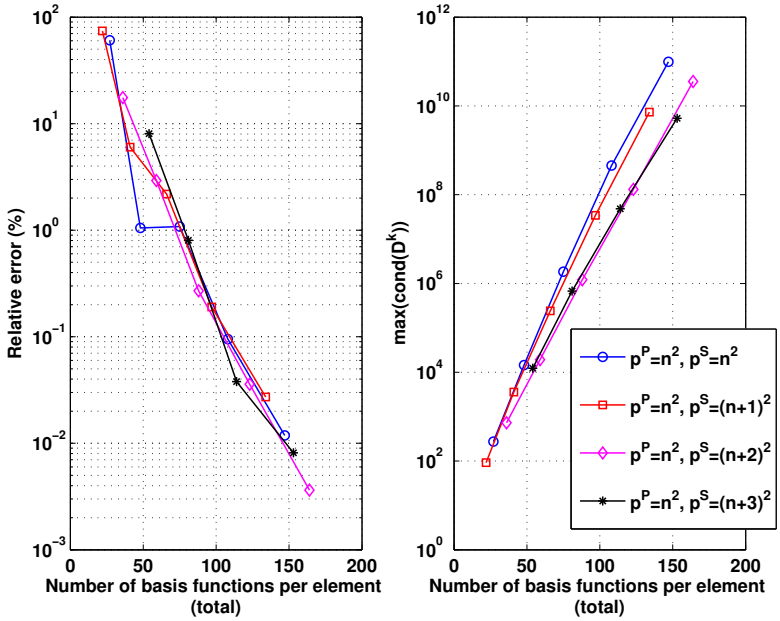

Figure 5.2: Results for elastic plane wave propagation in a unit cube with different number of basis functions p^P and p^S. The P-wave number is $\kappa_P = 8.5557$ and the S-wave number is $\kappa_S = 16.0062$.

The results shown in Figure 5.2 suggest that ratios p^P / p^S closer to one give larger condition numbers. This is expected since the P-wave and S-wave numbers are different. The results show surprisingly that the errors are rather similar regardless of the ratio of p^P / p^S.

The h-convergence was also examined in the article **II**. In this case the results were compared to the theoretical error estimate in (4.26). The frequency was taken to be $f = 1.2 \cdot 10^4$, angular frequency $\omega = 2\pi f = 7.5398 \cdot 10^4$, Young's modulus $E = 200 \cdot 10^9$, Poisson ratio $\nu = 0.3$, density $\rho = 7800$, P-wave number $\kappa_P = 12.8335$ and S-wave number $\kappa_S = 24.0093$. The number of P-wave basis functions was $p^P = 36$ and the number of S-wave basis functions was $p^S = 49$. That is $q_P = 5$ and $q_S = 6$ then $q_P \geq 2r_P + 1$ where $r_P \leq 2$ and similarly $q_S \geq 2r_S + 1$ where $r_S \leq 5/2$ (i.e. $r_S \leq 2$ since $r_S \in \mathbb{N}$).

The model problem again was elastic plane wave propagation in a unit cube and the incident direction of propagation was chosen as $\boldsymbol{d} = (-0.6838, 0.4558, 0.5698)$. Results are shown in Table 5.4 where the convergence rate for error is denoted by Order(error) and growth rate for the condition number is denoted by Order(cond).

Table 5.4: The h-convergence results for the elastic plane wave propagation. The P-wave number is $\kappa_P = 12.8335$ and the S-wave number is $\kappa_S = 24.0093$. The number of P-wave basis functions is $p^P = 36$ ($q_P = 5$) and S-wave basis functions $p^S = 49$ ($q_S = 6$).

h	error(%)	Order(error)	max(cond(D^k))	Order(cond)
1.0	54.1824	-	136.6296	-
0.5	25.1457	1.1075	1.4660e4	-6.7455
0.25	0.3063	6.3592	6.6385e7	-12.1448
0.125	0.0073	5.3909	1.7419e11	-11.3575

The results in Table 5.4 suggest that the order of convergence is similar to q^P or q^S (instead of r_P or r^S). This means that the theoretical error estimate in (4.26) could perhaps be improved. As discussed in **II**, an explanation for this is that error estimate (4.26) is derived via scalar and vector potential fields which may reduce the predicted order of convergence. At the finest mesh size the condition number is rather high.

Finally, in the article **II**, a case in which the theory does not predict convergence was investigated ($q_P = 2$ and $q_S = 4$). The

number of basis functions $p^P = 9$ and $p^S = 25$ were fixed and the mesh size h varied. If $q_P \geq 2r_P + 1$ and $q_S \geq 2r_S + 1$ that means $r_P \leq 1/2$ (i.e. $r_P = 0$ since $r_P \in \mathbb{N}$) and $r_S \leq 3/2$ (i.e. $r_S = 1$ since $r_S \in \mathbb{N}$). The P-wave number is $\kappa_P = 8.5557$ and the S-wave number is $\kappa_S = 16.0062$. Results are shown in Table 5.5.

Table 5.5: Results for the elastic plane wave propagation when $p^P = 9$ and $p^S = 25$. Then $q_P = 2$ and $r_P = 0$ and similarly $r_S \leq 3/2$ and $q_S = 4$.

h	error(%)	Order(error)	max(cond(D^k))	Order(cond)
1.0	90.6057	-	20.5633	-
0.5	38.8714	1.2209	200.2592	-3.3197
0.25	2.9209	3.7342	1.9154e4	-6.5796
0.125	0.1716	4.0893	2.0054e6	-6.7101
0.0625	0.0152	3.4969	1.5940e8	-6.3126

The results in Table 5.5 show convergence with $p^P = 9$ and $p^S = 25$ and the order of convergence is close to order 4. At the finest grid size, the condition number is high and growth in condition number is about order 6.5. Even though, the theory does not predict convergence, the numerical results show convergence, again indicating that better error estimates could likely be proved.

5.3 PAPER III: IMPROVEMENTS FOR THE UWVF

Element shapes and sizes affect the approximation and the robustness of the UWVF. In practice, the closer an element is to circular, the better condition numbers are expected since the regularity parameter is closer to one, see [51, 236]. Therefore, we investigated numerically how the element shapes affect the accuracy and conditioning of the UWVF. In particular, the use of mixed element meshes was investigated.

In addition to problems with singular solutions another challenging problem for plane wave based methods, such as the UWVF, are rapidly decaying (or evanescent) wave fields [47, 48]. Rapidly

decaying wave fields can be generated, for example, at fluid-fluid interfaces or in acoustic ducts, see [41, 237]. Strategies to improve the accuracy for the case of evanescent wave fields include, mesh refinement (h-version), increasing the number of basis functions (p-version), hp-version or the use of tailored basis functions. In DEM [49, 55] evanescent wave basis functions improved the accuracy in the fluid-fluid and fluid-solid interface problems when evanescent wave fields were present in the solution. Motivated by that work and results in [49, 55], the feasibility of using the evanescent wave basis functions (4.74) in the UWVF was tested numerically. The numerical results were for the fluid-fluid interface problems (straight interface and curved interface). Only the main numerical results in article **III**, will be outlined here.

5.3.1 Mixed element mesh

In practice the choice of basis functions, the element shapes and element sizes all affect the accuracy and conditioning of the UWVF. Therefore, our numerical tests included investigations of the effect of element shapes. The perfomance of the new scaled Bessel basis (4.73) was also examined.

First a very simple model problem, plane wave propagation in 2D, was considered. Let Ω be a computational domain with boundary Γ. The homogeneous Helmholtz problem is to find the time-harmonic pressure field p_a such that

$$\begin{aligned} \Delta p_a + \kappa^2 p_a &= 0 \text{ in } \Omega, \\ \frac{\partial p_a}{\partial \boldsymbol{n}} - i\eta p_a &= g \text{ on } \Gamma, \end{aligned}$$

where the Robin type boundary condition was used ($Q = 0$). The exact solution is

$$p_a = \exp(i\kappa \boldsymbol{d}_{\text{inc}} \cdot \boldsymbol{x}),$$

where the incident direction $\boldsymbol{d}_{\text{inc}} = (\cos(\pi/p), \sin(\pi/p))$ was not parallel to any of the directions used in the plane wave basis (3.15).

The wave number was chosen to be $\kappa = 40$. Relative errors were computed using equation (5.1).

The triangular mesh is shown in Figure 5.3 and results using this triangular mesh with 434 elements are shown in Table 5.6.

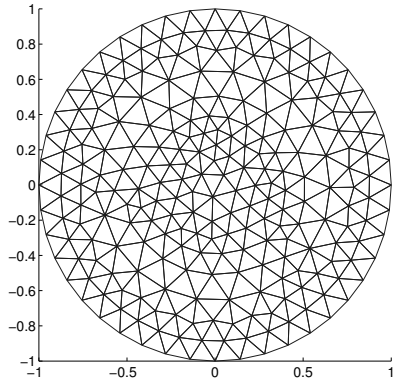

Figure 5.3: Triangular mesh with 434 elements.

Table 5.6: Results using triangular mesh with 434 elements and plane wave basis (3.15) and scaled Bessel basis (4.73).

Basis	p	error(%)	max(Dcond)	nnz($D - C$)
PW	7	70.40	60	8.3e4
	9	15.62	8.9e2	1.4e5
	11	1.74	2.7e4	2.0e5
	13	0.20	1.5e6	2.9e5
Bessel	7	36.20	68	8.3e4
	9	5.19	4.6e2	1.4e5
	11	0.71	4.4e3	2.0e5
	13	0.10	3.7e4	2.9e5

Results shown in Table 5.6 indicate that the accuracy is better when the scaled Bessel basis (4.73) is used compared with the results using the same number of plane wave basis functions (3.15).

In addition the condition number for the scaled Bessel basis (4.73) is smaller than for the plane wave basis (3.15). This implies that the scaling in the Bessel basis (4.73) has been a successful choice.

The mixed element mesh is shown in Figure 5.4 consisting of 226 triangular and 208 quadrilateral elements. The motivation for this study is that quadrilaterals can be used to fill the domain away from the boundary and triangles can be used to generate a mesh to approximate the complex details. However, the savings in time and the number of unknowns depends also on meshing strategies. In this particular example, the number of elements was chosen to be the same in the purely triangular mesh and in the mixed element mesh (that consists of triangles and quadrilaterals).

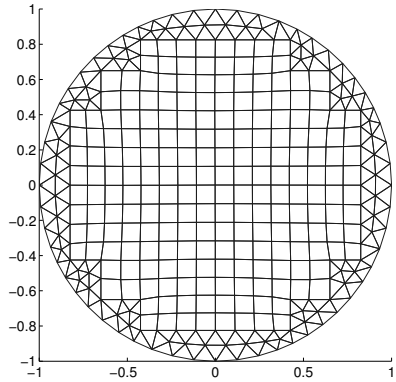

Figure 5.4: Mixed element mesh with 434 elements using 226 triangles and 208 quadrilaterals.

The results using the mixed element mesh are shown in Table 5.7, and suggest that the scaled Bessel (4.73) based UWVF has slightly better accuracy than the plane wave (3.15) based UWVF. The results in Table 5.7 are slightly better than those in Table 5.6 but this can partly be explained by the fact that the elements near the boundary are smaller in the mixed element case. The matrix filling is denser when using mixed elements due to the fact that the quadrilaterals have more edges than triangles and thus more neighboring elements. Therefore, the improvement in time and memory

Table 5.7: Results using mixed element mesh with 226 triangles and 208 quadrilaterals. Plane wave basis (3.15) and scaled Bessel basis (4.73) is used.

Basis	p_t	p_q	error(%)	max(Dcond)	nnz($D-C$)
PW	7	7	52.92	3.4e2	9.2e4
	9	9	6.56	8.1e3	1.5e5
	11	11	0.51	4.3e5	2.3e5
	13	13	0.08	4.6e7	3.2e5
Bessel	7	7	39.46	1.7e2	9.5e4
	9	9	3.84	1.7e3	1.5e5
	11	11	0.33	1.6e4	2.3e5
	13	13	0.06	1.4e5	3.2e5

requirements depend on the meshing strategy (and the choice of the number of basis functions per element which is not shown here). The results show that mixed elements can be successfully used in the UWVF but that improvements are less pronounced than we expected before the study.

5.3.2 Fluid-fluid interface problem with straight interface

Let Ω be divided into two subdomains $\Omega = \Omega^1 \cup \Omega^2$. Suppose the domain Ω^1 has refractive index n_1 and Ω^2 has refractive index n_2. The boundary of the domain Ω is denoted by Γ. The boundary of Ω^1 is denoted by $\partial\Omega^1$ and the boundary of Ω^2 is denoted by $\partial\Omega^2$. The 2D fluid-fluid interface problem is to find the pressure field p_a

such that

$$\Delta p_a^1 + n_1^2 \kappa^2 p_a^1 = 0 \quad \text{in } \Omega^1, \tag{5.5}$$

$$\Delta p_a^2 + n_2^2 \kappa^2 p_a^2 = 0 \quad \text{in } \Omega^2, \tag{5.6}$$

$$\frac{\partial p_a^1}{\partial \boldsymbol{n}} - i\eta p_a^1 = g \text{ on } \Gamma \cap \partial\Omega^1,$$

$$\frac{\partial p_a^2}{\partial \boldsymbol{n}} - i\eta p_a^2 = g \text{ on } \Gamma \cap \partial\Omega^2,$$

$$p_a^1 = p_a^2 \quad \text{on } \partial\Omega^1 \cap \partial\Omega^2, \tag{5.7}$$

$$\frac{\partial p_a^1}{\partial \boldsymbol{n}} = \frac{\partial p_a^2}{\partial \boldsymbol{n}} \quad \text{on } \partial\Omega^1 \cap \partial\Omega^2, \tag{5.8}$$

where n_i is the refractive index in domain Ω^i ($i = 1, 2$), η is an acoustic flux parameter and g is the source term on the boundary. The Robin type boundary condition $Q = 0$ was chosen.

The source term on the boundary Γ is

$$g = \frac{\partial p_a}{\partial \boldsymbol{n}} - in\kappa p_a$$

where n is either n_1 or n_2 and

$$p_a = \begin{cases} p_{\text{inc}} + p_R & \text{if } y < 0, \\ p_T & \text{if } y > 0. \end{cases} \tag{5.9}$$

In equation (5.9) the incident plane wave field was chosen $p_{\text{inc}} = \exp(i\kappa n_1(d_x x + d_y y))$ in Ω^1 where the incident direction

$$\boldsymbol{d} = (d_x, d_y) = (\cos(\theta_{\text{inc}}), \sin(\theta_{\text{inc}}))$$

with incident angle θ_{inc}. The reflected field can be written as $p_R = R\exp(i\kappa n_1(d_x x - d_y y))$ where the reflection coefficient is given by $R = -\frac{K_2 - \kappa n_1 d_y}{K_2 + \kappa n_1 d_y}$, where $K_1 = \kappa n_1 d_x$ and $K_2 = \kappa\sqrt{1 - n_1^2 d_x^2}$ with $\text{Im}(K_2) \geq 0$. The transmitted field in Ω^2 is $p_T = T\exp(i(K_1 x + K_2 y))$ where the transmission coefficient is $T = 1 + R = 1 - \frac{K_2 - \kappa n_1 d_y}{K_2 + \kappa n_1 d_y}$.

In our first tests, the enriched evanescent wave basis was only used on a one element layer in the domain Ω^2 where the evanescent wave fields were expected. In particular, only two evanescent wave

basis functions were used ($p_{ew} = 2$) since it has been shown to be an adequate choice for fluid-fluid interface problem in the original publication **III**. The matrix A in the evanescent wave basis (4.74) was chosen to be the 2×2 identity matrix. The wave number was chosen $\kappa = 25$ and the refractive indices $n_1 = 2$ and $n_2 = 1$. First, the h-convergence was investigated. The number of basis functions was chosen as $p_1 = 13$ in Ω^1, $p_2 = 7$ in Ω^2 and $p_3 = 9$ or $p_3 = p_2 + p_{EW}$ with $p_{EW} = 2$ in Ω^3. One of the meshes is represented in Figure 5.5.

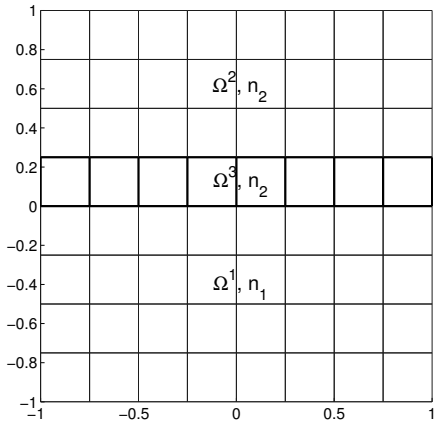

Figure 5.5: One of the meshes used in the simulation. The domain Ω^3 refers to the layer where the enriched evanescent wave basis functions (4.74) were used.

The results when the plane wave basis (3.15) is enriched with evanescent wave basis functions (4.74) are shown in Figure 5.6.

Figure 5.6 suggests that the evanescent wave basis (4.74) improves the accuracy and the condition numbers with enrichment and without enrichement are rather similar. The effect of the evanescent wave basis (4.74) is diminished at the finest element sizes. In this case the thickness of the layer where the evanescent wave basis (4.74) was used was the element size and hence this degeneration as h decreases is plausible (cf. the case in singularity studies earlier with highly refined non-uniform mesh).

The Bessel basis functions (4.73) with the enriched evanescent

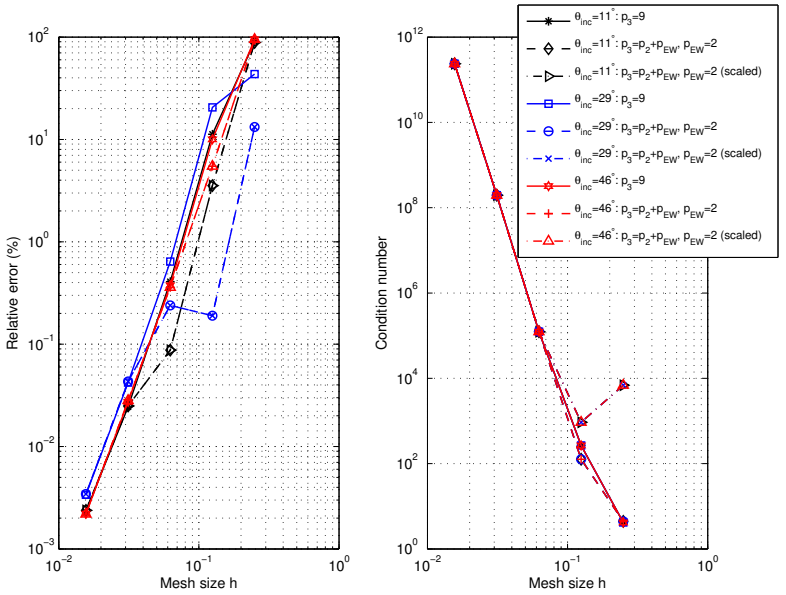

Figure 5.6: Results for h-convergence in the 2D fluid-fluid interface problem with fixed number of basis functions $p_1 = 13$ in Ω^1, $p_2 = 7$ in Ω^2 and $p_3 = 9$ or $p_3 = p_2 + p_{EW}$ with $p_{EW} = 2$ in Ω^3. The plane wave basis (3.15) was used and the plane wave basis (3.15) was enriched with the evanescent wave basis functions (4.74). Three different incident angles were considered $\theta_{\text{inc}} = 11^\circ$, $\theta_{\text{inc}} = 29^\circ$ and $\theta_{\text{inc}} = 46^\circ$. On the left figure is shown the results for the mesh size h versus the relative error (%). On the right figure is shown the condition number of matrix D^k versus the mesh size h.

wave basis (4.74) were also studied in the article **III**. The results are shown in Figure 5.7.

These results show that the Bessel based UWVF without enriched evanescent wave functions has the smallest condition numbers. However, when the Bessel basis (4.73) is enriched with the evanescent wave functions (4.74) the accuracy is improved but on the other hand the condition number is increased. The unscaled evanescent wave basis with Bessel basis has smaller condition numbers than Bessel basis with scaled enrichment. However, we see that the highest condition numbers in Figure 5.7 are smaller than the highest condition numbers in Figure 5.6.

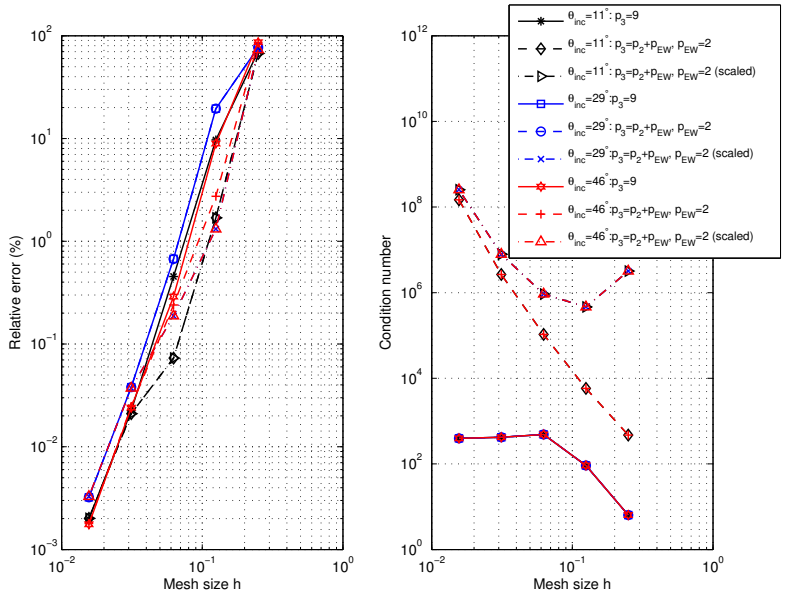

Figure 5.7: Results for h-convergence in the 2D fluid-fluid interface problem with fixed number of basis functions $p_1 = 13$ in Ω^1, $p_2 = 7$ in Ω^2 and $p_3 = 9$ or $p_3 = p_2 + p_{EW}$ with $p_{EW} = 2$ in Ω^3. The Bessel basis (4.73) was used and the Bessel basis (4.73) was enriched with the evanescent wave basis functions (4.74). Three different incident angles were considered $\theta_{\text{inc}} = 11°$, $\theta_{\text{inc}} = 29°$ and $\theta_{\text{inc}} = 46°$. On the left figure is shown the results for the mesh size h versus the relative error (%). On the right figure is shown the condition number of matrix D^k versus the mesh size h.

In the final numerical test case for a straight fluid-fluid interface in the article **III**, the number of basis functions was chosen based on the condition number. This strategy was originally introduced in [132] and was tailored in **III** to take into account the evanescent wave basis functions (4.74), for more details see the paper **III**. The strategy was to choose the number of plane wave basis functions so that the condition number does not exceed the set limit $(1 \cdot 10^6)$. Then, for the elements in the domain Ω^2 an enriched basis was accepted with $p_k - 2 + p_{ew}$ basis functions and $p_{ew} = 2$ if the resulting element condition number did not exceed the limit $(1 \cdot 10^6)$. In this case the thickness of the layer Ω^3 was based on the condition num-

ber and it could be less, equal or greater than one element. The results in Figure 5.7 imply that the evanescent wave basis (4.74) is not that well coupled (produces high condition number) with Bessel basis functions (4.73) (compared with the enriched plane wave basis (3.15) in Figure 5.6).

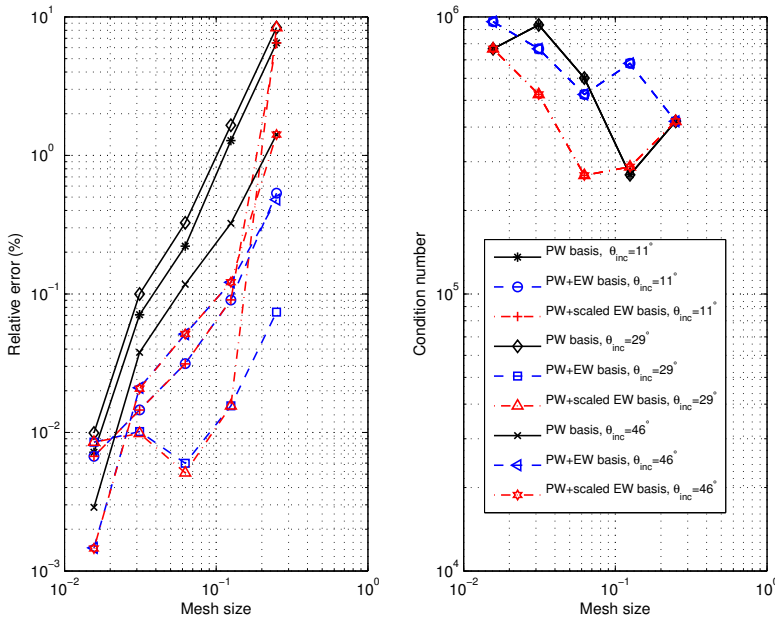

Figure 5.8: Results for the 2D fluid-fluid interface problem using plane wave basis functions (3.15) and plane wave basis (3.15) enriched with the evanescent wave basis functions (4.74).

The results shown in Figure 5.8 indicate that the effect of the evanescent wave basis (4.74) on improving accuracy is now more visible (compared to Figures 5.6 and 5.7). Our results show that a careful use of an evanescent wave basis improves the accuracy of the UWVF.

5.3.3 Transmission problem with curved interface

The transmission problem considered next is the model problem used in [132]. Again the behavior of the UWVF using plane wave basis (3.15) and plane wave basis (3.15) enriched with the evanescent wave basis functions (4.74) were in focus because this problem has regions with total internal reflection. The governing equations are shown in (5.5), (5.6), (5.7) and (5.8) and the following boundary condition was chosen

$$\frac{\partial p_a^1}{\partial r} - i\kappa p_a^1 = \left(\frac{\partial p_a^{\text{inc}}}{\partial r} - i\kappa p_a^{\text{inc}} \right) \quad \text{on } \Gamma, \tag{5.10}$$

where the incident field is $p_a^{\text{inc}} = \exp(i\kappa x)$.

Triangles with curved edges can easily be implemented in the UWVF. In particular, the contribution of integrals on the curved edge was computed as in [132] using quadrature.

The matrix A in the evanescent wave basis (4.74) was chosen to allow the direction of evanescence to change. In particular, we used

$$\mathrm{A} = \begin{pmatrix} \tau_1 & \nu_1 \\ \tau_2 & \nu_2 \end{pmatrix} \tag{5.11}$$

where $\boldsymbol{\nu}_{\mathrm{A}} = (\nu_1, \nu_2)$ was chosen to be the unit normal for the circle pointing at the origin so $\boldsymbol{\nu}_{\mathrm{A}} = ((0,0) - \boldsymbol{x}_0)/(\|(0,0) - \boldsymbol{x}_0\|_2)$ with $\boldsymbol{x}_0$ denoting the centroid of the element. The tangential unit vector was chosen as $\boldsymbol{\tau}_{\mathrm{A}} = (\tau_1, \tau_2) = (\nu_2, -\nu_1)$. The plane wave basis (3.15) was enriched with the evanescent wave basis (4.74) in the interior circle ($r_2 = 0.6$) and in $0.6 < r \leq 1.0$ pure plane wave basis functions (3.15) were used.

The triangular mesh and a schematic figure for choosing the evanescent wave basis functions are shown in Figure 5.9. The wave number was chosen to be $\kappa = 15$. The refractive indices were chosen to be $n_1 = 4$ and $n_2 = 1$. The results using pure plane wave basis functions (3.15) in the UWVF are shown in Table 5.8.

The results using plane wave basis functions (3.15) enriched with the evanescent wave basis functions (4.74) are shown in Ta-

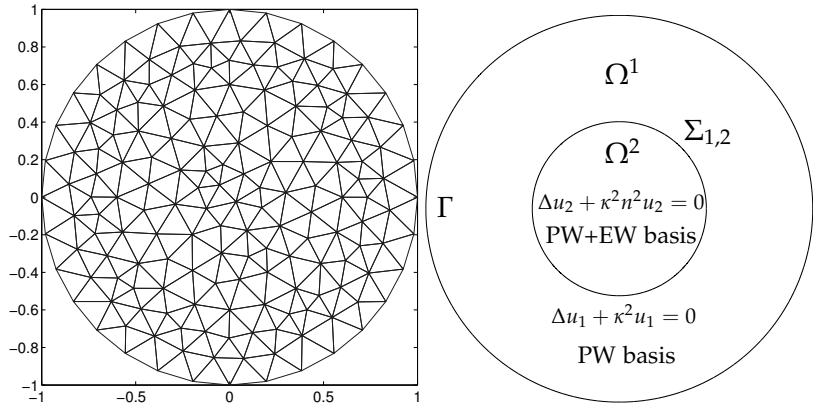

Figure 5.9: On the left is shown a mesh used in the simulations. The inner radius is $r_2 = 0.6$ and the outer radius is $r_1 = 1$. The mesh consists of 298 elements. On the right is a schematic figure where the enriched evanescent wave basis functions were used.

Table 5.8: Results for the transmission problem using pure plane wave basis functions (3.15). In the domain Ω^1 the number of basis functions is denoted by p_1 and in Ω^2 by p_2.

p_1	p_2	error (%)	max(Dcond)	length(b)
15	7	28.49	1.6e4	3.7e3
15	9	22.13	2.0e5	3.9e3
15	11	12.30	2.9e7	4.1e3
15	13	4.60	8.1e9	4.3e3
15	15	1.52	2.2e12	4.5e3
17	7	28.80	2.8e5	4.0e3
17	9	22.45	2.8e5	4.3e3
17	11	13.09	2.9e7	4.5e3
17	13	5.13	8.1e9	4.7e3

ble 5.9. In addition, the use of a different number of evanescent wave basis functions (4.74) is tested for a curved interface problem.

Results in Tables 5.8 and 5.9 imply that the evanescent wave basis functions (4.74) improves the accuracy. The results show that it is possible to use different numbers of evanescent wave basis

Table 5.9: Results for the transmission problem using plane wave basis (3.15) enriched with the evanescent wave basis functions (4.74). In the domain Ω^1 the number of plane wave basis functions is denoted by p_1 and in Ω^2 by p_2 and in Ω^2 the number of evanescent wave basis functions is denoted by p_{EW}.

p_1	p_2	p_{EW}	error (%)	max(Dcond)	length(b)
15	5	2	14.12	8.6e4	3.7e3
15	7	2	5.53	2.0e5	3.9e3
15	9	2	1.65	8.4e7	4.1e3
15	11	2	0.87	1.0e10	4.3e3
17	5	2	14.15	2.8e5	4.0e3
17	7	2	5.71	2.0e6	4.3e3
17	9	2	1.57	8.4e7	4.5e3
17	11	2	0.53	1.0e10	4.7e3
17	7	4	0.55	3.0e7	4.5e3
17	9	4	0.35	2.2e9	4.7e3
17	5	8	0.41	1.4e8	4.7e3

functions and interestingly the condition numbers are slightly lower when $p_{EW} = 4$ or $p_{EW} = 8$ are used. Perhaps, due to the rather general form of the evanescent wave basis in (4.74) with (5.11), it can be applied to other type of problems where evanescent wave fields are present.

5.4 PAPER IV: VIBRATION OF A THIN CLAMPED PLATE

Thin plate problems (and vibro-acoustic problems) occur in various fields in industry, for example, in the car industry. To date, the UWVF has been applied to second order elliptic PDEs (see Table 3.1). However, the WBM [123], VTCR [56] and DEM [174] have been successfully applied to Kirchhoff's thin plate problems. The dynamic Kirchhoff thin plate equation (4.27) is a fourth order PDE and two boundary conditions (4.28) and (4.29) are needed in order to solve the problem uniquely. This motivated us to investigate

the feasibility of the UWVF for thin clamped plate problems. The UWVF presented in the original publication **IV** and in this thesis is restricted to clamped plate type boundary conditions. This is the first attempt to approximate fourth order elliptic problems using the UWVF. In this section we give a review of the main numerical results of the paper **IV**.

5.4.1 Thin clamped plate problem

The inhomogeneous Kirchhoff plate equation with the clamped plate boundary conditions can be written as finding the displacement field w such that

$$\Delta^2 w - \kappa_b^4 w = \delta(\boldsymbol{x} - \boldsymbol{x}_0) \quad \text{in } \Omega, \tag{5.12}$$

$$w = 0 \quad \text{on the boundary } \Gamma, \tag{5.13}$$

$$\frac{\partial w}{\partial \boldsymbol{n}} = 0 \quad \text{on the boundary } \Gamma, \tag{5.14}$$

where $\delta(\boldsymbol{x} - \boldsymbol{x}_0)$ is Dirac's δ-function. The location of the volume source was chosen at the origin i.e. $\boldsymbol{x}_0 = (0, 0)$.

The derivation of the exact solution for the circular thin clamped plate problem is given in the original publication **IV**. The exact solution is

$$w = -\frac{i}{8\kappa^2}(H_0^{(1)}(i\kappa_b r) + H_0^{(2)}(\kappa r)) + a_0 J_0(\kappa_b r) + b_0 I_0(\kappa_b r) \tag{5.15}$$

where $H_0^{(1)}(\cdot)$ is the Hankel function of first kind and order zero, $H_0^{(2)}(\cdot)$ is the Hankel function of second kind and order zero, and the unknown coefficients a_0 and b_0 can be solved so that the exact solution satisfies the boundary conditions (5.13) and (5.14)) that is

$$\begin{pmatrix} J_0(\kappa_b r_1) & J_0(i\kappa_b r_1) \\ -\kappa_b J_1(\kappa_b r_1) & -i\kappa_b J_1(i\kappa_b r_1) \end{pmatrix} \begin{pmatrix} a_0 \\ b_0 \end{pmatrix} = \frac{i}{8\kappa_b^2} \begin{pmatrix} H_0^{(1)}(i\kappa_b r_1) + H_0^{(2)}(\kappa_b r_1) \\ -i\kappa_b H_1^{(1)}(i\kappa_b r_1) - \kappa H_1^{(2)}(\kappa_b r_1) \end{pmatrix}$$

where the radius of the computational domain is denoted by r_1.

It has been reported in [35, 125] that the UWVF approximation (or expected convergence rate) is not good for inhomogeneous problems compared to homogeneous problems when the inhomogeneous problem is approximated directly. Therefore, in the article **IV**, the solution w was first divided in two parts such that

$$w = w_{\text{smth}} + w_{\text{fund}}, \tag{5.16}$$

where $w_{\text{smth}} = a_0 J_0(\kappa_b r) + b_0 I_0(\kappa_b r)$ satisfies the homogeneous equation

$$\Delta^2 w_{\text{smth}} - \kappa_b^4 w_{\text{smth}} = 0 \quad \text{in } \Omega.$$

and $w_{\text{fund}} = -\frac{i}{8\kappa^2}(H_0^{(1)}(i\kappa_b r) + H_0^{(2)}(\kappa_b r))$ satisfies the inhomogeneous equation

$$\Delta^2 w_{\text{fund}} - \kappa_b^4 w_{\text{fund}} = \delta(x - x_0) \quad \text{in } \Omega.$$

We treated the field w_{smth} as unknown and sought to approximate it using the UWVF. Using the thin plate equation (5.12), the clamped plate boundary conditions (5.13), (5.14) and equation (5.16), we obtained the problem of finding the field w_{smth} so that

$$\begin{aligned} \Delta^2 w_{\text{smth}} - \kappa_b^4 w_{\text{smth}} &= 0 \quad \text{in } \Omega, \\ w_{\text{smth}} &= -w_{\text{fund}} \quad \text{on } \Gamma, \\ \frac{\partial w_{\text{smth}}}{\partial \boldsymbol{n}} &= -\frac{\partial w_{\text{fund}}}{\partial \boldsymbol{n}} \quad \text{on } \Gamma. \end{aligned}$$

In the UWVF the boundary conditions were implemented by setting $Q_1 = -1$, $Q_2 = 1$ and $g_1 = 2i\sigma_1 w_{\text{fund}}$ and $g_2 = -2\frac{\partial w_{\text{fund}}}{\partial \boldsymbol{n}}$ in (4.28) and (4.29). Again, the strategy introduced in [132] was used to model the curved boundary using quadrature. When the unknown field w_{smth} was solved using the UWVF, the total field w could be easily recovered using equation (5.16).

The plate bending wave number was $\kappa_b = 20$ and meshes are shown in Figure 5.10.

The basis functions in the UWVF were chosen to be the plane wave basis (4.62) together with the evanescent wave basis (4.63).

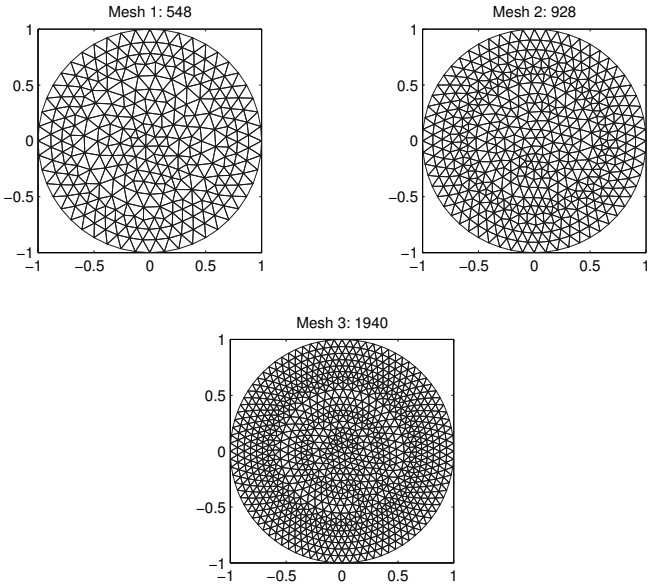

Figure 5.10: Meshes used in the clamped plate simulations. The number of triangular elements on the top left mesh is 548, on the top right mesh is 928. On the bottom row mesh consists of 1940 triangular elements.

The element sizes are roughly the same and a uniform number of basis functions per element was used. For the results shown here, the number of plane wave (4.62) and evanescent wave (4.63) basis functions was chosen to be equal. However, in the submitted conference paper [238] we investigated the thin plate problem using different numbers of basis functions per element. The results for p-convergence of the UWVF are shown in Figure 5.11. Relative errors were computed by applying equation (5.1).

The results in Figure 5.11 imply that the UWVF can accurately model the thin clamped plate problems. The results demonstrate p-convergence and suggest also h-convergence as expected. It is also shown that the accuracy plateaus for large p due to higher condition numbers.

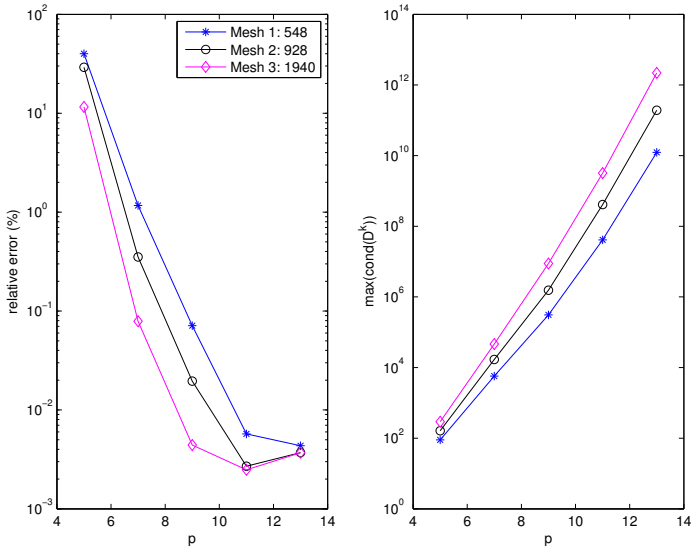

Figure 5.11: Results for thin circular clamped plate problem using three different meshes. The number of plane wave basis is p (as well as the number of evanescent wave basis functions). The plate bending wave number was $\kappa_b = 20$.

6 Conclusions

In this thesis the UWVF has been developed starting from first order systems of the PDEs and using an upwind DG scheme. The goal of the Ph.D. project was to improve the accuracy and stability of the UWVF in acoustics and further develop the method in mechanics applications including elasticty. In linear elasticity the main aim was to derive error estimate for the UWVF and extend the code for 3D problems. Finally, the first step of the UWVF towards the elastic thin plate problems was considered. In particular, the focus was to investigate the behavior of the UWVF with different basis functions.

For the acoustic UWVF, the Bessel basis improves the condition number and shows similar performance in convergence to plane waves. In particular, the accuracy of results using the Bessel basis tends to be better at the point when the plane wave basis suffers from ill-conditioning. The results indicate that Bessel bases are more stable than the plane wave basis. In addition, more general corner functions (similar to WBM [43]) can be applied in future in the UWVF in order to improve the accuracy near singularities in 2D.

In the case of fluid-fluid interface problems tailored evanescent wave bases are able to capture rapidly decaying wave fields. The plane wave and evanescent wave basis functions are more practical to use compared to the Bessel basis due to the fact that the integrals in the UWVF can be computed efficiently in closed form. In general, different basis function choices improved the accuracy of the UWVF in the presence of corner singularities and rapidly decaying waves. However, we still need to find a balance between the robustness of the method and the use of a priori information of the problem when choosing the basis.

The elastic UWVF was extended to 3D. The basis functions were chosen to be plane waves: P-wave, SH-wave (horizontal S-wave)

and SV-wave (vertical S-wave). To derive the UWVF, the Navier equation was written as a first order system and the UWVF was derived via a DG scheme. The error estimates were motivated by the work in [35, 39, 51, 52, 125, 152, 153]. The preliminary numerical results show that the UWVF is a feasible method to solve 3D elastic wave problems. In addition, based on numerical results, the error estimate of the elastic-UWVF could perhaps be improved.

The UWVF was tailored to thin clamped plate problems and thus the formulation is fairly simple and no "additional corner modes" are needed in the formulation (cf. twisting moments, see [55, 56, 123]). Numerical results show that the UWVF can cope with fourth order PDEs. The boundary conditions are written as "impedance type" and motivated by the integration by parts formula (see details in **IV**). In particular, the UWVF is derived from a first order system of equations via a DG scheme. In the UWVF, a plane wave basis and a decaying evanescent wave basis (similar to corner wave) need to be combined. This is consistent with theoretical work by Vekua [231], who showed that the solution of the fourth order Kirchhoff thin plate equation can be written as a sum of a solution of the Helmholtz equation and solution of the modified Helmholtz equation. Other basis functions that satisfy the Helmholtz equation or the modified Helmholtz equation could also be used.

Further research on applications of the UWVF could include general plate problems with free plate and simply supported boundary conditions. In this case the formulation most likely needs to have corner moments (twisting moments) and the UWVF becomes more complex. One option is to follow the DEM approach [50] by using Lagrange multipliers (but only at the vertices). In addition, error estimates for the plate-UWVF could be investigated (using the approximation of plane waves and evanescent waves). It might also be interesting to investigate the use of evanescent (edge) basis functions for plate vibration problems. In addition, as in [68], perhaps wave-bands could be studied in determine conditioning and investigate theoretical error estimates, for example, in acoustic problems.

Motivated by Table 3.1, the advection-diffusion or poroelastic problems could also be investigated using the UWVF with tailored basis functions. Now it is also possible to extend, the 2D fluid-solid code [48] to a 3D fluid-solid problem with the evanescent wave basis, which could provide a useful solver for high intensity focused ultrasound (HIFU) applications.

Bibliography

[1] I. M. Babuška and S. A. Sauter, "Is the Pollution Effect of the FEM Avoidable for the Helmholtz Equation Considering High Wave Numbers?," *SIAM Review* **42,** pp. 451–484 (2000).

[2] S. Marburg, "Six Boundary Elements per Wavelength: Is That Enough?," *Journal of Computational Acoustics* **10,** 25–51 (2002).

[3] R. H. Lyon, *Statistical energy analysis of dynamical systems: theory and applications* (MIT Press, 1975).

[4] I. Harari and T. J. Hughes, "Galerkin/least-squares finite element methods for the reduced wave equation with non-reflecting boundary conditions in unbounded domains," *Computer Methods in Applied Mechanics and Engineering* **98,** 411 – 454 (1992).

[5] O. Z. Mehdizadeh and M. Paraschivoiu, "Investigation of a two-dimensional spectral element method for Helmholtz's equation," *Journal of Computational Physics* **189,** 111 – 129 (2003).

[6] F. Ihlenburg and I. Babuška, "Finite Element Solution of the Helmholtz Equation with High Wave Number Part II: The h-p Version of the FEM," *SIAM Journal on Numerical Analysis* **34,** 315–358 (1997).

[7] J. Melenk and S. Sauter, "Convergence analysis for finite element discretizations of the Helmholtz equation with Dirichlet-to-Neumann boundary conditions," *Mathematics of Computation* **79,** 1871–1914 (2010).

[8] J. Melenk and S. Sauter, "Wavenumber Explicit Convergence Analysis for Galerkin Discretizations of the Helmholtz

Equation," *SIAM Journal on Numerical Analysis* **49,** 1210–1243 (2011).

[9] W. H. Reed and T. R. Hill, "Triangular Mesh Methods for the Neutron Transport Equation," *Los Alamos Report LA-UR-73-479* (1973).

[10] X. Feng and H. Wu, "Discontinuous Galerkin Methods for the Helmholtz Equation with Large Wave Number," *SIAM Journal on Numerical Analysis* **47,** 2872–2896 (2009).

[11] X. Feng and H. Wu, "hp-discontinuous Galerkin methods for the Helmholtz equation with large wave number," *Mathematics of Computation* **80,** 1997–2024 (2011).

[12] X. Feng and Y. Xing, "Absolutely stable local discontinuous Galerkin methods for the Helmholtz equation with large wave number," *Mathematics of Computation* **82,** 1269–1296 (2013).

[13] H. Wu, "Pre-asymptotic error analysis of CIP-FEM and FEM for Helmholtz equation with high wave number. Part I: Linear version," *IMA Journal of Numerical Analysis* (2013), To appear.

[14] L. Zhu and H. Wu, "Pre-asymptotic Error Analysis of CIP-FEM and FEM for Helmholtz Equation with High Wave Number. Part II: hp version," *SIAM Journal on Numerical Analysis* (2013), To appear.

[15] L. Demkowicz and J. Gopalakrishnan, "A class of discontinuous Petrov-Galerkin methods. Part II: Optimal test functions," *Numerical Methods for Partial Differential Equations* **27,** 70–105 (2011).

[16] J. Zitelli, I. Muga, L. Demkowicz, J. Gopalakrishnan, D. Pardo, and V. Galo, "A class of discontinuous Petrov-Galerkin methods. The optimal test norm and time-harmonic wave propagation in 1D ," *Journal of Computational Physics* **230,** 2406–2432 (2011).

[17] L. Demkowicz, J. Gopalakrishnan, I. Muga, and J. Zitelli, "Wavenumber explicit analysis of a DPG method for the multidimensional Helmholtz equation," *Computer Methods in Applied Mechanics and Engineering* **213-216,** 126 – 138 (2012).

[18] G. Fix, S. Gulati, and G. Wakoff, "On the use of singular functions with finite element approximations," *Journal of Computational Physics* **13,** 209 – 228 (1973).

[19] S. E. Benzley, "Representation of singularities with isoparametric finite elements," *International Journal for Numerical Methods in Engineering* **8,** 537–545 (1974).

[20] E. Byskov, "The calculation of stress intensity factors using the finite element method with cracked elements," *International Journal of Fracture Mechanics* **6,** 159–167 (1970).

[21] P. Bettess and O. C. Zienkiewicz, "Diffraction and refraction of surface waves using finite and infinite elements," *International Journal for Numerical Methods in Engineering* **11,** 1271–1290 (1977).

[22] K. Gerdes and L. Demkowicz, "Solution of 3D-Laplace and Helmholtz equations in exterior domains using hp-infinite elements," *Computer Methods in Applied Mechanics and Engineering* **137,** 239 – 273 (1996).

[23] R. J. Astley, "Wave envelope and infinite elements for acoustical radiation," *International Journal for Numerical Methods in Fluids* **3,** 507–526 (1983).

[24] J. M. Melenk, *On Generalized Finite Element Methods*, PhD thesis (University of Maryland, 1995).

[25] J. M. Melenk and I. Babuška, "The partition of unity finite element method: Basic theory and applications," *Computer methods in applied mechanics and engineering* **139,** 289–314 (1996).

[26] P. Mayer and J. Mandel, "The Finite Ray Element Method For The Helmholtz Equation Of Scattering: First Numerical Experiments," (1997).

[27] A. De La Bourdonnaye, "A microlocal discretization method and its utilization for a scattering problem," *Comptes rendus de l'Académie des sciences. Serie 1, Mathématique* **318,** 385–388 (1994).

[28] A. De La Bourdonnaye, "High frequency approximation of integral equations modeling scattering phenomena," *Mathematical Modelling and Numerical Analysis* **28,** 223–241 (1994).

[29] E. Perrey-Debain, J. Trevelyan, and P. Bettess, "New special wave boundary elements for short wave problems," *Communications in Numerical Methods in Engineering* **18,** 259–268 (2002).

[30] T. Strouboulis, I. Babuška, and K. Copps, "The design and analysis of the Generalized Finite Element Method," *Computer Methods in Applied Mechanics and Engineering* **181,** 43–69 (2000).

[31] E. Trefftz, "Ein gegenstuck zum ritzschen verfahren," *In Proceedings of the 2nd International Congress of Applied Mechanics* 131-137 (1926).

[32] E. A. W. Maunder, "Trefftz in translation," *Computer Assisted Mechanics and Engineering Sciences* **10,** 545–563 (2003).

[33] V. Kupradze and M. Aleksidze, "The method of functional equations for the approximate solution of certain boundary value problems," *USSR Computational Mathematics and Mathematical Physics* **4,** 82 – 126 (1964).

[34] B. Després, "Sur une formulation variationnelle de type ultra-faible," *Comptes rendus de l'Académie des sciences. Serie 1, Mathématique* **318,** 939–944 (1994).

[35] O. Cessenat, *Application d'une nouvelle formulation variationnelle aux équations d'ondes harmoniques. Probl'emes de Helmholtz 2D et de Maxwell 3D*, PhD thesis (Université Paris IX Dauphine, 1996).

[36] P. Ladevèze, "Une nouvelle approche pour le calcul des vibrations moyennes fréquences," *Comptes rendus de l'Académie des sciences. Série II, Mécanique, physique, chimie, astronomie* **322,** 849–856 (1996).

[37] W. Desmet, *A wave based prediction technique for coupled vibro-acoustic analysis*, PhD thesis (Katholieke Universiteit Leuven, 1998).

[38] M. Stojek, "Least-squares Trefftz-type elements for the Helmholtz equation," *International Journal for Numerical Methods in Engineering* **41,** 831–849 (1998).

[39] P. Monk and D.-Q. Wang, "A least squares method for the Helmholtz equation," *Computer Methods in Applied Mechanics and Engineering* **175,** 121–136 (1999).

[40] C. Farhat, I. Harari, and L. P. Franca, "A discontinuous enrichment method," *Computer Methods in Applied Mechanics and Engineering* **190,** 6455–6479 (2001).

[41] T. Huttunen, P. Gamallo, and R. J. Astley, "Comparison of two wave element methods for the Helmholtz problem," *Communications in Numerical Methods in Engineering* **25,** 35–52 (2009).

[42] A. H. Barnett and T. Betcke, "An Exponentially Convergent Nonpolynomial Finite Element Method for Time-Harmonic Scattering from Polygons," *SIAM Journal on Scientific Computing* **32,** 1417–1441 (2010).

[43] C. Vanmaele, D. Vandepitte, and W. Desmet, "An efficient wave based prediction technique for dynamic plate bending problems with corner stress singularities," *Computer Methods in Applied Mechanics and Engineering* **198,** 2227–2245 (2009).

[44] C. Vanmaele, K. Vergote, D. Vandepitte, and W. Desmet, "Simulation of in-plane vibrations of 2D structural solids with singularities using an efficient wave based prediction technique," *Computer Assisted Methods in Engineering and Science* **19,** 135–171 (2012).

[45] E. Deckers, B. Bergen, B. Van Genechten, D. Vandepitte, and W. Desmet, "An efficient Wave Based Method for 2D acoustic problems containing corner singularities," *Computer Methods in Applied Mechanics and Engineering* **241-244,** 286 – 301 (2012).

[46] E. Deckers, B. Van Genechten, D. Vandepitte, and W. Desmet, "Efficient treatment of stress singularities in poroelastic wave based models using special purpose enrichment functions," *Computers & Structures* **89,** 1117 – 1130 (2011), Computational Fluid and Solid Mechanics 2011 Proceedings Sixth MIT Conference on Computational Fluid and Solid Mechanics.

[47] E. Perrey-Debain, "Plane wave decomposition in the unit disc: convergence estimates and computational aspects," *Journal of Computational and Applied Mathematics* **193,** 140–156 (2006).

[48] T. Huttunen, P. Monk, F. Collino, and J. P. Kaipio, "The ultra weak variational formulation for elastic wave problems," *SIAM Journal on Scientific Computing* **25,** 1717–1742 (2004).

[49] R. Tezaur, L. Zhang, and C. Farhat, "A discontinuous enrichment method for capturing evanescent waves in multiscale fluid and fluid/solid problems," *Computer Methods in Applied Mechanics and Engineering* **197,** 1680–1698 (2008).

[50] P. Massimi, R. Tezaur, and C. Farhat, "A discontinuous enrichment method for three-dimensional multiscale harmonic wave propagation problems in multi-fluid and fluid-solid media," *International Journal for Numerical Methods in Engineering* **76,** 400–425 (2008).

[51] A. Buffa and P. Monk, "Error estimates for the ultra weak variational formulation of the Helmholtz equation," *ESAIM: Mathematical Modelling and Numerical Analysis* **42,** 925–940 (2008).

[52] A. Moiola, "Plane wave approximation in linear elasticity," *Applicable Analysis* (In press).

[53] R. Hiptmair, A. Moiola, and I. Perugia, "Plane wave discontinuous Galerkin methods for the 2D Helmholtz equation: analysis of the *p*-version," *SIAM Journal on Numerical Analysis* **49,** 264–284 (2011).

[54] C. Vanmaele, *Development of a wave based prediction technique for the efficient analysis of low- and mid-frequency structural vibrations*, PhD thesis (Katholieke Universiteit Leuven Faculteit Toegepaste Wetenschappen Arenbergkasteel, B-3001 Heverlee (Leuven), Belgium, 2007).

[55] P. Massimi, R. Tezaur, and C. Farhat, "A discontinuous enrichment method for the efficient solution of plate vibration problems in the medium-frequency regime," *International Journal for Numerical Methods in Engineering* **84,** 127–148 (2010).

[56] P. Ladevèze, L. Arnaud, P. Rouch, and C. Blanzé, "The variational theory of complex rays for the calculation of medium-frequency vibrations," *Engineering Computations* **18,** 193–214 (2001).

[57] K. Graff, *Wave Motion in Elastic Solids* (Dover Publications, 1975).

[58] T. Huttunen, *The ultra weak variational formulation for ultrasound transmission problems*, PhD thesis (University of Kuopio, 2004).

[59] A. W. Leissa, *Vibration of plates* (NASA, Washington, DC, 1969).

[60] G. Dunavaut and J. Lions, *Inequalities in Mechanics and Physics* (Springer-Verlag, Berlin, 1976).

[61] S. Timoshenko and S. Woinowsky-Krieger, *Theory of plates and shells* (McGraw-Hill Book Company, Inc., 1959).

[62] J. Cuenca, *Wave models for the flexural vibrations of thin plates*, PhD thesis (Université du Maine, Le Mans, France, 2009).

[63] L. Cremer, M. Heckl, and B. A. Petersson, *Structure-borne sound: structural vibrations and sound radiation at audio frequencies* (Springer, 2005).

[64] F. Ihlenburg, *Finite element analysis of acoustic scattering*, Vol. 132, (Springer, 1998).

[65] D. Colton and R. Kress, *Inverse Acoustic and Electromagnetic Scattering Theory* (Springer, 1998).

[66] L. L. Thompson, "A review of finite-element methods for time-harmonic acoustics," *The Journal of the Acoustical Society of America* **119,** 1315–1330 (2006).

[67] O. Laghrouche and P. Bettess, "Short Wave Modelling Using Special Finite Elements.," *Journal of Computational Acoustics* **8,** 189 (2000).

[68] T. Strouboulis and R. Hidajat, "Partition of unity method for Helmholtz equation: q-convergence for plane-wave and wave-band local bases," *Applications of Mathematics* **51,** 181–204 (2006).

[69] H. Riou, P. Ladevèze, and B. Sourcis, "The multiscale VTCR approach applied to acoustics problems," *Journal of Computational Acoustics* **16,** 487–505 (2008).

[70] O. Laghrouche and M. Mohamed, "Locally enriched finite elements for the Helmholtz equation in two dimensions," *Computers & Structures* **88,** 1469 – 1473 (2010), Special Issue: Association of Computational Mechanics - United Kingdom.

[71] J. M. Melenk and I. Babuška, "Approximation with harmonic and generalized harmonic polynomials in the partition of unity method," *Computer Assisted Methods in Engineering and Science* **4,** 607–632 (1997).

[72] I. Babuška and J. M. Melenk, "The partition of unity method," *International Journal for Numerical Methods in Engineering* **40,** 727–758 (1997).

[73] P. Ortiz and E. Sanchez, "An improved partition of unity finite element model for diffraction problems," *International Journal for Numerical Methods in Engineering* **50,** 2727–2740 (2001).

[74] O. Laghrouche, P. Bettess, and R. J. Astley, "Modelling of short wave diffraction problems using approximating systems of plane waves," *International Journal for Numerical Methods in Engineering* **54,** 1501–1533 (2002).

[75] L. Xi-kui and Z. Hao-yang, "Partition of unity finite element method for short wave propagation in solids," *Applied Mathematics and Mechanics* **26,** 1056–1063 (2005).

[76] O. Laghrouche, P. Bettess, E. Perrey-Debain, and J. Trevelyan, "Plane wave basis finite-elements for wave scattering in three dimensions," *Communications in Numerical Methods in Engineering* **19,** 715–723 (2003).

[77] E. Perrey-Debain, O. Laghrouche, P. Bettess, and J. Trevelyan, "Plane-wave basis finite elements and boundary elements for three-dimensional wave scattering," *Philosophical Transactions of the Royal Society of London. Series A: Mathematical, Physical and Engineering Sciences* **362,** 561–577 (2004).

[78] E. De Bel, P. Villon, and P. Bouillard, "Forced vibrations in the medium frequency range solved by a partition of unity method with local information," *International Journal for Numerical Methods in Engineering* **62,** 1105–1126 (2005).

[79] A. El Kacimi and O. Laghrouche, "Numerical modeling of elastic wave scattering in frequency domain by partition of unity finite element method," *International Journal for Numerical Methods in Engineering* **77,** 1646–1669 (2009).

[80] P. Bettess, J. Shirron, O. Laghrouche, B. Peseux, R. Sugimoto, and J. Trevelyan, "A numerical integration scheme for special finite elements for the Helmholtz equation," *International Journal for Numerical Methods in Engineering* **56,** 531–552 (2003).

[81] R. Astley and P. Gamallo, "Special short wave elements for flow acoustics," *Computer Methods in Applied Mechanics and Engineering* **194,** 341 – 353 (2005), Selected papers from the 11th Conference on The Mathematics of Finite Elements and Applications.

[82] P. Gamallo and R. J. Astley, "The partition of unity finite element method for short wave acoustic propagation on non-uniform potential flows," *International Journal for Numerical Methods in Engineering* **65,** 425–444 (2006).

[83] O. Laghrouche, P. Bettess, E. Perrey-Debain, and J. Trevelyan, "Wave interpolation finite elements for Helmholtz problems with jumps in the wave speed," *Computer Methods in Applied Mechanics and Engineering* **194,** 367 – 381 (2005), Selected papers from the 11th Conference on The Mathematics of Finite Elements and Applications.

[84] O. Laghrouche, A. El-Kacimi, and J. Trevelyan, "Extension of the PUFEM to Elastic Wave Propagation in Layered Media," *Journal of Computational Acoustics* **20,** 1240006 (2012).

[85] W. G. Facco, E. J. Silva, R. Adriano, A. S. Moura, and N. Z. Lima, "Handling material discontinuities in a nonconforming generalized finite element method to solve wave propagation problems," *Microwave and Optical Technology Letters* **54,** 2709–2716 (2012).

[86] A. El Kacimi and O. Laghrouche, "Improvement of PUFEM for the numerical solution of high-frequency elastic wave scattering on unstructured triangular mesh grids," *International Journal for Numerical Methods in Engineering* **84,** 330–350 (2010).

[87] S. Essahbi, E. Perrey-Debain, M. Ben Tahar, L. Hammami, and M. Haddar, "Plane Wave Based Method: Analytic Integration and Frequency Behaviour," *WSEAS Transactions on Applied and Theoretical Mechanics* **7** (2012).

[88] G. Gabard, "Exact integration of polynomial-exponential products with application to wave-based numerical methods," *Communications in Numerical Methods in Engineering* **25,** 237–246 (2009).

[89] E. A. Munts, S. J. Hulshoff, and R. des Borst, "The partition-of-unity method for linear diffusion and convection problems: accuracy, stabilization and multiscale interpretation," *International Journal for Numerical Methods in Fluids* **43,** 199–213 (2003).

[90] M. S. Mohamed, M. Seaid, J. Trevelyan, and O. Laghrouche, "A partition of unity FEM for time-dependent diffusion problems using multiple enrichment functions," *International Journal for Numerical Methods in Engineering* **93,** 245–265 (2013).

[91] F. Ihlenburg and I. Babuška, "Solution of Helmholtz problems by knowledge-based FEM," *Computer Assisted Mechanics and Engineering Sciences* **4,** 397–416 (1997).

[92] E. Perrey-Debain, J. Trevelyan, and P. Bettess, "Plane wave interpolation in direct collocation boundary element method for radiation and wave scattering: numerical aspects and applications," *Journal of Sound and Vibration* **261,** 839 – 858 (2003).

[93] E. Perrey-Debain, J. Trevelyan, and P. Bettess, "P-wave and S-wave decomposition in boundary integral equation for plane

elastodynamic problems," *Communications in Numerical Methods in Engineering* **19,** 945–958 (2003).

[94] E. Perrey-Debain, J. Trevelyan, and P. Bettess, "Use of Wave Boundary Elements for Acoustic Computations," *Journal of Computational Acoustics* **11,** 305–321 (2003).

[95] E. Perrey-Debain, J. Trevelyan, and P. Bettess, "Wave boundary elements: a theoretical overview presenting applications in scattering of short waves," *Engineering Analysis with Boundary Elements* **28,** 131 – 141 (2004).

[96] G. Gabard, P. Gamallo, and T. Huttunen, "A comparison of wave-based discontinuous Galerkin, ultra-weak and least-square methods for wave problems," *International Journal for Numerical Methods in Engineering* **85,** 380–402 (2011).

[97] M. Stojek, M. Markiewicz, and O. Mahrenholtz, "Diffraction loads on multiple vertical cylinders with rectangular cross section by Trefftz-type finite elements," *Computers & Structures* **75,** 335 – 345 (2000).

[98] E. Zheng, F. Ma, and D. Zhang, "A least-squares non-polynomial finite element method for solving the polygonal-line grating problem," *Journal of Mathematical Analysis and Applications* **397,** 550 – 560 (2013).

[99] P. Ladevèze, P. Rouch, H. Riou, and X. Bohineust, "Analysis of Medium-Frequency Vibrations in a Frequency Range," *Journal of Computational Acoustics* **11,** 255–283 (2003).

[100] P. Ladevèze and H. Riou, "Calculation of medium-frequency vibrations over a wide frequency range," *Computer Methods in Applied Mechanics and Engineering* **194,** 3167 – 3191 (2005).

[101] H. Riou, P. Ladevèze, and P. Rouch, "Extension of the variational theory of complex rays to shells for medium-frequency vibrations," *Journal of Sound and Vibration* **272,** 341 – 360 (2004).

[102] L. Kovalevsky, P. Ladevèze, and H. Riou, "The Fourier version of the Variational Theory of Complex Rays for medium-frequency acoustics," *Computer Methods in Applied Mechanics and Engineering* **225-228,** 142 – 153 (2012).

[103] L. Kovalevsky, H. Riou, and P. Ladevèze, "On the use of the Variational Theory of Complex Rays for the analysis of 2-D exterior Helmholtz problem in an unbounded domain," *Wave Motion* **50,** 428–436 (2013).

[104] L. Kovalevsky, P. Ladevèze, H. Riou, and M. Bonnet, "The variational theory of complez rays for three-dimensional Helmholtz problems," *Journal of Computational Acoustics* **20,** 1250021 (2012).

[105] H. Riou, P. Ladevèze, B. Sourcis, B. Faverjon, and L. Kovalevsky, "An adaptive numerical strategy for the medium-frequency analysis of helmholtz's problem," *Journal of Computational Acoustics* **20,** 1250001 (2012).

[106] P. Ladevèze and M. Chevreuil, "A new computational method for transient dynamics including the low- and the medium-frequency ranges," *International Journal for Numerical Methods in Engineering* **64,** 503–527 (2005).

[107] M. Chevreuil, P. Ladevèze, and P. Rouch, "Transient analysis including the low- and the medium-frequency ranges of engineering structures," *Computers & Structures* **85,** 1431 – 1444 (2007), Computational Structures Technology.

[108] H. Riou and P. Ladevèze, "A new numerical strategy for the resolution of high-Péclet advection-diffusion problems," *Computer Methods in Applied Mechanics and Engineering* **241-244,** 302 – 310 (2012).

[109] I. Kalashnikova, C. Farhat, and R. Tezaur, "A discontinuous enrichment method for the finite element solution of high

Péclet advection-diffusion problems," *Finite Elements in Analysis and Design* **45,** 238 – 250 (2009), The Twentieth Annual Robert J. Melosh Competition.

[110] B. Pluymers, B. Hal, D. Vandepitte, and W. Desmet, "Trefftz-Based Methods for Time-Harmonic Acoustics," *Archives of Computational Methods in Engineering* **14,** 343–381 (2007).

[111] W. Desmet, P. Sas, and D. Vandepitte, "An indirect Trefftz method for the steady-state dynamic analysis of coupled vibro-acoustic systems," *Computer Assisted Mechanics and Engineering Sciences* **8,** 271–288 (2001).

[112] W. Desmet, B. van Hal, P. Sas, and D. Vandepitte, "A computationally efficient prediction technique for the steady-state dynamic analysis of coupled vibro-acoustic systems," *Advances in Engineering Software* **33,** 527 – 540 (2002), Engineering Computational Technology & Computational Structures Technology.

[113] B. Van Genechten, B. Bergen, D. Vandepitte, and W. Desmet, "A Trefftz-based numerical modelling framework for Helmholtz problems with complex multiple-scatterer configurations," *Journal of Computational Physics* **229,** 6623 – 6643 (2010).

[114] B. van Hal, W. Desmet, D. Vandepitte, and P. Sas, "A Coupled Finite Element-Wave Based Approach for the Steady-State Dynamic Analysis of Acoustic Systems.," *Journal of Computational Acoustics* **11,** 285 – 303 (2003).

[115] B. van Hal, W. Desmet, D. Vandepitte, and P. Sas, "Hybrid Finite Element - Wave Based Method for acoustic problems," *Computer Assisted Mechanics and Engineering Sciences* **10,** 479–494 (2003).

[116] B. van Hal, W. Desmet, and D. Vandepitte, "Hybrid finite element-wave-based method for steady-state interior

structural-acoustic problems," *Computers & Structures* **83,** 167 – 180 (2005), Advances in Analysis of Fluid Structure Interaction Advances in Analysis of Fluid Structure Interaction.

[117] B. Van Genechten, D. Vandepitte, and W. Desmet, "A direct hybrid finite element - Wave based modelling technique for efficient coupled vibro-acoustic analysis," *Computer Methods in Applied Mechanics and Engineering* **200,** 742 – 764 (2011).

[118] B. Van Genechten, B. Pluymers, D. Vandepitte, and W. Desmet, "A hybrid wave based-modally reduced finite element method for the efficient analysis of low-and mid-frequency car cavity acoustics," *SAE International Journal of Passenger Cars-Mechanical Systems* **2,** 1494–1504 (2009).

[119] K. Vergote, B. Van Genechten, D. Vandepitte, and W. Desmet, "On the analysis of vibro-acoustic systems in the mid-frequency range using a hybrid deterministic-statistical approach," *Computers & Structures* **89,** 868 – 877 (2011), Computational Fluid and Solid Mechanics 2011 Proceedings Sixth MIT Conference on Computational Fluid and Solid Mechanics.

[120] B. Pluymers, W. Desmet, D. Vandepitte, and P. Sas, "Application of an efficient wave-based prediction technique for the analysis of vibro-acoustic radiation problems," *Journal of Computational and Applied Mathematics* **168,** 353 – 364 (2004), Selected Papers from the Second International Conference on Advanced Computational Methods in Engineering (ACOMEN 2002).

[121] J. Rejlek, B. Pluymers, A. Hepberger, H.-H. Priebsch, and W. Desmet, "Application of the Wave Based Technique for steady-state semi-infinite sound radiation analysis," *Computer Assisted Mechanics and Engineering Sciences* **15,** 337–351 (2008).

[122] B. Bergen, B. V. Genechten, D. Vandepitte, and W. Desmet, "An Efficient Trefftz-Based Method for Three-Dimensional

Helmholtz Problems in Unbounded Domains," *CMES: Computer Modeling in Engineering & Sciences* **61,** 155–176 (2010).

[123] C. Vanmaele, D. Vandepitte, and W. Desmet, "An efficient wave based prediction technique for plate bending vibrations," *Computer Methods in Applied Mechanics and Engineering* **196,** 3178–3189 (2007).

[124] E. Deckers, N.-E. Hörlin, D. Vandepitte, and W. Desmet, "A Wave Based Method for the efficient solution of the 2D poroelastic Biot equations," *Computer Methods in Applied Mechanics and Engineering* **201-204,** 245 – 262 (2012).

[125] O. Cessenat and B. Després, "Application of an ultra weak variational formulation of elliptic PDEs to the two-dimensional Helmholtz problem," *SIAM Journal on Numerical Analysis* **35,** 255–299 (1998).

[126] P. Gamallo and R. J. Astley, "A comparison of two Trefftz-type methods: the ultraweak variational formulation and the least-squares method, for solving shortwave 2-D Helmholtz problems," *International Journal for Numerical Methods in Engineering* **71,** 406–432 (2007).

[127] T. Huttunen, M. Malinen, and P. Monk, "Solving Maxwell's equations using the ultra weak variational formulation," *Journal of Computational Physics* **223,** 731–758 (2007).

[128] G. Gabard, "Discontinuous Galerkin methods with plane waves for time-harmonic problems," *Journal of Computational Physics* **225,** 1961–1984 (2007).

[129] Z. Badics and Y. Matsumoto, "Trefftz discontinuous Galerkin methods for time-harmonic electromagnetic and ultrasound transmission problems," *International Journal of Applied Electromagnetics and Mechanics* **28,** 17–24 (2008).

[130] L.-M. Imbert-Gérard and B. Després, "A generalized plane wave numerical method for smooth non constant coeffIcients," (2011).

[131] C. J. Howarth, S. N. Chandler-Wilde, S. Langdon, and P. N. Childs, "Enriching a Hankel Basis by Ray Tracing in the Ultra Weak Variational Formulation," *Proceedings of Waves 2013, The 11th international conference on mathematical and numerical aspects of waves* (2013).

[132] T. Huttunen, P. Monk, and J. P. Kaipio, "Computational aspects of the ultra-weak variational formulation," *Journal of Computational Physics* **182,** 27–46 (2002).

[133] E. Darrigrand and P. Monk, "Coupling of the ultra-weak variational formulation and an integral representation using a fast multipole method in electromagnetism," *Journal of Computational and Applied Mathematics* **204,** 400 – 407 (2007), Special Issue: The Seventh International Conference on Mathematical and Numerical Aspects of Waves (WAVES'05).

[134] E. Darrigrand and P. Monk, "Combining the Ultra-Weak Variational Formulation and the multilevel fast multipole method," *Applied Numerical Mathematics* **62,** 709 – 719 (2012), Advances in Boundary Integral Equations and Related Topics: On the Occasion of Professor George C. Hsiao's 75th Birthday.

[135] P. Monk, J. Schöberl, and A. Sinwel, "Hybridizing Raviart-Thomas Elements for the Helmholtz Equation," *Electromagnetics* **30,** 149–176 (2010).

[136] T. Huttunen, J. P. Kaipio, and P. Monk, "An ultra-weak method for acoustic fluid-solid interaction," *Journal of Computational and Applied Mathematics* **213,** 1667–1685 (2008).

[137] T. Huttunen, P. Monk, and J. P. Kaipio, "The perfectly matched layer for the ultra weak variational formulation of

the 3D Helmholtz equation," *International Journal for Numerical Methods in Engineering* **61,** 1072–1092 (2004).

[138] T. Huttunen, M. Malinen, J. P. Kaipio, P. J. White, and K. Hynynen, "A full-wave Helmholtz model for continuous-wave ultrasound transmission," *IEEE Transactions on Ultrasonics, Ferroelectrics and Frequency Control* **52,** 397–409 (2005).

[139] T. Huttunen, E. T. Seppälä, O. Kirkeby, A. Kärkkäinen, and L. Kärkkäinen, "Simulation of the transfer function for a head-and-torso model over the entire audible frequency range," *Journal of Computational Acoustics* **15,** 429–448 (2007).

[140] L. Ding, T. Van Renterghem, and D. Botteldooren, "Estimating the Effect of Semi-Transparent Low-Height Road Traffic Noise Barriers with Ultra Weak Variational Formulation," *Acta Acustica united with Acustica* **97,** 391–402 (2011).

[141] M. Loeser and B. Witzigmann, "The Ultra Weak Variational Formulation Applied to Radiation Problems With Macroscopic Sources in Inhomogeneous Domains," *Selected Topics in Quantum Electronics, IEEE Journal of* **15,** 1144 –1155 (2009).

[142] F. Cakoni and P. Monk, "The 3D Inverse Electromagnetic Scattering Problem for a Coated Dielectric," in *Numerical Mathematics and Advanced Applications*, A. de Castro, D. Gmez, P. Quintela, and P. Salgado, eds. (Springer Berlin Heidelberg, 2006), pp. 119-134.

[143] D. Colton and P. Monk, "Target identification of coated objects," *Antennas and Propagation, IEEE Transactions on* **54,** 1232 – 1242 (2006).

[144] P. Monk and V. Selgas, "Near field sampling type methods for the inverse fluid–solid interaction problem," *Inverse Problems and Imaging (IPI)* **5,** 465–483 (2011).

[145] M. Malinen, S. R. Duncan, T. Huttunen, and J. P. Kaipio, "Feedforward and feedback control of ultrasound surgery," *Applied Numerical Mathematics* **56,** 55 – 79 (2006).

[146] M. Malinen, T. Huttunen, and J. P. Kaipio, "Thermal dose optimization method for ultrasound surgery," *Physics in Medicine and Biology* **48,** 745 (2003).

[147] M. Malinen, T. Huttunen, and J. P. Kaipio, "An optimal control approach for ultrasound induced heating," *International Journal of Control* **76,** 1323–1336 (2003).

[148] J. M. J. Huttunen, T. Huttunen, M. Malinen, and J. P. Kaipio, "Determination of heterogeneous thermal parameters using ultrasound induced heating and MR thermal mapping," *Physics in Medicine and Biology* **51,** 1011 (2006).

[149] T. Huttunen and P. Monk, "The Use of Plane Waves to Approximate Wave Propagation in Anisotropic Media," *Journal of Computational Mathematics* **25,** 350–367 (2007).

[150] C. J. Gittelson, R. Hiptmair, and I. Perugia, "Plane wave discontinuous Galerkin methods: Analysis of the *h*-version," *ESAIM: Mathematical Modelling and Numerical Analysis* **43,** 297–331 (2009).

[151] A. Moiola, *Trefftz-Discontinuous Galerkin Methods for Time-Harmonic Wave Problems*, PhD thesis (ETH Zürich, 2011).

[152] A. Moiola, R. Hiptmair, and I. Perugia, "Plane wave approximation of homogeneous Helmholtz solutions," *Zeitschrift für angewandte Mathematik und Physik* **65,** 809–837 (2011).

[153] R. Hiptmair, A. Moiola, and I. Perugia, "Error analysis of Trefftz-discontinuous Galerkin methods for the time-harmonic Maxwell equations," *Mathematics of Computation* **82,** 247–268 (2013).

[154] C. Gittelson and R. Hiptmair, "Dispersion Analysis of Plane Wave Discontinuous Galerkin Methods," (2012).

[155] R. Hiptmair, A. Moiola, and I. Perugia, "Trefftz discontinuous Galerkin methods for acoustic scattering on locally refined meshes," *Applied Numerical Mathematics* - (2013).

[156] L. Yuan and C.-W. Shu, "Discontinuous Galerkin method based on non-polynomial approximation spaces," *Journal of Computational Physics* **218,** 295 – 323 (2006).

[157] B. Cockburn and C. Shu, "The Local Discontinuous Galerkin Method for Time-Dependent Convection-Diffusion Systems," *SIAM Journal on Numerical Analysis* **35,** 2440–2463 (1998).

[158] B. Cockburn and C.-W. Shu, "Runge-Kutta Discontinuous Galerkin Methods for Convection-Dominated Problems," *Journal of Scientific Computing* **16,** 173–261 (2001).

[159] L. Yuan and C.-W. Shu, "Discontinuous Galerkin method for a class of elliptic multi-scale problems," *International Journal for Numerical Methods in Fluids* **56,** 1017–1032 (2008).

[160] W. Wang and C.-W. Shu, "The WKB Local Discontinuous Galerkin Method for the Simulation of Schrodinger Equation in a Resonant Tunneling Diode," *Journal of Scientific Computing* **40,** 360–374 (2009).

[161] F. Kretzschmar, S. Schnepp, I. Tsukerman, and T. Weiland, "Discontinuous Galerkin Methods with Trefftz Approximation," *arXiv preprint arXiv:1302.6459* (2013), Submitted to Journal of Computational Physics.

[162] C. Farhat, I. Harari, and U. Hetmaniuk, "A discontinuous Galerkin method with Lagrange multipliers for the solution of Helmholtz problems in the mid-frequency regime," *Computer Methods in Applied Mechanics and Engineering* **192,** 1389 – 1419 (2003).

[163] C. Farhat, I. Harari, and U. Hetmaniuk, "The discontinuous enrichment method for multiscale analysis," *Computer Methods in Applied Mechanics and Engineering* **192,** 3195 – 3209

(2003), Multiscale Computational Mechanics for Materials and Structures.

[164] C. Farhat, P. Wiedemann-Goiran, and R. Tezaur, "A discontinuous Galerkin method with plane waves and Lagrange multipliers for the solution of short wave exterior Helmholtz problems on unstructured meshes," *Wave Motion* **39,** 307 – 317 (2004), New computational methods for wave propagation.

[165] C. Farhat, R. Tezaur, and P. Wiedemann-Goiran, "Higher-order extensions of a discontinuous Galerkin method for mid-frequency Helmholtz problems," *International Journal for Numerical Methods in Engineering* **61,** 1938–1956 (2004).

[166] R. Tezaur and C. Farhat, "Three-dimensional discontinuous Galerkin elements with plane waves and Lagrange multipliers for the solution of mid-frequency Helmholtz problems," *International Journal for Numerical Methods in Engineering* **66,** 796–815 (2006).

[167] M. Amara, R. Djellouli, and C. Farhat, "Convergence Analysis of a Discontinuous Galerkin Method with Plane Waves and Lagrange Multipliers for the Solution of Helmholtz Problems," *SIAM Journal on Numerical Analysis* **47,** 1038–1066 (2009).

[168] G. Gabard, "Discontinuous Galerkin methods with plane waves for the displacement-based acoustic equation," *International Journal for Numerical Methods in Engineering* **66,** 549–569 (2006).

[169] L. Zhang, R. Tezaur, and C. Farhat, "The discontinuous enrichment method for elastic wave propagation in the medium-frequency regime," *International Journal for Numerical Methods in Engineering* **66,** 2086–2114 (2006).

[170] I. Harari, R. Tezaur, and C. Farhat, "A study of higher-order discontinuous Galerkin and quadratic least-squares stabilized

finite element computations for acoustics," *Journal of Computational Acoustics* **14,** 1 – 19 (2006).

[171] I. Harari and N. Makmel, "Dispersion Analysis of the Discontinuous Enrichment Method for Plane-strain Elasticity," *International Journal for Computational Methods in Engineering Science and Mechanics* **10,** 303–316 (2009).

[172] E. Grosu and I. Harari, "Studies of the discontinuous enrichment method for two-dimensional acoustics," *Finite Elements in Analysis and Design* **44,** 272 – 287 (2008), The Nineteenth Annual Robert J. Melosh Competition.

[173] E. Grosu and I. Harari, "Three-dimensional element configurations for the discontinuous enrichment method for acoustics," *International Journal for Numerical Methods in Engineering* **78,** 1261–1291 (2009).

[174] P. Massimi, R. Tezaur, and C. Farhat, "A discontinuous enrichment method for the efficient solution of plate vibration problems in the medium-frequency regime," *International Journal for Numerical Methods in Engineering* **84,** 127–148 (2010).

[175] C. Farhat, I. Kalashnikova, and R. Tezaur, "A higher-order discontinuous enrichment method for the solution of high Péclet advection-diffusion problems on unstructured meshes," *International Journal for Numerical Methods in Engineering* **81,** 604–636 (2010).

[176] I. Kalashnikova, R. Tezaur, and C. Farhat, "A discontinuous enrichment method for variable-coefficient advection-diffusion at high Péclet number," *International Journal for Numerical Methods in Engineering* **87,** 309–335 (2011).

[177] S. Brogniez, C. Farhat, and E. Hachem, "A high-order discontinuous Galerkin method with Lagrange multipliers for advection-diffusion problems," *Computer Methods in Applied Mechanics and Engineering* **264,** 49 – 66 (2013).

[178] C. Farhat and J. Toivanen, "A hybrid discontinuous Galerkin method for computing the ground state solution of Bose-Einstein condensates," *Journal of Computational Physics* **231,** 4709 – 4722 (2012).

[179] A. Gillman, R. Djellouli, and M. Amara, "A mixed hybrid formulation based on oscillated finite element polynomials for solving Helmholtz problems," *Journal of Computational and Applied Mathematics* **204,** 515 – 525 (2007), Special Issue: The Seventh International Conference on Mathematical and Numerical Aspects of Waves (WAVES'05).

[180] M. Grigoroscuta-Strugaru, *Contribution à la résolution numérique des problèmes de Helmholtz*, PhD thesis (Université de Pau et des Pays de l'Adour, 2009).

[181] M. Grigoroscuta-Strugaru, M. Amara, H. Calandra, and R. Djellouli, "A Modified Discontinuous Galerkin Method for Solving Efficiently Helmholtz Problems.," *Communications in Computational Physics* **11,** 335 (2012).

[182] M. Amara, H. Calandra, R. Djellouli, and M. Grigoroscuta-Strugaru, "A stable discontinuous Galerkin-type method for solving efficiently Helmholtz problems," *Computers & Structures* **106-107,** 258 – 272 (2012).

[183] D. Wang, R. Tezaur, J. Toivanen, and C. Farhat, "Overview of the discontinuous enrichment method, the ultra-weak variational formulation, and the partition of unity method for acoustic scattering in the medium frequency regime and performance comparisons," *International Journal for Numerical Methods in Engineering* **89,** 403–417 (2012).

[184] S. Esterhazy and J. Melenk, "On Stability of Discretizations of the Helmholtz Equation," in *Numerical Analysis of Multiscale Problems*, Vol. 83, I. G. Graham, T. Y. Hou, O. Lakkis, and R. Scheichl, eds. (Springer Berlin Heidelberg, 2012), pp. 285-324.

[185] Q. Hu and L. Yuan, "A Weighted Variational Formulation with Wave Basis Functions for Solving Helmholtz Equations," (2012).

[186] C. Farhat, R. Tezaur, and J. Toivanen, "A domain decomposition method for discontinuous Galerkin discretizations of Helmholtz problems with plane waves and Lagrange multipliers," *International Journal for Numerical Methods in Engineering* **78,** 1513–1531 (2009).

[187] S. Petersen, C. Farhat, and R. Tezaur, "A spacetime discontinuous Galerkin method for the solution of the wave equation in the time domain," *International Journal for Numerical Methods in Engineering* **78,** 275–295 (2009).

[188] T. Betcke and J. Phillips, "Approximation by dominant wave directions in plane wave methods ," (2012).

[189] R. Hiptmair, A. Moiola, I. Perugia, and C. Schwab, "Approximation by harmonic polynomials in star-shaped domains and exponential convergence of Trefftz hp-DGFEM," (2012).

[190] I. Babuška and Z. Zhang, "The partition of unity method for the elastically supported beam," *Computer Methods in Applied Mechanics and Engineering* **152,** 1 – 18 (1998), Containing papers presented at the Symposium on Advances in Computational Mechanics.

[191] R. Sugimoto and P. Bettess, "Coupling of mapped wave infinite elements and plane wave basis finite elements for the Helmholtz equation in exterior domains," *Communications in Numerical Methods in Engineering* **19,** 761–777 (2003).

[192] P. Ortiz, "Finite elements using a plane-wave basis for scattering of surface water waves," *Philosophical Transactions of the Royal Society of London. Series A: Mathematical, Physical and Engineering Sciences* **362,** 525–540 (2004).

[193] R. Kechroud, A. Soulaimani, and X. Antoine, "A performance study of plane wave finite element methods with a Padé-type artificial boundary condition in acoustic scattering," *Advances in Engineering Software* **40,** 738 – 750 (2009).

[194] A. E. Kacimi and O. Laghrouche, "Numerical analysis of two plane wave finite element schemes based on the partition of unity method for elastic wave scattering," *Computers & Structures* **88,** 1492 – 1497 (2010), Special Issue: Association of Computational Mechanics - United Kingdom.

[195] O. Laghrouche, A. El-Kacimi, and J. Trevelyan, "A comparison of NRBCs for PUFEM in 2D Helmholtz problems at high wave numbers," *Journal of Computational and Applied Mathematics* **234,** 1670 – 1677 (2010), Eighth International Conference on Mathematical and Numerical Aspects of Waves (Waves 2007).

[196] M. Mohamed, O. Laghrouche, and A. El-Kacimi, "Some numerical aspects of the PUFEM for efficient solution of 2D Helmholtz problems," *Computers & Structures* **88,** 1484 – 1491 (2010), Special Issue: Association of Computational Mechanics - United Kingdom.

[197] A. El-Kacimi and O. Laghrouche, "Wavelet based ILU preconditioners for the numerical solution by PUFEM of high frequency elastic wave scattering," *Journal of Computational Physics* **230,** 3119 – 3134 (2011).

[198] S. Essahbi, E. Perry-Debain, M. Haddar, L. Hammami, and M. Ben Tahar, "On the use of the plane wave based method for vibro-acoustic problems," *Multidiscipline Modeling in Materials and Structures* **7,** 356 – 369 (2011).

[199] J.-D. Chazot, B. Nennig, and E. Perrey-Debain, "Performances of the Partition of Unity Finite Element Method for the analysis of two-dimensional interior sound fields with ab-

sorbing materials," *Journal of Sound and Vibration* **332,** 1918–1929 (2013).

[200] M. S. Mohamed, M. Seaid, J. Trevelyan, and O. Laghrouche, "Time-independent hybrid enrichment for finite element solution of transient conduction-radiation in diffusive grey media," *Journal of Computational Physics* - (2013).

[201] O. Cessenat and B. Després, "Using plane waves as base functions for solving time harmonic equations with the ultra weak variational formulation," *Journal of Computational Acoustics* **11,** 227–238 (2003).

[202] T. Huttunen, J. P. Kaipio, and K. Hynynen, "Modeling of anomalies due to hydrophones in continuous-wave ultrasound fields," *IEEE Transactions in Ultrasonics, Felloelectric and Frequency Control* **50,** 1486–1500 (2003).

[203] T. Luostari, T. Huttunen, and P. Monk, Chap 6. Plane Wave Methods for Approximating the Time Harmonic Wave Equation in *Highly oscillatory problems* (Cambridge University Press, 2009).

[204] J. Melenk, A. Parsania, and S. Sauter, "Generalized DG-Methods for Highly Indefinite Helmholtz Problems based on the Ultra-Weak Variational Formulation," (2012).

[205] P. Ladevèze, L. Blanc, P. Rouch, and C. Blanzé, "A multiscale computational method for medium-frequency vibrations of assemblies of heterogeneous plates," *Computers and Structures* **81,** 1267–1276 (2003).

[206] P. Rouch and P. Ladevèze, "The variational theory of complex rays: a predictive tool for medium-frequency vibrations," *Computer Methods in Applied Mechanics and Engineering* **192,** 3301 – 3315 (2003), Multiscale Computational Mechanics for Materials and Structures.

[207] C. Blancé and P. Rouch, "Analysis of structures with stochastic interfaces in the medium-frequency range," *Journal of Computational Acoustics* **13,** 711–729 (2005).

[208] O. Dorival, P. Rouch, and O. Allix, "A substructured version of the variational theory of complex rays dedicated to the calculation of assemblies with dissipative joints in the medium-frequency range," *Engineering Computations* **23,** 729 – 748 (2006).

[209] L. Blanc, C. Blanzé, and P. Rouch, "A multiscale "Trefftz" computational method for medium-frequency vibrations of assemblies of heterogeneous plates with uncertainties," *Computers & Structures* **85,** 595 – 605 (2007), Stochastic Structural Analysis, Optimization and Re-Analysis.

[210] B. Pluymers, W. Desmet, D. Vandepitte, and P. Sas, "On the use of a wave based prediction technique for steady-state structural-acoustic radiation analysis," *CMES: Computer Modeling in Engineering & Sciences* **7,** 173–184 (2005).

[211] X.-S. He, Q.-B. Huang, and W.-C. Peng, "Wave based method for mid-frequency analysis of coupled vibro-acoustic problem," *International Journal of Mechanics and Materials in Design* **4,** 21–29 (2008).

[212] R. Lanoye, G. Vermeir, W. Lauriks, F. Sgard, and W. Desmet, "Prediction of the sound field above a patchwork of absorbing materials," *The Journal of the Acoustical Society of America* **123,** 793–802 (2008).

[213] J. Jegorovs, "Wave based method: new applicability areas," (2009).

[214] J. Jegorovs, "On the extension of the wave based method," in *Days on Diffraction (DD), 2010* (2010), pp. 85 –92.

[215] B. Van Genechten, K. Vergote, D. Vandepitte, and W. Desmet, "A multi-level wave based numerical modelling framework

for the steady-state dynamic analysis of bounded Helmholtz problems with multiple inclusions," *Computer Methods in Applied Mechanics and Engineering* **199,** 1881 – 1905 (2010).

[216] A. Dijckmans, G. Vermeir, and W. Lauriks, "Sound transmission through finite lightweight multilayered structures with thin air layers," *The Journal of the Acoustical Society of America* **128,** 3513–3524 (2010).

[217] K. Koo, B. Pluymers, W. Desmet, and S. Wang, "Vibro-acoustic design sensitivity analysis using the wave-based method," *Journal of Sound and Vibration* **330,** 4340 – 4351 (2011), COMPUTATIONAL AERO-ACOUSTICS (CAA) FOR AIRCRAFT NOISE PREDICTION - PART B.

[218] E. Deckers, B. Drofmans, B. Van Genechten, B. Bergen, D. Vandepitte, and W. Desmet, "Spline-based boundaries: A first step towards generic geometric domain descriptions for efficient mid-frequency acoustic analysis using the Wave Based Method," *Journal of Computational and Applied Mathematics* **235,** 2679 – 2693 (2011).

[219] B. Bergen, B. Pluymers, B. Van Genechten, D. Vandepitte, and W. Desmet, "A Trefftz based method for solving Helmholtz problems in semi-infinite domains," *Engineering Analysis with Boundary Elements* **36,** 30 – 38 (2012), Special Issue on Trefftz Method.

[220] K. Vergote, C. Vanmaele, D. Vandepitte, and W. Desmet, "An efficient wave based approach for the time-harmonic vibration analysis of 3D plate assemblies," *Journal of Sound and Vibration* **332,** 1930 – 1946 (2013).

[221] E. Deckers, D. Vandepitte, and W. Desmet, "A Wave Based Method for the axisymmetric dynamic analysis of acoustic and poroelastic problems," *Computer Methods in Applied Mechanics and Engineering* **257,** 1 – 16 (2013).

[222] A. Dijckmans and G. Vermeir, "Development of a hybrid wave based–transfer matrix model for sound transmission analysis," *The Journal of the Acoustical Society of America* **133,** 2157–2168 (2013).

[223] S. Jonckheere, E. Deckers, B. V. Genechten, D. Vandepitte, and W. Desmet, "A direct hybrid Finite Element Wave Based Method for the steady-state analysis of acoustic cavities with poro-elastic damping layers using the coupled HelmholtzBiot equations," *Computer Methods in Applied Mechanics and Engineering* **263,** 144 – 157 (2013).

[224] V. D. Kupradze, *Potential methods in the theory of elasticity* (Israel Program for Scientific Translations, 1965).

[225] Y.-H. Pao, "Betti's identity and transition matrix for elastic waves," *Journal of the Acoustical Society of America* **64,** 302–310 (1978).

[226] D. N. Arnold, F. Brezzi, B. Cockburn, and L. D. Marini, "Unified analysis of discontinuous Galerkin methods for elliptic problems," *SIAM Journal on Numerical Analysis* **39,** 1749–1779 (2002).

[227] R. Womersley and I. Sloan, "Interpolation and cubature on the sphere," (2004), Electronic: http://web.maths.unsw.edu.au/˜rsw/Sphere.

[228] I. Sloan and R. Womersley, "Extremal systems of points and numerical integration on the sphere," *Advances in Computational Mathematics* **21,** 107–125 (2004).

[229] P. Cummings and X. Feng, "Sharp regularity coefficient estimates for complex-valued acoustic and elastic Helmholtz equations," *Mathematical Models and Methods in Applied Sciences* **16,** 139–160 (2006).

[230] E. H. Georgoulis and P. Houston, "Discontinuous Galerkin Methods for the Biharmonic Problems," *IMA Journal of Numerical Analysis* **29,** 573–594 (2009).

[231] I. Vekua, *New methods for solving elliptic equations* (North Holland, 1967).

[232] J. Oden, C. Duarte, and O. Zienkiewicz, "A new cloud-based hp finite element method," *Computer Methods in Applied Mechanics and Engineering* **153,** 117 – 126 (1998).

[233] L. Marin, "Treatment of singularities in the method of fundamental solutions for two-dimensional Helmholtz-type equations," *Applied Mathematical Modelling* **34,** 1615 – 1633 (2010).

[234] H.-S. Oh and I. Babuška, "The p-version of the finite element method for the elliptic boundary value problems with interfaces," *Computer Methods in Applied Mechanics and Engineering* **97,** 211 – 231 (1992).

[235] Q. Carayol and F. Collino, "Error estimates in the fast multipole method for scattering problems Part 1: Truncation of the Jacobi-Anger series," *ESAIM: Mathematical Modelling and Numerical Analysis* **38,** 371–394 (2004).

[236] P. Monk and E. Süli, "The Adaptive Computation of Far-Field Patterns by A Posteriori Error Estimation of Linear Functionals," *SIAM Journal on Numerical Analysis* **36,** 251–274 (1998).

[237] T. Luostari, T. Huttunen, and P. Monk, "The Ultra Weak Variational Formulation Using Evanescent Basis Functions," *10th International Conference on Theoretical and Computational Acoustics, ICTCA 2011, Taipei, Taiwan April 24-28, 2011, Proceeding* (2011).

[238] T. Luostari, T. Huttunen, and P. Monk, "Simulation of structural dynamics using a non-polynomial method," *Proceedings of 21st International Congress on Acoustics, ICA 2013.* (2013).

Teemu Luostari

Non-polynomial Approximation Methods in Acoustics and Elasticity

Acoustic and elastic wave models are often encountered in engineering. This thesis focuses on simulating time-harmonic wave propagation problems in acoustic and elastic media using a non-polynomial method called the ultra weak variational formulation (UWVF). A particular concern is the choice of basis functions in the acoustic UWVF. In addition, new error estimates for the elastic UWVF are presented and a new UWVF is introduced to solve vibration problems in thin elastic plates.

UNIVERSITY OF
EASTERN FINLAND

Publications of the University of Eastern Finland
Dissertations in Forestry and Natural Sciences

ISBN 978-952-61-1248-0